IMPACT OF PRICE REDUCTIONS ON THE LONG-TERM PAVEMENT PERFORMANCE OF HMA MIXES IN NORTH CAROLINA

Final Report
(Report No. FHWA/NC/2005-09)

To North Carolina Department of Transportation
(Research Project No. HWY-2002-07)

Submitted by

Y. Richard Kim, Ph.D., P.E.
Campus Box 7908
Department of Civil, Construction & Environmental Engineering
North Carolina State University
Raleigh, NC 27695-7908
Ph: 919-515-7758
Fax: 919-515-7908
E-mail: kim@ncsu.edu

Sugjoon Lee, Ph.D.
Northboro Research & Development Center
Saint-Gobain Technical Fabrics

Youngguk Seo, Ph.D.
Highway & Transportation Technology Institute
Korea Highway Corporation

Omar El-Haggan
Scott Wilson Kirkpatrick & Co.
England

Department of Civil, Construction & Environmental Engineering
North Carolina State University
Raleigh, NC

August 2005

Technical Report Documentation Page

1. Report No. **FHWA/NC/2005-09**	2. Government Accession No.	3. Recipient's Catalog No.
4. Title and Subtitle **Impact of Price Reductions on the Long-Term Pavement Performance of HMA Mixes in North Carolina**		5. Report Date **August 8, 2005** 6. Performing Organization Code
7. Author(s) **Y. Richard Kim, Sugjoon Lee, Youngguk Seo, and Omar El-Haggan**		8. Performing Organization Report No.
9. Performing Organization Name and Address **Campus Box 7908** **Dept. of Civil, Construction & Environmental Engineering** **North Carolina State University, Raleigh, NC 27695-7908**		10. Work Unit No. (TRAIS) 11. Contract or Grant No.
12. Sponsoring Agency Name and Address **NC Department of Transportation** **Research and Analysis Group** **1 South Wilmington Street** **Raleigh, NC 27601**		13. Type of Report and Period Covered **Final Report** **July 2001 – May 2004** 14. Sponsoring Agency Code **2002-07**

15. Supplementary Notes

16. Abstract

Article 105-3 of the North Carolina Department of Transportation (NCDOT) Standard Specifications for Road and Structures provides guidance on price adjustments for hot mix asphalt pavements that are not within reasonably close conformity with the specifications but for which the work is to be accepted and remains in place. Although the impact of this Article is enormous, no research has been done in North Carolina to support whether the current practice is adequate. The primary objective of the research reported herein is to determine whether price reduction calculations under the provisions of Article 105-3 are adequate.

The type of pavement deficiency addressed in this research is *in situ* density. Both fatigue and rutting performance are evaluated. The following laboratory tests were performed on two North Carolina Superpave mixtures with varying air void contents: (1) axial compression dynamic modulus tests for modulus determination; (2) indirect tension tests for fatigue performance evaluation; (3) repeated load triaxial tests for rutting evaluation; and (4) accelerated pavement tests on laboratory pavement slabs for fatigue and rutting evaluation using the third-scale Model Mobile Loading Simulator (MMLS3). Air void models for the dynamic modulus, fatigue cracking, and rutting are developed using the laboratory test data.

The results from the material level performance tests and the MMLS3 tests allowed the calculation of the PRF values. It was found that the PRF values are not sensitive to the testing methodology used (i.e., the MMLS3 vs. IDT or TRLPD tests); rather they are significantly different, depending upon which performance characteristic is used (i.e., fatigue cracking vs. rutting).

Pavement performance prediction methodologies were developed that predict the fatigue life and permanent deformation growth of the asphalt pavement under the MMLS3 loading. These methodologies are based on material level performance models, multilayered elastic analysis, and the time-temperature superposition principle to account for the differences between the material level testing conditions and the MMLS3 testing conditions. The fatigue life prediction algorithm adopts a cumulative damage analysis; the permanent deformation prediction algorithm uses a sublayering method. It was found that the prediction methodologies yield reasonable predictions of fatigue life and permanent deformation growth of asphalt slabs under the MMLS3 loading.

These pavement performance prediction methodologies were implemented into the computer program called AP^4 (Asphalt Pavement Performance Prediction Program). This program allows the determination of the service life for fatigue cracking and rutting based on the inputs of air void contents in all the HMA layers. Case studies of five density deficient pavements were conducted, which resulted in reasonable price reductions.

17. Key Words	18. Distribution Statement		
Price Reduction, Performance Related Specification, Density, Rutting, Fatigue Cracking, MMLS3, Mechanistic-Empirical			
19. Security Classif. (of this report) Unclassified	20. Security Classif. (of this page) Unclassified	21. No. of Pages 96	22. Price

Form DOT F 1700.7 (8-72) **Reproduction of completed page authorized**

DISCLAIMER

The contents of this report reflect the views of the authors and not necessarily the views of North Carolina State University. The authors are responsible for the facts and the accuracy of the data presented herein. The contents do not necessarily reflect the official views or policies of either the North Carolina Department of Transportation or the Federal Highway Administration at the time of publication. This report does not constitute a standard, specification, or regulation.

ACKNOWLEDGMENTS

This research was sponsored by the North Carolina Department of Transportation and the Federal Highway Administration. Our Steering and Implementation Committee consisted of Judith Corley-Lay, Ph.D., P.E., Chair; Cecil Jones, P.E.; Shannon Sweitzer, P.E.; Jack Cowsert, P.E.; Chris Bacchi, P.E.; Jim Phillips, P.E.; Rodger Rochelle, P.E.; and Mustan Kadibhai, P.E. These advisors have given invaluable direction and support to us throughout the project. The principal investigator wishes to thank these people for their significant contributions to the research.

TABLE OF CONTENTS

LIST OF TABLES

LIST OF FIGURES

CHAPTER 1 INTRODUCTION

1.1 Background

Recent advancements in testing and analysis techniques for hot mix asphalt (HMA) mixtures and asphalt pavements have allowed for more realistic predictions of pavement performance. Additional capabilities inherent in these techniques make it possible to address more complicated, but nonetheless crucial, aspects of engineering within state highway agencies. One immediate area in need of improvement is the development of specifications that are based on the performance of asphalt mixtures and pavements, i.e., performance-related specifications (PRS). Such specifications will allow state highway agencies to determine pay factors of HMA mixtures under various conditions using more realistic and sound engineering principles than are currently in use.

The recognition for the need to develop performance-related specifications (PRS) for asphalt concrete pavements dates back to the early 1980s. Such specifications were deemed necessary to achieve the goals of the SHRP initiative and to foster cooperation and teamwork between the contractor and the owner, as well as to be equitable to both sides (Fernando et al. 1987). Extensive research in this area has been sponsored/conducted by private industry, academia, state DOTs, and the SHRP, NCHRP, FHWA, in addition to other national and international agencies. Conducted research varies in scope from discussion of the philosophy and evolution of PRS (Hughes 1984) to the development of comprehensive PRS frameworks that have been proposed and implemented by state DOTs.

PRS frameworks may be divided broadly into two categories. For the first category, which has been adopted by many highway agencies in the United States, the acceptance criteria for these specifications are generally based on traditional materials and construction variables such as asphalt content, air voids, density, and pavement thickness. The acceptance levels (based on deviations from the mean or percent within limit) for most specifications are selected from historical records to penalize those contractors with high levels of variability or large departures from the target values. However, these penalties are not related directly to poor pavement performance and, thus, may not ensure that the desired design life is attained (Anderson et al. 1990). For that reason, this category of PRS frameworks is starting to phase out in favor of the second category.

For the second category of frameworks, non-conformance penalties are directly related to an anticipated loss in pavement life and increase in life-cycle costs. In such frameworks, a series of algorithms based on laboratory and/or accelerated pavement testing is employed to develop the relationship between materials and construction variables and fundamental response variables, and the relationship between the fundamental response variables and pavement performance distresses. Consequently, the determination of pavement life and life-cycle costs may then be predicted using mathematical models and calibrated by sampling and testing in-service pavements (Shook et al. 1993; Buttlar and Harrell 1998). Ultimately, the decrease in pavement life and increase in life-cycle costs are transformed to pay factors that are incurred by the contractor.

All existing frameworks employ rational and practical models that perform effectively to some extent. However, Weed (1999) concludes that precise models may not be ready for several years to come and that more research is needed to link construction quality to expected life and ultimately to value expressed in the form of penalties.

One excellent candidate for improvement, using the PRS approach, is the North Carolina Department of Transportation Article 105-3 of Standard Specifications for Road and Structures. It provides, in part: "In the event the Engineer finds the materials or the finished product in which the materials are used are not within reasonably close conformity with the plans and specifications but that reasonably acceptable work has been produced, he will then make a determination if the work is to be accepted and remain in place. If the Engineer determines that the work is to be accepted, he will then have the authority to make such adjustment in contract price as he deems warranted based upon engineering judgment and the final estimate will be paid accordingly."

For HMA pavements in North Carolina, price adjustments are made for such material characteristics that include, but are not limited to, insufficient asphalt cement content, insufficient density, or excess air voids. The reduced payments result in fewer first cost funds being expended by the NCDOT, but no attempt has been made to quantify the long-term costs based upon HMA performance. One would assume that the practice of reducing payments under Article 105-3 would accelerate the need for pavement maintenance, but no research has been done in North Carolina to substantiate that assumption. For example, Article 609-9 of the NCDOT Specifications for Road and Structures presents the following formula to calculate reduced pay due to deficiency in HMA density:

$$R = 10 \times D^{1.465} \tag{1-1}$$

where R = the percentage of reduced pay and
D = the average deficiency in density not to exceed 3.0%.

This formula was developed based on the assumption of a 50% price reduction for a 3% deficiency in *in situ* density and the exponential relationship between price reduction and percent deficiency in density. However, there are no supporting data for this relationship, leaving the NCDOT vulnerable to possible challenges from contractors.

Based on these needs, the North Carolina Department of Transportation sponsored a research project for North Carolina State University to conduct a comprehensive laboratory study to verify, calibrate, or modify Article 105-3 and/or Article 609-9. The findings from this research project are summarized in the following chapters.

1.2 Objectives and Scope

The primary objectives of this research are:

(1) to refine/develop fatigue and rutting performance prediction models of HMA that can be used to determine appropriate price reductions due to mixture deficiencies in density;
(2) to determine whether price reductions under the provisions of Article 105-3 and other supporting Articles are adequate based on economic analysis; and
(3) to develop a new recommendation for the application of Article 105-3 and other supporting Articles should the current policy be found to be inadequate.

The scope of this research project covers asphalt pavements that are applicable to Article 105-3 due to insufficient density in the asphalt layer. The performance measures to be evaluated include fatigue cracking and rutting.

1.3 Overall Research Approach and Report Organization

It was recognized at the beginning of this research project that the performance reduction due to insufficient density of the HMA depends upon the pavement structure, the location of the deficient HMA in the pavement structure, and the type of performance in question. For example, a deficient HMA at the bottom of a thick asphalt layer would not affect the rutting performance as significantly as the same deficient mix at the top of the layer. At the same time, the deficient HMA at the bottom of the asphalt layer would have a more significant effect on the bottom-up fatigue cracking than the same mix at the top of the layer.

Based on these observations, it is inevitable that a research approach is adopted that involves both a pavement performance prediction model and a pavement response model that are expressed as a function of the HMA density (i.e., air voids). The overall research approach in this project follows a mechanistic pavement analysis method similar to the one used in the NCHRP 1-37A Mechanistic-Empirical Pavement Design Guide (MEPDG) (AASHTO 2004). The research approach is composed of the following three phases:

Phase I: Laboratory testing and analysis to develop air void models for the modulus and performance of HMA mixtures.
Phase II: Scaled-down accelerated pavement testing to verify the asphalt pavement performance prediction methodology and to determine the price reduction factors in the laboratory setting.
Phase III: Development of a computer program that is capable of performing the pavement performance prediction methodology, verified in Phase II, to determine the price reduction factors as a function of pavement structure, the degree of density deficiency, and the location of the deficient HMA.

CHAPTER 2 discusses materials, specimen fabrication, testing setup and experimental testing details incorporated in the research. The air void models developed from the laboratory testing for the dynamic modulus, fatigue cracking, and rutting performance are presented in CHAPTER 3. CHAPTER 4 describes the experimental program of the

accelerated pavement testing using the third-scale Model Mobile Loading Simulator (MMLS3). Fatigue cracking and the rutting performance of asphalt slabs with different air voids are evaluated using the MMLS3. The pavement performance prediction methodology is developed based on the incremental damage concept and applied to the MMLS3 results. CHAPTER 5 tackles the challenging task of developing a computer program (AP^4) that adopts the pavement performance prediction methodology. Various modules included in the computer program are described in detail. CHAPTER 6 presents the analysis of the results obtained from the laboratory performance tests, MMLS3 tests, and case studies using the AP^4 study results. CHAPTER 7 offers conclusions and future research recommendations.

CHAPTER 2 LABORATORY PERFORMANCE TESTING

This chapter describes the laboratory testing and analysis for the development of performance prediction models that can be used to determine the effects of air voids on asphalt pavement performance.

2.1 Materials and Specimen Fabrication

Two mixture types were used in this study: I19.0C which is an intermediate course mix with a 19 mm nominal maximum size of aggregate (NMSA), and S9.5C which is a surface course mix with a 9.5 mm NMSA. These two mixes are the most commonly used HMAs in asphalt pavement construction in North Carolina. Granite aggregate from the Martin-Marietta Garner quarry and binders obtained from the Citgo refinery in Wilmington, North Carolina were used to produce both mixes. Both binders include a 0.5% anti-strip additive. The target aggregate gradations are listed in Table 2-1 and plotted in Figure 2-1. Mix design information is presented in Table 2-2. All mixtures were aged at 135°C for four hours (i.e., short-term oven aging) before compaction.

Table 2-1. Target aggregate gradations

	Sieve Size (mm)	I19.0C	S9.5C
% Passing	25.0	100	100
	19.0	99	100
	12.5	89	100
	9.50	78	95
	4.75	43	65
	2.36	28	47
	1.18	22	39
	0.60	16	30
	0.43	-	-
	0.30	10	18
	0.18	-	-
	0.15	8	12
	0.075	4.9	5.4

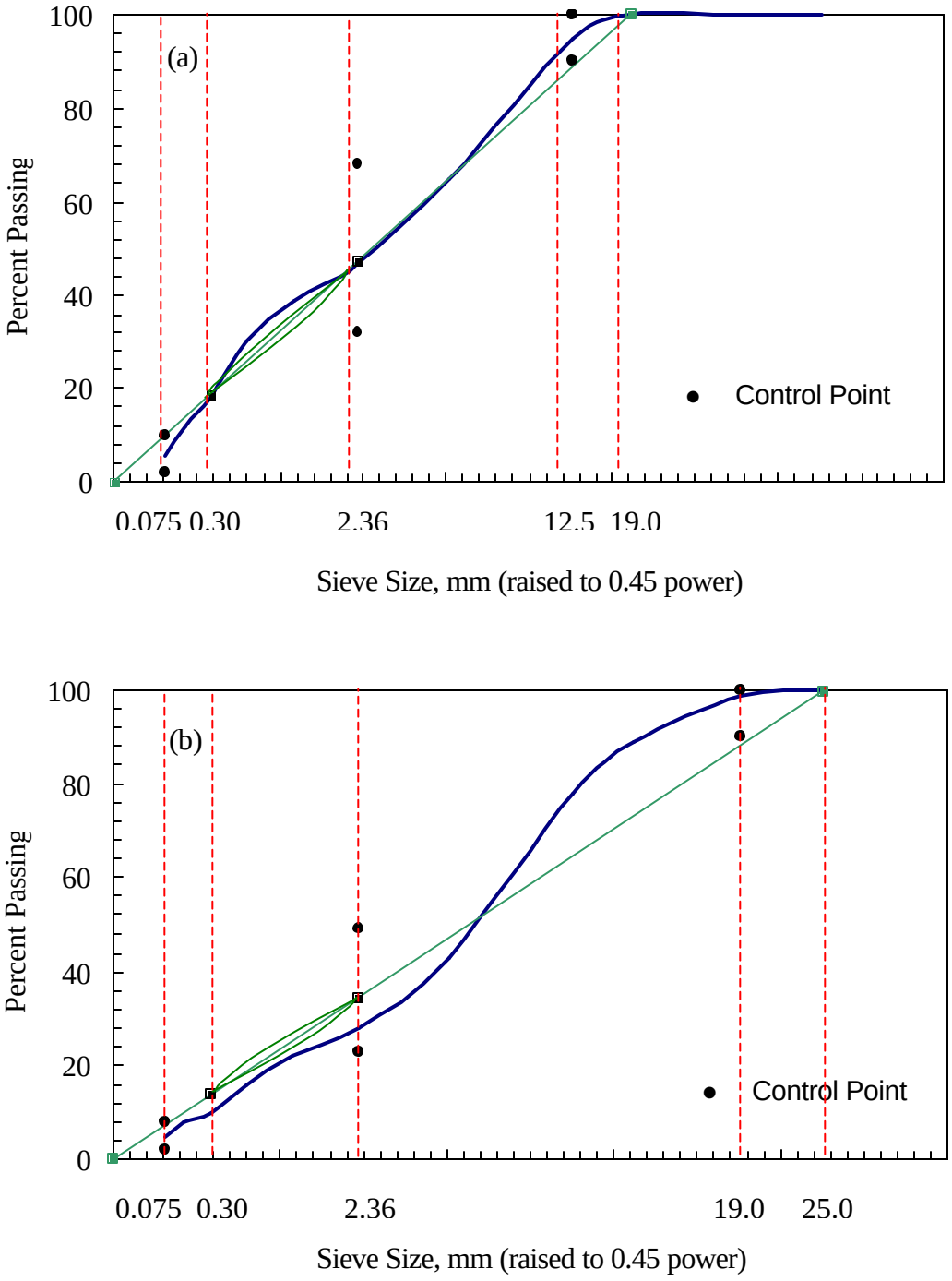

Figure 2-1. Aggregate gradations for: (a) S9.5C mix; (b) I19.0C mix

Table 2-2. Mix design information

Mix Type	Binder Grade	Asphalt Content	Mixing Temperature (°C)	Compaction Temperature (°C)	G_{mm}
S9.5C	PG 64-22	4.7%	158	145	2.464
I19.0C	PG 70-22	5.2%	166	155	2.469

Gyratory specimens with a 150 mm diameter were prepared using the ServoPac Superpave Gyratory Compactor, manufactured by Industrial Process Controls (IPC) in Australia. Specimens were fabricated with two different heights: a 178 mm height for the axial compression test and a 50 mm height for the indirect tension (IDT) test. Axial specimens were cut and cored to the final specimen size of 100 mm diameter and 150 mm height. Final dimensions of the IDT specimens were 150 mm in diameter and 38 mm in height. The compaction effort was adjusted in both axial compression and IDT specimens so that the air void content in the final testing specimens (cut and cored) would fall within ±0.5% of the target air void content.

The target air void contents for this research were determined according to the NCDOT specifications. These specifications call for a minimum 92% of maximum specific gravity (G_{mm}) for newly constructed asphalt pavements. Asphalt pavements with a density between 89% and 92% were considered for price reduction, and those with a density lower than 89% were rejected and had to be reconstructed. Therefore, density levels that require the penalty calculation fall between 89% and 92% (i.e., 8% to 11% of *initial* air voids). In order to determine the target air void contents for laboratory testing, densification processes both in the field and in the laboratory had to be carefully studied and compared. The following section presents the air void reduction study using field cores from which the target air void contents for the fatigue and permanent deformation testing were selected.

2.2 Air Void Reduction Study

This project requires the laboratory testing of HMA specimens that are comprised of air void contents that are different than those expected in the field. One important issue related to the target air void content is that it changes during the actual service life of the pavement due to traffic densification. Depending on the type of laboratory test method, this densification process may or may not be simulated properly in the laboratory. For example, the triaxial repeated load permanent deformation (TRLPD) test used in this study simulates the field densification relatively well, whereas the densification process in the IDT test adopted in this study for fatigue cracking evaluation is quite different from that in the field.

To study the air void reduction in asphalt pavements, two sets of field data were collected. One data set was obtained from an air void reduction study conducted by the National Center for Asphalt Technology (NCAT 2002), the objective of which was to refine the Superpave gyratory compaction requirements. The other data set was obtained

from I-85 in North Carolina after two years of traffic. The initial air void contents of the I-85 pavement were not available. However, assuming that the lane center cores could yield some information regarding the initial air void content, cores from the I-85 pavement were obtained from both the wheel path and lane center. Both the NCAT data (dotted lines) and the I-85 data (solid lines) are presented in Figure 2-2. The initial air void contents for the I-85 cores in this figure are actually the air void contents of the 2-year-old cores from the lane center. The initial air void contents of the NCAT study were measured immediately after construction.

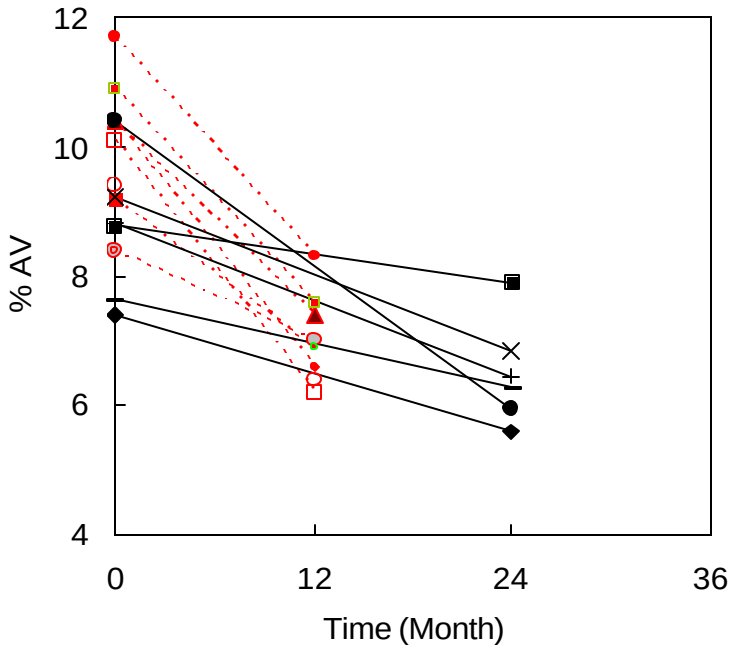

Figure 2-2. Reduction of air void contents

One should note that the *initial* air void contents for the 2-year data from I-85 are about 1% lower than those from the NCAT study, whereas the air void contents after one year are in the same range for both sets of data. This observation suggests that there may have been about a 1% air void reduction in the lane center during the 2-year period. Some amount of densification in the lane center is realistic considering traffic wander and densification due to the pavement's own weight at high temperatures.

To account for this discrepancy, a 1% air void was added to the initial air void content of the 2-year data, as shown in Figure 2-3. It is shown that a significant air void reduction develops during the first year. Much less densification occurs during the second year, and the trend seems to suggest that little densification occurs after the second year. Hanson et al. (1994) also proved that the mechanical properties of field cores remain constant after two years of traffic densification.

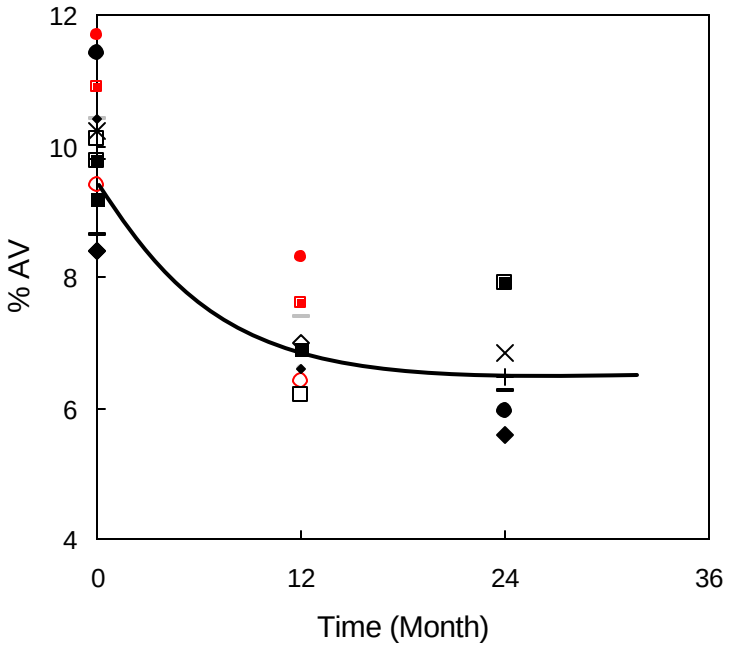

Figure 2-3. Reduction of air voids after the adjustment of the *initial* air void contents for the I-85 cores

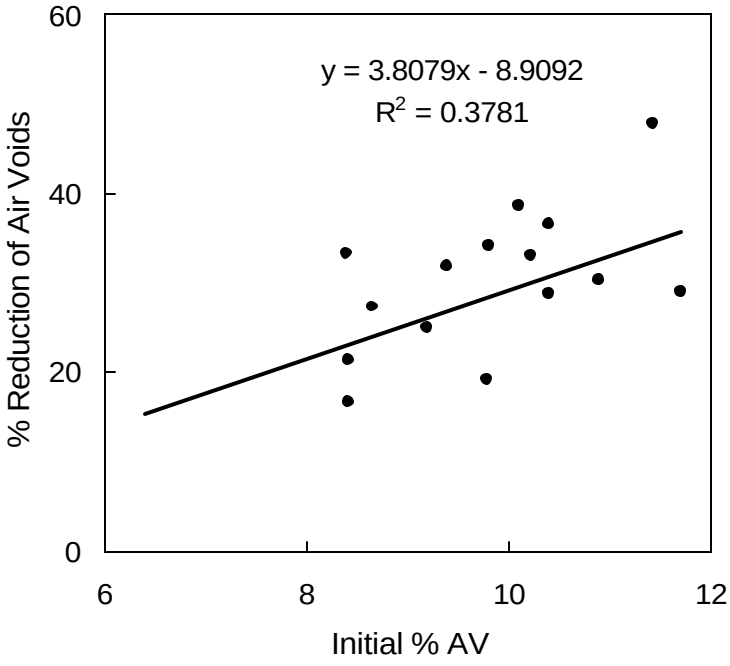

Figure 2-4. Percent air void reduction after two years

Figure 2-4 shows the percent air void reduction after 2 years. It is observed that a higher initial air void content yields larger air void reductions during the densification process. Field air voids investigated in this study are reduced by 20% to 40% of the original air voids.

Density levels that require the penalty calculation fall between 89% and 92% (i.e., 8% to 11% of initial air voids). Therefore, the target air void contents for the laboratory testing must be designed so that the test can simulate the performance of the asphalt mixtures within this air void range. For permanent deformation testing using the TRLPD test, the target air void contents should follow those of the initial air void contents in the field. However, as was mentioned earlier in this section, the IDT fatigue testing requires an adjustment of these air void contents to represent the field conditions most accurately. Knowing that the most densification occurs during the first two years and that the air void content after the first two years remains relatively constant, it was decided to choose the target air void contents obtained by the fatigue testing as those of the asphalt pavements after two years in service. The amount of densification in the first two years that corresponded to each initial air void content was approximated using the regression line shown in Figure 2-4. Table 2-3 summarizes the findings from this study. It was found that 8% to 11% initial air void contents become about 6% to 8% after two years of densification. Based on this information, it was determined that the laboratory IDT fatigue testing should be conducted on HMA specimens with air voids between 6% and 8% (i.e., 6, 7, and 8%) to simulate the fatigue cracking performance of HMAs with initial air voids ranging from 8% to 11% in the field. The target air void contents for the TRLPD testing were selected as 8, 8.75, 9.5, and 11%. Different air void contents were obtained by varying the total mass of the gyratory specimen.

Table 2-3. Initial air void contents and laboratory target air void contents for the IDT fatigue testing

Initial air voids	IDT target air voids
8.0	6.3
8.75	6.5
9.5	6.7
11.0	7.2

2.3 Test and Analysis Methods

The dynamic modulus, fatigue cracking, and rutting performance were investigated in this research. The following test methods were used for these engineering properties:

- Dynamic Modulus – Uniaxial and triaxial compression tests
- Fatigue Cracking – Indirect tensile test
- Rutting – Triaxial repeated load permanent deformation test

In the following subsections, the test setups, test protocols, and data analysis methods are described for each test method.

2.3.1 Test Setup

Two servo-hydraulic testing machines, MTS 810 and UTM-25, were used in testing. The UTM-25 was manufactured by IPC in Australia. It has a loading capacity of 25 kN and is capable of applying loads over a wide range of frequencies, ranging from 0.01 Hz to 25 Hz. The temperature control system of the UTM-25 is refrigeration-based with a heating element to achieve high temperatures. The temperature control system was able to achieve the required testing temperatures, ranging from -10°C to 50°C. The MTS 810 has a loading capacity of 100 kN, and its temperature chamber is a liquid nitrogen based system, which controls test temperatures effectively.

In both machines, an asphalt concrete dummy specimen with a temperature probe inserted in the middle of the specimen was placed inside the chamber in order to check the actual temperature of the specimen during testing. In the triaxial test, this dummy specimen was placed in the triaxial cell to avoid any errors due to the temperature difference between the inside and outside of the cell.

Deformations were measured by linear variable differential transformers (LVDTs). For axial testing, four loose-core type LVDTs were mounted to the surface at 90° radial intervals using a 100 mm gauge length in the mid-height of the specimen. For IDT fatigue testing, two loose-core type miniature LVDTs were mounted on each side of the specimen using a 50.8 mm gauge length.

The LabView data acquisition system was used for data collection. It is fully computer controlled and is capable of measuring and recording data from multiple channels simultaneously. A maximum of 11 channels were used in the TRLPD test: four for the vertical LVDTs, four for the radial LVDTs, one for the load cell, one for the actuator, and one for confining pressure. For the IDT test, six channels were used: four for the surface-mounted LVDTs, one for the actuator, and one for the load cell.

The Load Guide Device (LGD), developed out of the Strategic Highway Research Program (SHRP), was used as the loading apparatus in the IDT fatigue test. From the NCHRP 1-28 study, it was found that when compared against other loading devices with no column or four columns, the SHRP LGD with its two guide columns resulted in the least amount of "rocking" of the IDT specimen without causing significant friction between the upper loading plate and guide columns under repetitive loading (Barksdale et al. 1997).

The setups for the axial compression dynamic modulus test and the TRLPD test followed the specifications developed from NCHRP 1-37A (2002[a], 2002[b]). The same test setup was used in the uniaxial and triaxial compression tests, except the triaxial test was conducted in the triaxial cell. In the TRLPD test of an 11% air void content specimen at 50°C, the axial deformation was too large to be covered by the LVDTs used in this

research. Therefore, the displacement measured by the actuator was evaluated as a substitute for the on-specimen LVDT measurements. The main concern over this substitute is the end effect and machine compliance, which may result in different strains when displacements are measured from the actuator and from on-specimen LVDTs. Deformations measured from both the on-specimen LVDTs and the actuator were analyzed, and it was found that the strain calculated from the actuator displacement matches quite well with the strain calculated from the displacement measured by the on-specimen LVDTs. This agreement suggests firstly that machine compliance was not a significant factor at this temperature and, secondly, that the end effect was minimal. The first observation is reasonable because the stiffness of the asphalt specimen at 50°C was much lower than the stiffness of the machine and mechanical parts in the testing apparatus. Also, the silicon grease lubrication and the use of two rubber membranes between the loading plate and the specimen end seemed to work quite well in minimizing the end effect. Consequently, it was decided to use the actuator measurement in cases where vertical deformation is too high for the on-specimen LVDTs to cover.

2.3.2 Test Protocols

Complex Modulus Testing

Complex modulus testing was performed for the construction of the linear viscoelastic (LVE) mastercurves for the dynamic modulus $|E^*|$ and phase angle (ϕ). Axial compression tests with and without confining pressure were used in this research. The test protocol for these test methods followed the protocol developed from the NCHRP 1-37A (2002[a]) except for the application of the confining pressure. The complex modulus tests were performed at multiple frequency-temperature combinations that were determined to be adequate to develop a dynamic modulus mastercurve. The testing frequencies range from 0.01 to 25 Hz and the testing temperature from -10° to 55°C.

Testing was conducted at temperatures from the lowest to the highest, and frequencies were applied at each temperature from the fastest to the slowest. Before applying the first frequency, a preconditioning load was applied at 25 Hz. The load amplitude was adjusted based on the material stiffness, air void content, temperature, and frequency to keep the strain response within 60-75 microstrains (the target range). After each frequency application, a five-minute rest period was allowed so that the specimen could recover before the next frequency was applied.

In the triaxial complex modulus test, a confining pressure of 20 psi was applied to the specimen before starting the test. The radial deformation was monitored with the confining pressure, and the complex modulus test was initiated after the radial strain was stabilized. Two to three replicate tests were conducted on each of the two mixtures with 8, 8.75, 9.5, and 11% air void contents.

Fatigue Testing

The IDT fatigue test was adopted to evaluate the fatigue response of the HMAs. Three air void contents were selected for fatigue testing: 6, 7, and 8% which were determined from the air void reduction study in Section 2.2. A stress-controlled, continuous haversine pulse consisting of a 0.1 sec loading followed by a 0.9 sec rest period was applied until the horizontal average strain fell between 3 ~ 4%. In this strain range, it was observed that fatigue damage in the specimen accelerates regardless of testing conditions. Therefore, caution was practiced to protect the LVDTs and loading apparatus once the measured strains reached that range.

Fatigue testing was conducted at three temperatures (1.5°, 10°, and 20°C) for the I19.0C mix and at two temperatures (10° and 20°C) for the S9.5C mix. More testing was done on the I19.0C mix because the mechanistic pavement performance prediction methodology developed in this research project considers only traditional bottom-up fatigue cracking. In this methodology, the tensile strain at the bottom of the lowest asphalt layer is the primary pavement response that is related to the fatigue life of the pavement. Since most asphalt pavements have the intermediate course under the surface course, the fatigue characteristics of the intermediate course are more important, according to the pavement performance prediction methodology.

Before starting the fatigue test, the complex modulus test was performed at the testing temperature in order to obtain a linear viscoelastic fingerprint of the specimen being tested. To induce a wide range of fatigue lives, three load levels (low, medium, and high) were selected for each testing temperature, air void, and mix type. Two replicates were tested on each of the two mixtures. However, a third replicate was introduced if a large discrepancy was found between the fatigue lives of the two replicates.

Permanent Deformation Testing

Rutting characteristics of HMAs with different air voids were determined using the TRLPD test. The NCHRP 1-37A test protocol (2002[b]) was followed. Based on a study of effective temperatures for different climatic regions of North Carolina, 30°, 40°, and 50°C were selected as the test temperatures. For each of the three temperatures, two replicates were tested at four air void contents: 8, 8.75, 9.5, and 11%.

In this research, a statistical model, developed by Hafez (1997), was used to estimate the deviator stress in the asphalt layer and then the deviator stress in the TRLPD test. This model is able to estimate the deviator stress for a given pavement structure, material quality, and tire pressure, as shown below:

$$s_d = -43.82 + 62.54E_{ac} + .0004E_{sg} + 0.585p_c + 14.78z_{cr} \qquad (2\text{-}1)$$

where
σ_d = deviator stress, psi,
E_{ac} = asphalt layer modulus, 10^6 psi,

E_{sg} = subgrade modulus, psi,
p_c = tire pressure, psi, and
z_{cr} = depth within the asphalt layer, inches.

Moduli values were assumed to be 1,000 ksi for the asphalt layer and 25 ksi for the subgrade layer. Tire pressure was assumed to be 100 psi. Critical depth was assumed to be 2 inches. According to the Hafez model under these conditions, the deviator stress was determined to be 116.8 psi. Consequently, 120 psi was selected as the deviator stress in the TRLPD test in this research.

As for confining pressure, it ranges between 5 and 30 psi, according to the draft test protocol for the simple performance test for permanent deformation (NCHRP 2002[b]). Consequently, a confining stress of 20 psi was used for all permanent deformation tests in this project.

The TRLPD test was performed using a haversine pulse load of 0.1 sec duration, followed by a rest period of 0.9 sec. Twenty psi confining pressure and 120 psi deviator stress were applied to simulate *in situ* stress conditions. Before starting the TRLPD test, the dynamic modulus test was performed at the TRLPD testing temperature in order to obtain a fingerprint of the specimen being tested. This was done by applying 40 cycles at a frequency of 10 Hz.

2.3.3 Data Analysis

Complex Modulus Testing

LVDT and load cell measurements were collected using a National Instruments data acquisition board and LabView software. The raw data were previewed before any analysis was begun to ensure that strain readings were within the target range (between 60 and 75 microstrains) and that all of the LVDTs read properly. Readings from four LVDTs spaced at 90° intervals were averaged, and the axial strain was calculated from the averaged deformation.

LabView software was used in analyzing the stress and strain data. This program uses the Levenberg-Marquardt algorithm which is a least squares approach to curve fitting. The last five cycles of data were analyzed and fitted according to the following function:

$$F(t) = m_1 + m_2 t + m_3 \cos(wt + f) \qquad (2\text{-}2)$$

where $F(t)$ is load or deformation time history;
t is time;
m_1, m_2, and m_3 are regression coefficients;
f is the phase angle; and
w is the angular frequency.

Coefficient m_3 represents the amplitude of the sinusoidal waveform, and the dynamic modulus is then calculated from the ratio of these coefficients from load and deformation histories. The difference in the phase angles from the load and deformation analyses represents the phase angle of the material. It was found that there is a slight difference between the intended loading frequency and the actual loading frequency. In this study, the actual loading frequency was used in developing and representing the mastercurves.

Fatigue Testing

In the IDT fatigue testing, the horizontal strain was calculated by dividing the measured horizontal displacement by the gauge length (i.e., 2 in.). The horizontal strains from both sides of the specimen were averaged for further analysis. The fatigue life of each test was determined from the horizontal strain versus the number of cycles graph by the bisection method, as shown in Figure 2-5. The bisection method basically finds a straight line that bisects the angle between two tangent lines of the strain versus the number of loading cycles curve. Then, the fatigue life is the number of cycles at which the straight line crosses the strain curve.

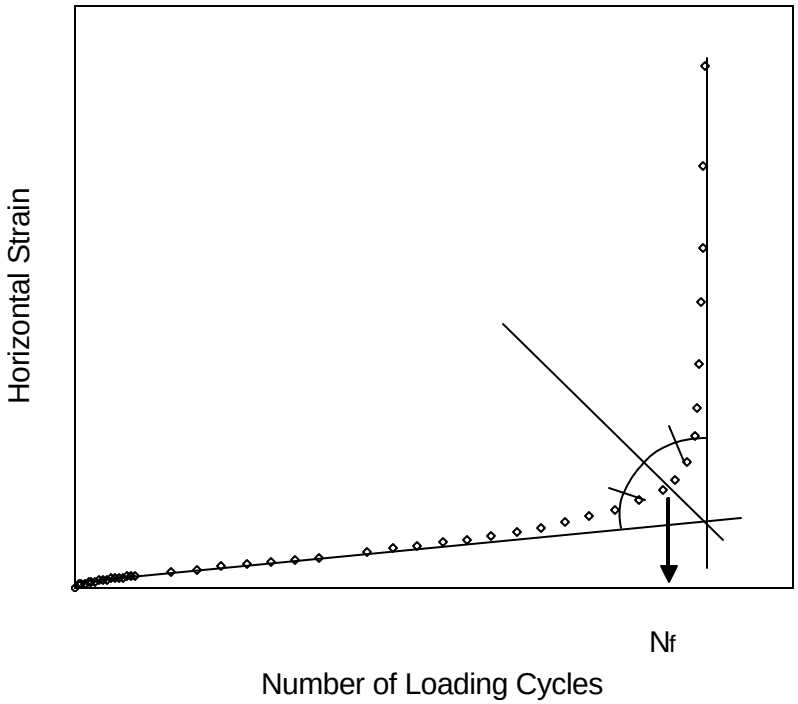

Figure 2-5. Schematic representation of determining the number of cycles to failure

As the specimen reached the fatigue life, macrocracks (several parallel cracks) were initiated at or near the center of the specimen and were propagated along the vertical plane. However, some specimens tested at 20°C resulted in a V-shaped localized failure around the top and/or bottom loading strips before complete rupture, indicating a

significant accumulated permanent deformation under the loading strips. In such cases, test data were discarded from the analysis.

Permanent Deformation Testing

Permanent strain was averaged from displacements measured from four vertical on-specimen LVDTs with 100 mm gauge lengths. Then, the permanent strain was plotted against the number of cycles in a log-log scale, and only the straight portion (secondary zone) of the curve was used for the analysis. In the TRLPD testing of 11% specimens at 50°C, the actuator strain substituted for the LVDT strains. Resilient strain was obtained from the recoverable portion of the total strain and was found to be constant throughout the test.

CHAPTER 3 DEVELOPMENT OF AIR VOID MODELS

In this section, data from the laboratory tests are analyzed to evaluate the effect of air void content on the asphalt mixture modulus and performance. For an assessment of the effect of air voids on the asphalt pavement performance, it is necessary to include a pavement structural analysis, which will be presented in the next chapters. This section focuses on the development of material-level models as a function of air void content.

3.1 Dynamic Modulus Model

Mastercurves were developed from complex modulus testing on specimens with different air voids. All the individual mastercurves with 20 psi confining pressure are plotted in Figure 3-1 and Figure 3-2 for the S9.5C and I19.0C mixtures, respectively. For both mixes, the sample-to-sample variation and similarity of the data from individual tests make it difficult to observe a clear effect of air voids on the dynamic modulus. Therefore, it was decided to average the mastercurves from two replicates of each of the four air void contents. The averaged mastercurves are plotted in Figure 3-3 and Figure 3-4 for the two mixes, respectively.

For the I19.0C mix (Figure 3-4), it is noticed that the dynamic modulus value decreases as the air void content increases, since the specimen becomes softer at high air voids. The data for the 8% and 8.45% mastercurves are similar to each other since there is only a small difference in air voids. The same general trend of the dynamic modulus decreasing as the air void content increases is found in Figure 3-3 for the S9.5C mix, except that the 8.6 and 9.65% air void mastercurves are reversed in position.

Mastercurves from unconfined complex modulus testing are plotted in Figure 3-5 and Figure 3-6 for the S9.5C and I19.0C mixes, respectively. The effect of air void content is not clear in Figure 3-5 for the S9.5C mix due to the relatively small difference in air void contents, but it is evident in Figure 3-6 for the I19.0C mix with widespread air void contents.

The following is the sigmoidal function which was used in fitting each mastercurve:

$$\log|E^*| = a + \frac{b}{1 + \frac{1}{\exp^{d+e(\log f_R)}}} \qquad (3\text{-}1)$$

where

$|E^*|$ = dynamic modulus in MPa,
a, b, d, e = regression coefficients,
f_R = reduced frequency in Hz (= $f \times a_T$),
f = frequency, and
a_T = shift factor.

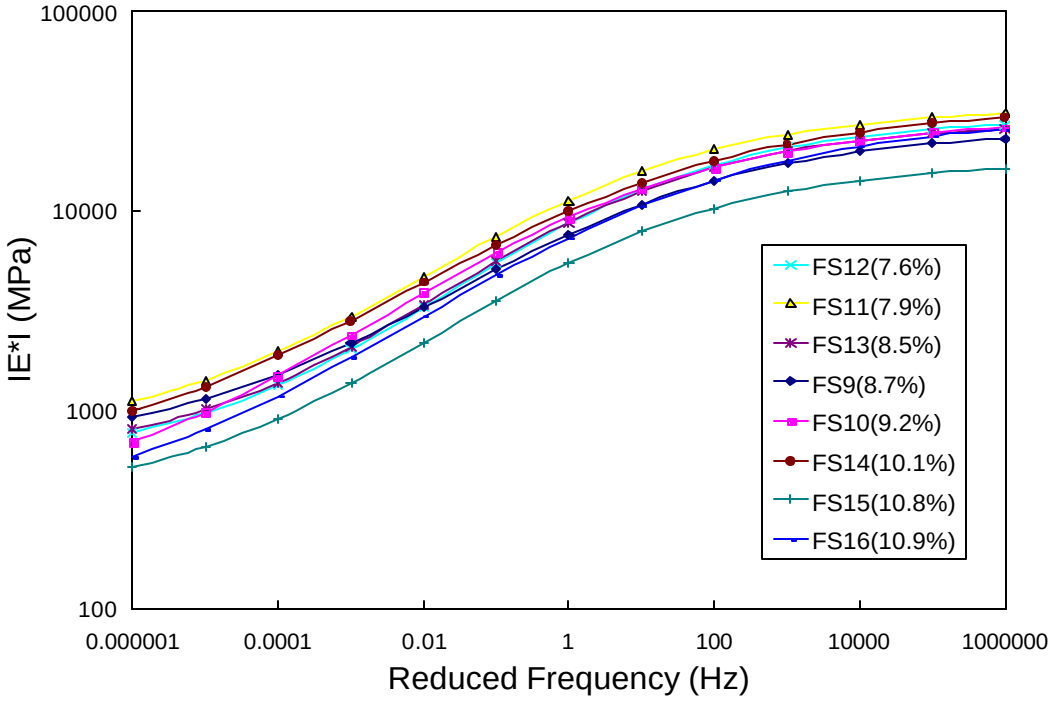

Figure 3-1. Effect of air void content on dynamic modulus with 20 psi confining pressure (S9.5C)

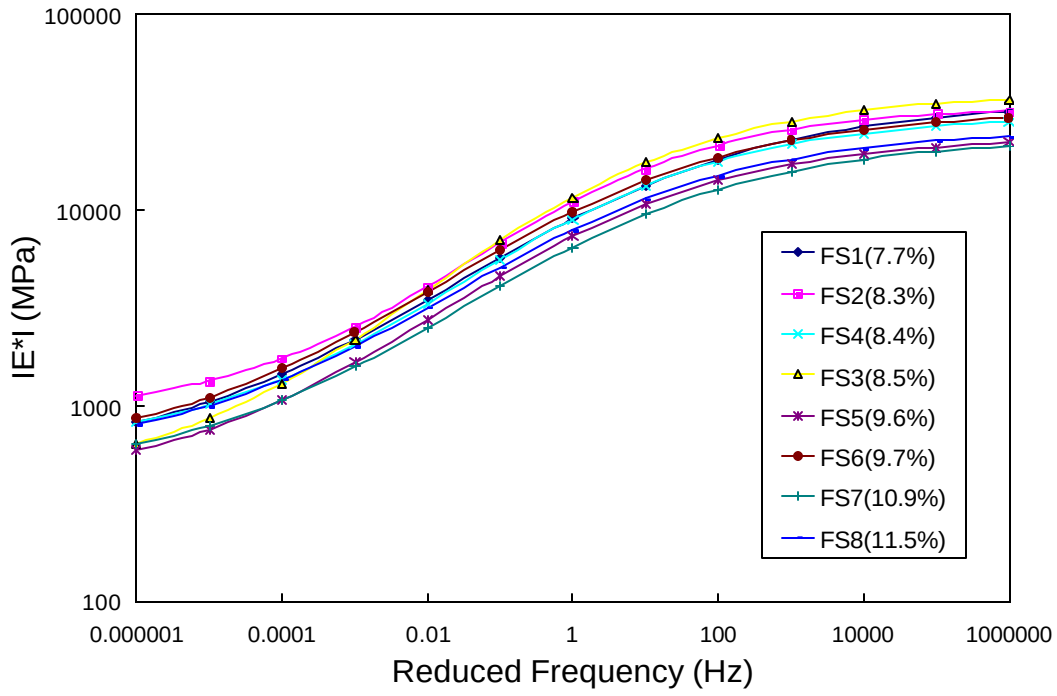

Figure 3-2. Effect of air void content on dynamic modulus with 20 psi confining pressure (I19.0C)

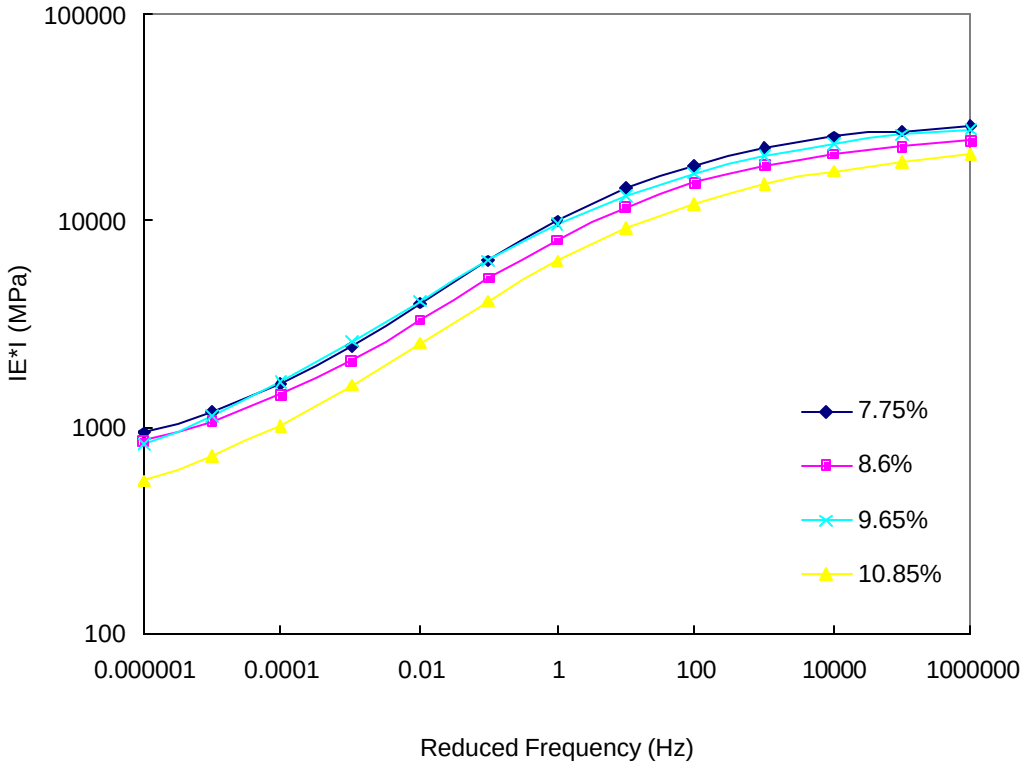

Figure 3-3. Averaged mastercurves for S9.5C mix with 20 psi confining pressure

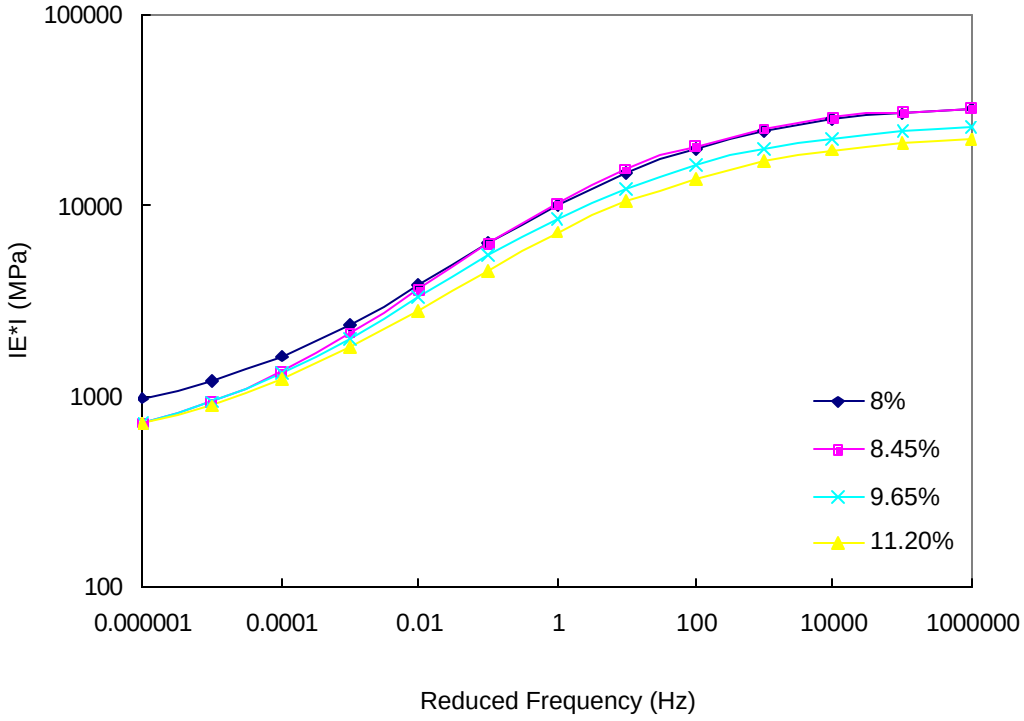

Figure 3-4. Averaged mastercurves for I19.0C mix with 20 psi confining pressure

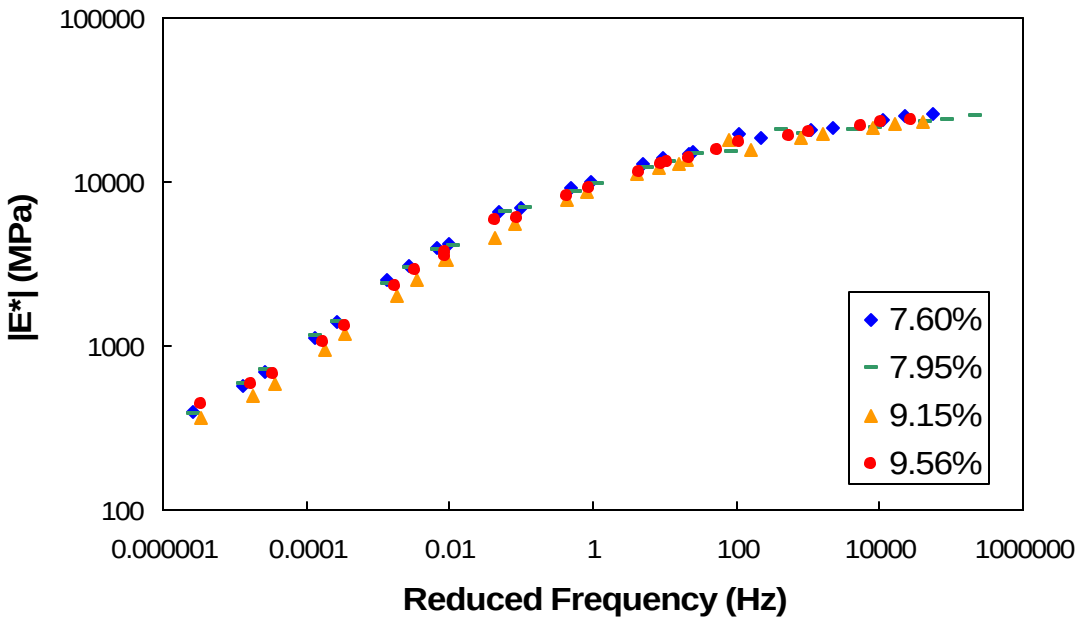

Figure 3-5. Averaged mastercurves for S9.5C mix without confining pressure

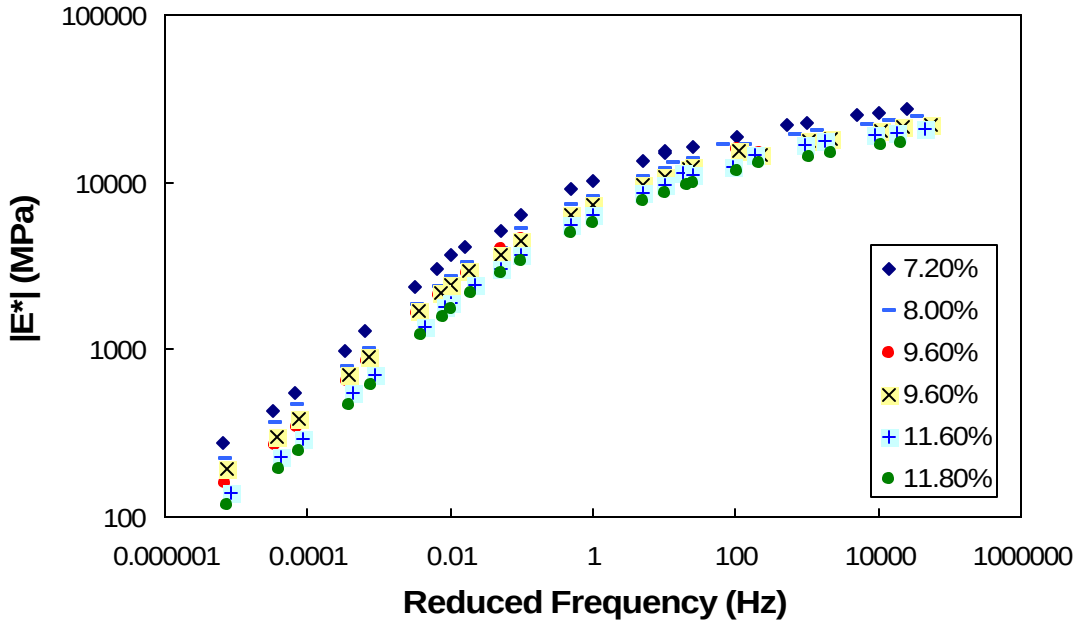

Figure 3-6. Averaged mastercurves for I19.0C mix without confining pressure

For each mixture, the coefficients *a*, *b*, *d*, and *e* in Eq. (3-1) were plotted against the air void content. It was found that a linear relationship exists between each of these coefficients and the air void content. This relationship is expressed as follows:

$$a,b,d,e = r \times (\%AV) + k \qquad (3\text{-}2)$$

where *%AV* is the air void content, and *?* and *?* are regression constants. The values of *?* and *?* for the two mixes are summarized in Table 3-1 for the unconfined dynamic modulus.

Table 3-1. Regression coefficients for |*E| sigmoidal function**

Coefficients of Sigmoidal Function in Eq. (3-2)	Mix Types			
	S9.5C		I19.0C	
	r	*k*	*r*	*k*
a	0.2147	-0.1853	-0.0893	1.9427
b	-0.2368	4.8201	0.0580	2.7716
d	-0.1428	2.8738	-0.0091	1.7504
e	0.0298	0.1723	0.0005	0.4452

When shift factors were plotted against temperature for all the air void contents (Figure 3-7 and Figure 3-8), it was found that the shift factor versus temperature relationship can be represented by a quadratic function, Eq. (3-3). Also, no trend was seen in shift factor as a function of air void content, and the shift factor versus temperature curves are essentially the same for the different air void contents.

$$a_T = aT^2 + bT + g \qquad (3\text{-}3)$$

where *T* is the temperature, and *a*, *ß*, and *?* are regression coefficients. The shift factor versus temperature relationship of a 9.6% air void content was selected as the representative, and its coefficients are presented in Table 3-2.

Eqs. (3-1) and (3-2) are combined to express the dynamic modulus as a function of frequency, temperature, and air void content, as follows:

$$\log|E^*| = a(\%AV) + \frac{b(\%AV)}{1 + \frac{1}{\exp^{d(\%AV) + e(\%AV)\log[f \square a_T(T)]}}} \qquad (3\text{-}4)$$

where the parenthesis means that the variable in front of the parenthesis is a function of the variable inside the parenthesis.

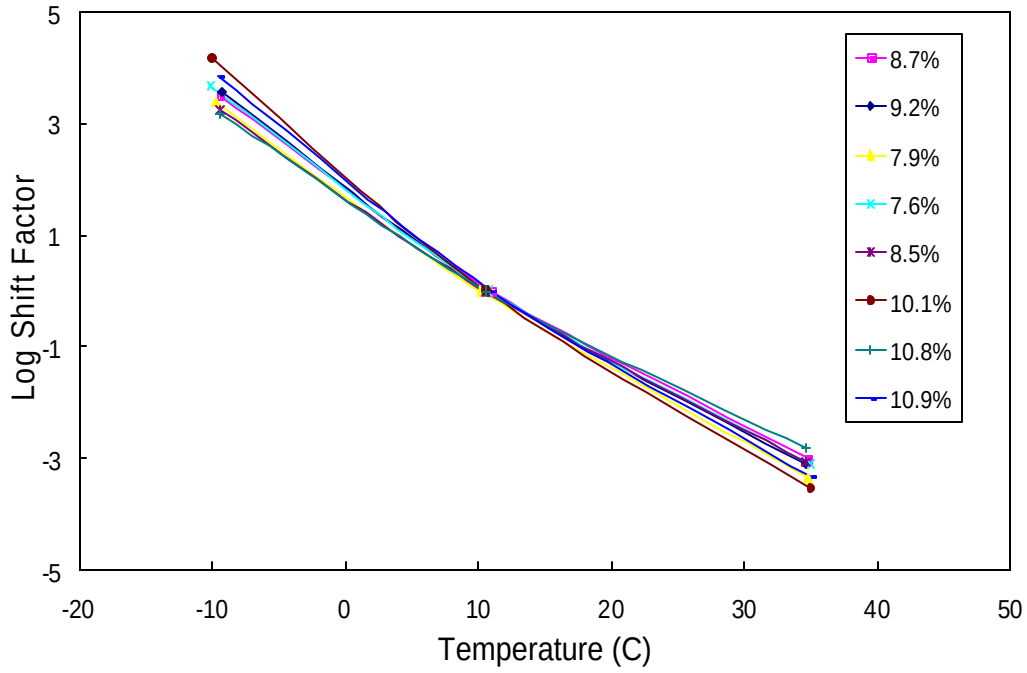

Figure 3-7. Shift factor versus temperature (S9.5C)

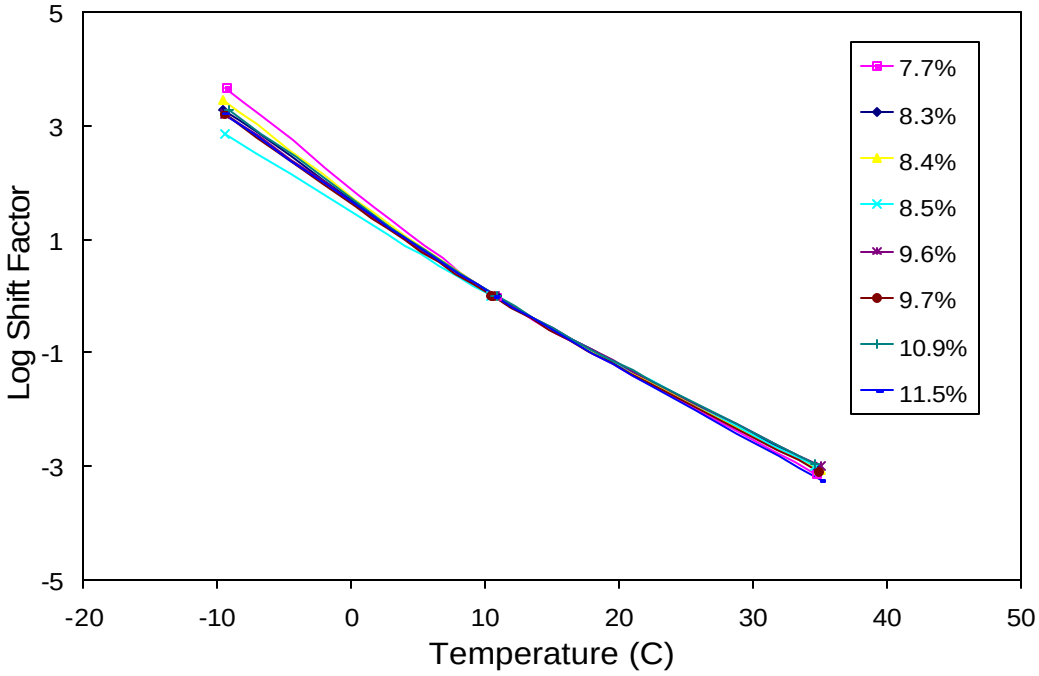

Figure 3-8. Shift factor versus temperature (I19.0C)

Table 3-2. Regression coefficients for the shift factor versus temperature relationship

Coefficients in Eq. (3-3)	Mix Type	
	S9.5C	I19.0C
a	6.56E-4	8.61E-4
b	-0.169	-0.165
g	1.626	1.546

Eq. (3-4) allows the determination of the dynamic modulus as a function of the air void content of the mix and the location of the mix in the pavement structure. If the location (i.e., depth) of a mixture in the pavement structure is known, the temperature and loading frequency in that location can be determined using predictive models. Knowing the air void content, temperature, and loading frequency, one can determine the dynamic modulus of the mixture at that location using Eq. (3-4).

Effect of Confining Pressure on $|E^*|$

The dynamic moduli of the mixtures determined from unconfined and confined axial compression tests are compared in this section. The comparison for the S9.5C mix is presented in Figure 3-9 and Figure 3-10.

Figure 3-9 displays the dynamic moduli of the S9.5C mixture as determined from uniaxial and triaxial tests in a semi-log scale. Although the effect of confinement seems to be insignificant in this figure, further analysis is necessary because the normal scale used in this figure for the dynamic modulus axis suppresses the information at the lower reduced frequencies. Therefore, the same data were plotted in a log-log scale in Figure 3-10. The effect of confinement is found to be significant at low reduced frequencies (i.e., a high temperature and/or low loading frequency).

This observation is also supported by Figure 3-11 where the uniaxial and triaxial dynamic moduli of the S9.5C mixture at low, medium, and high reduced frequencies are presented for various air void contents. The dynamic modulus versus air void content relationships are essentially the same between the uniaxial and triaxial data for 10,000 and 1 Hz, whereas at 0.0005 Hz the uniaxial dynamic moduli are smaller than the triaxial ones. This finding is somewhat expected because, as the temperature increases or loading frequency decreases, the asphalt binder becomes softer, and the effect of confinement on the aggregate structure becomes more significant. The confinement makes the asphalt-aggregate mixture more resistant to stress in these conditions and, thus, the triaxial test yields a greater dynamic modulus than the uniaxial test.

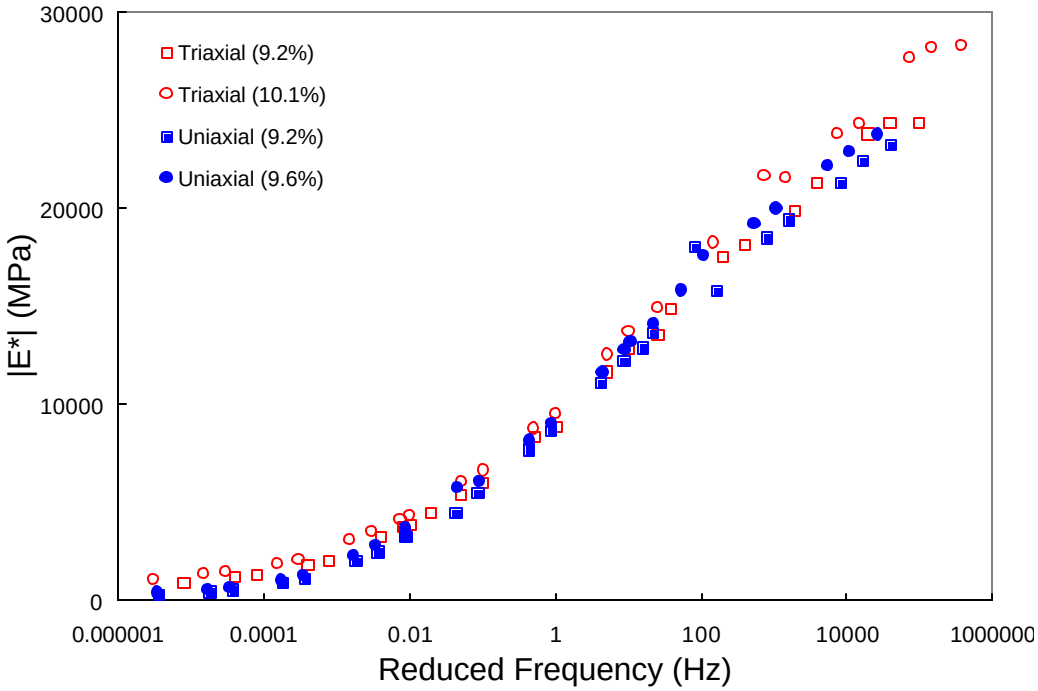

Figure 3-9. l*El Comparison between triaxial and uniaxial tests in semi-log scale (S9.5C)**

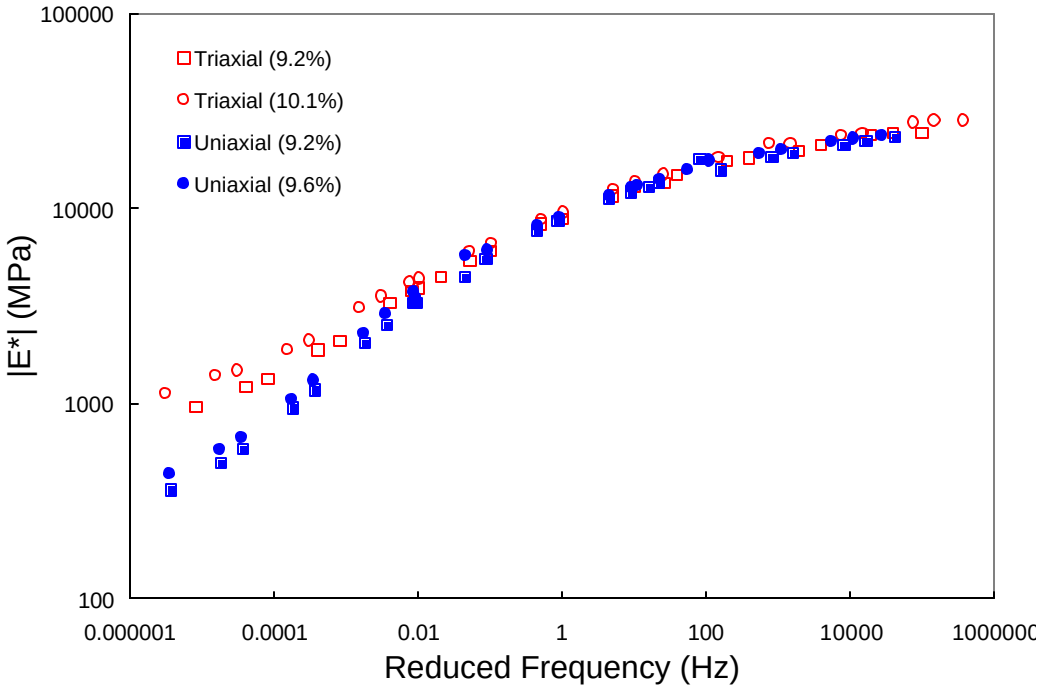

Figure 3-10. |*E| comparison between triaxial and uniaxial tests in log-log scale (S9.5C)**

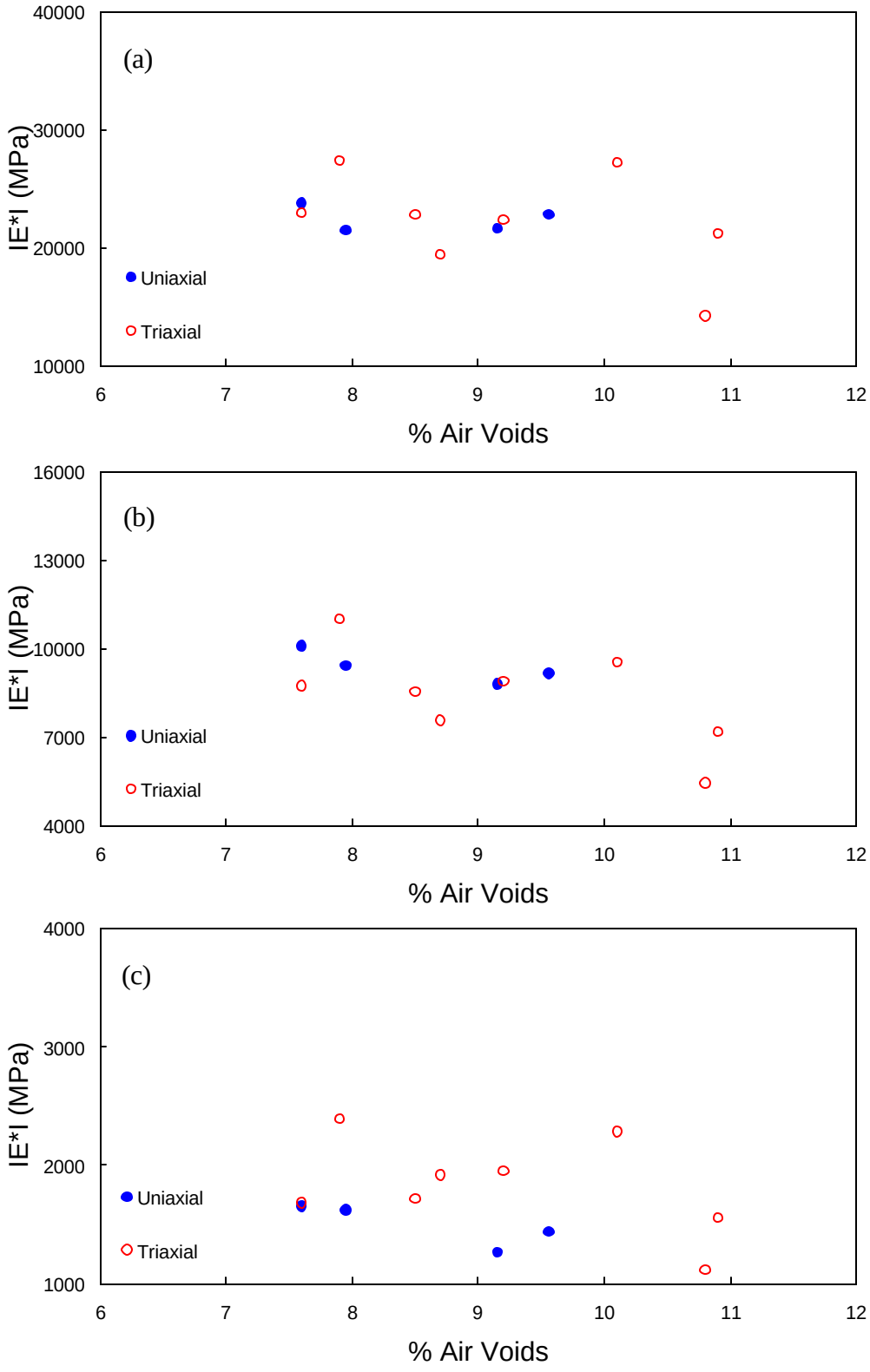

Figure 3-11. l*El versus air void content at: (a) 10,000 Hz; (b) 1 Hz; (c) 0.0005 Hz (S9.5C)**

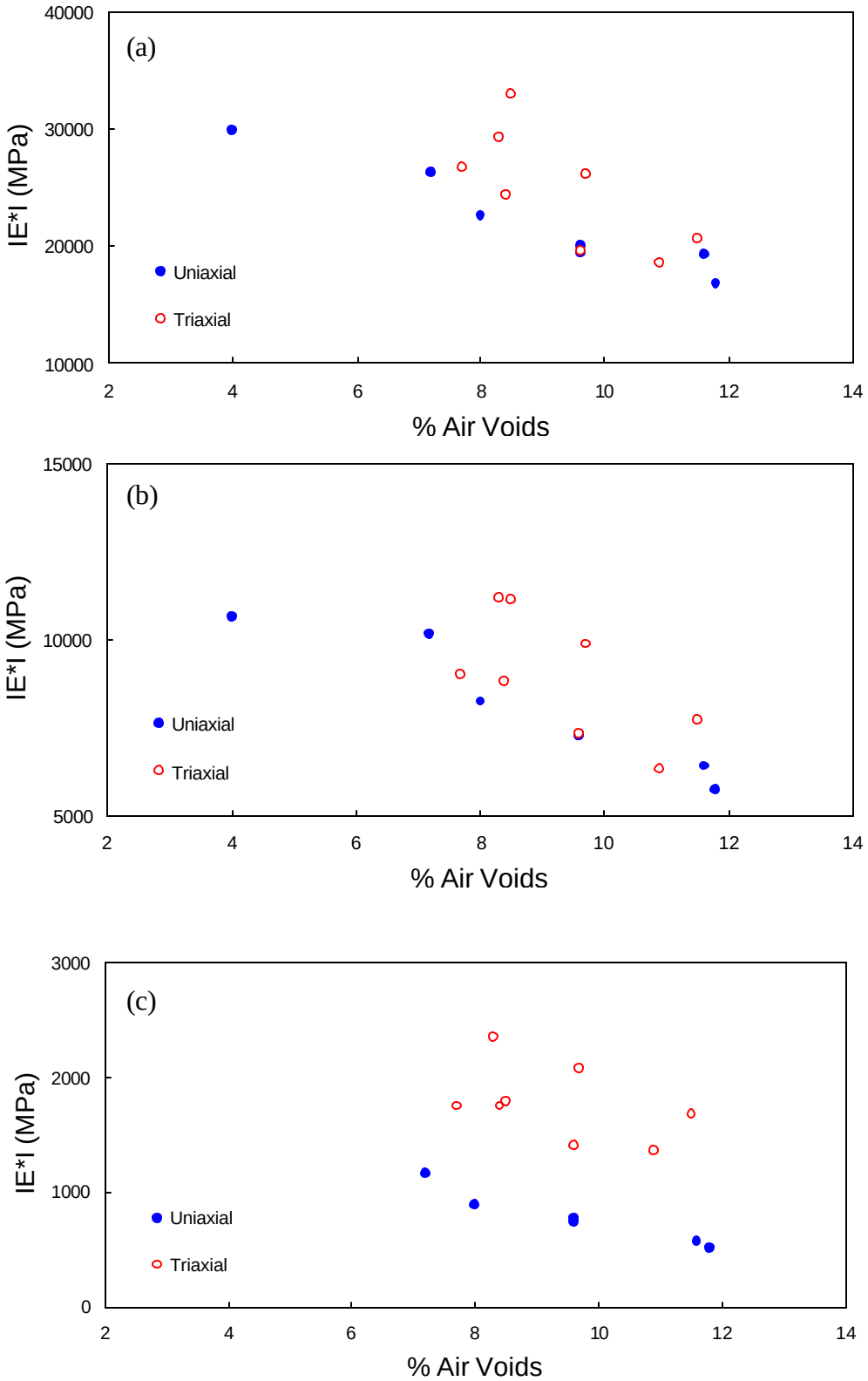

Figure 3-12. l*El versus air void content at: (a) 10,000 Hz; (b) 1 Hz; (c) 0.0005 Hz (I19.0C)**

The dynamic moduli of the I19.0C mixture at the three reduced frequencies are plotted in Figure 3-12. Different from Figure 3-11 for the S9.5C mixture, the triaxial dynamic moduli are, in general, larger than those determined from the uniaxial test. The difference is much greater at 0.0005 Hz. This observation is different from the one made from the S9.5C data. It is probably due to the fact that the I19.0C mix has larger aggregate particles and, therefore, the effect of confinement becomes greater. The reduction in the dynamic modulus as the %AV increases is greater (i.e., the slope is steeper) in the triaxial data than in the uniaxial data.

3.2 Fatigue Life Prediction Model

IDT fatigue test results were analyzed to determine the horizontal strain at the center of the specimen (et) and the number of cycles to failure (Nf). Typical data from the IDT fatigue testing are shown in Figure 3-13. In general, the horizontal strain increases more quickly as the air void content increases, although this trend is often violated due to the large variability in the fatigue test results. The number of cycles to failure was determined using the bisection method illustrated in Figure 2-5.

Table 3-3 and Table 3-4 summarize the N_f values for various air void contents of the S9.5C and I19.0C mixes, respectively. The same data are plotted in Figure 3-14 and Figure 3-15 to display the effect of air void content on the fatigue life of the two mixes more effectively. Although the data are more scattered due to testing and sample-to-sample variability, the reduction of fatigue life due to an increased air void content is clearly seen in these figures.

A traditional way of presenting the fatigue data is to plot the tensile strain (e_t) against the number of cycles to failure (N_f). All the fatigue test results are plotted in this manner in Figure 3-16 and Figure 3-17 for the S9.5C and I19.0C mixes. In general, it can be observed that the effect of air void content is not significant on the fatigue relationship, except for the I19.0C mix at 20°C (Figure 3-17(a)) in which a slight air void dependence can be found. In order to demonstrate the effect of temperature, the same data in Figure 3-16 and Figure 3-17 are plotted in Figure 3-18 without differentiating among the different air void contents. For both the S9.5C and I19.0C mixes, the effect of temperature was found to be significant; that is, the higher temperature, the steeper the slope of the fatigue relationship.

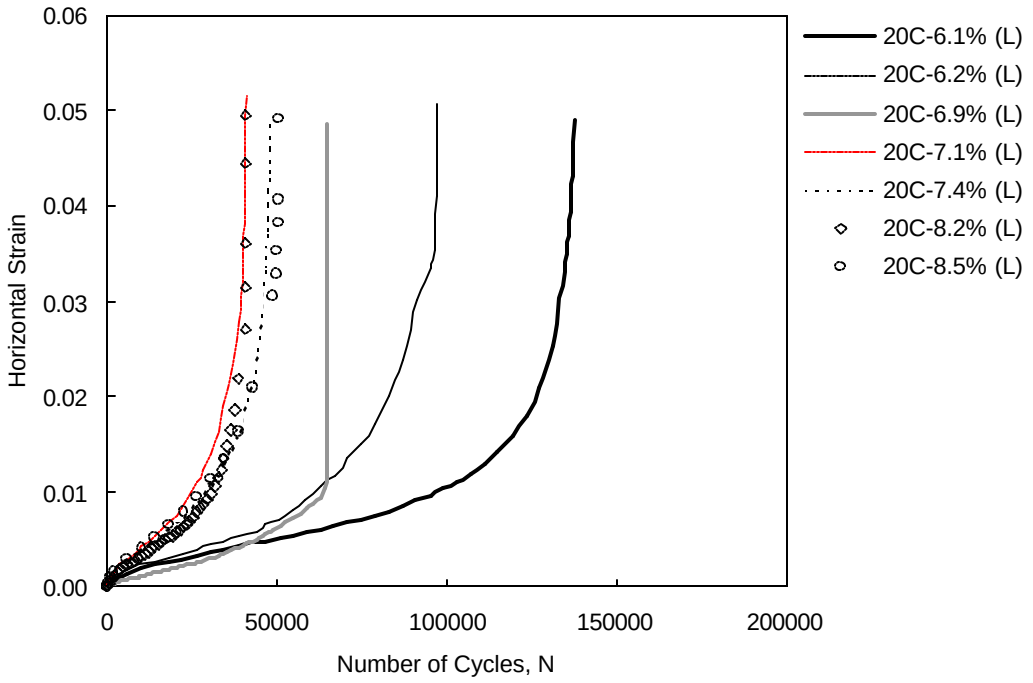

Figure 3-13. Horizontal strain growth as a function of air void content observed from the IDT fatigue testing of I19.0C at 20°C

Table 3-3. Number of cycles to failure as a function of air void content (S9.5C)

Load Level	20°C		10°C	
	%AV	N_f	%AV	N_f
High	5.9	6,170	6.0	23,200
	6.2	2,440	-	-
	7.1	1,690	7.1	10,610
	7.2	1,635	7.2	9,880
	8.1	1,460	-	-
	8.2	1,380	8.0	3,730
Medium	6.1	9,400	-	-
	6.2	22,400	6.1	44,300
	7.0	12,500	7.0	28,450
	7.4	14,450	7.1	22,125
	7.9	12,010	7.8	16,230
	8.0	6,560	8.4	20,500
Low	6.0	194,500	6.0	146,270
	6.1	330,000	-	-
	7.1	75,900	7.0	80,000
	7.3	71,900	7.1	83,250
	7.8	29,450	-	-
	8.0	56,000	8.0	65,250

Table 3-4. Number of cycles to failure as a function of air void content (I19.0C)

Load Level	20°C		10°C		1.5°C	
	%AV	N_f	%AV	N_f	%AV	N_f
High	5.7	4,250	6.1	94,000	5.5	7,469
	6.0	9,700	-	-	6.1	7,514
	6.7	3,320	6.8	68,384	6.7	4,180
	7.3	1,850	6.9	95,130	6.8	5,269
	8.0	2,110	8.0	17,412	7.8	1,252
	8.4	2,100	-	-	8.3	2,091
Medium	6.0	21,700	6.3	27,000	6.0	100,800
	6.2	25,250	-	-	-	-
	6.5	9,250	6.6	19,883	6.8	32,000
	6.8	17,500	7.1	14,650	6.9	59,176
	7.6	6,882	-	-	-	-
	7.9	17,416	7.9	6,682	7.6	22,501
	8.1	3,650	8.1	11,950	7.6	10,409
Low	6.1	122,000	6.1	278,000	5.9	125,310
	6.2	81,000	6.5	247,429	6.3	145,000
	7.1	35,200	6.7	132,800	7.2	54,000
	7.4	41,800	-	-	7.2	65,045
	8.2	36,700	7.5	89,200	7.8	27,988
	8.5	44,900	7.9	76,083	-	-

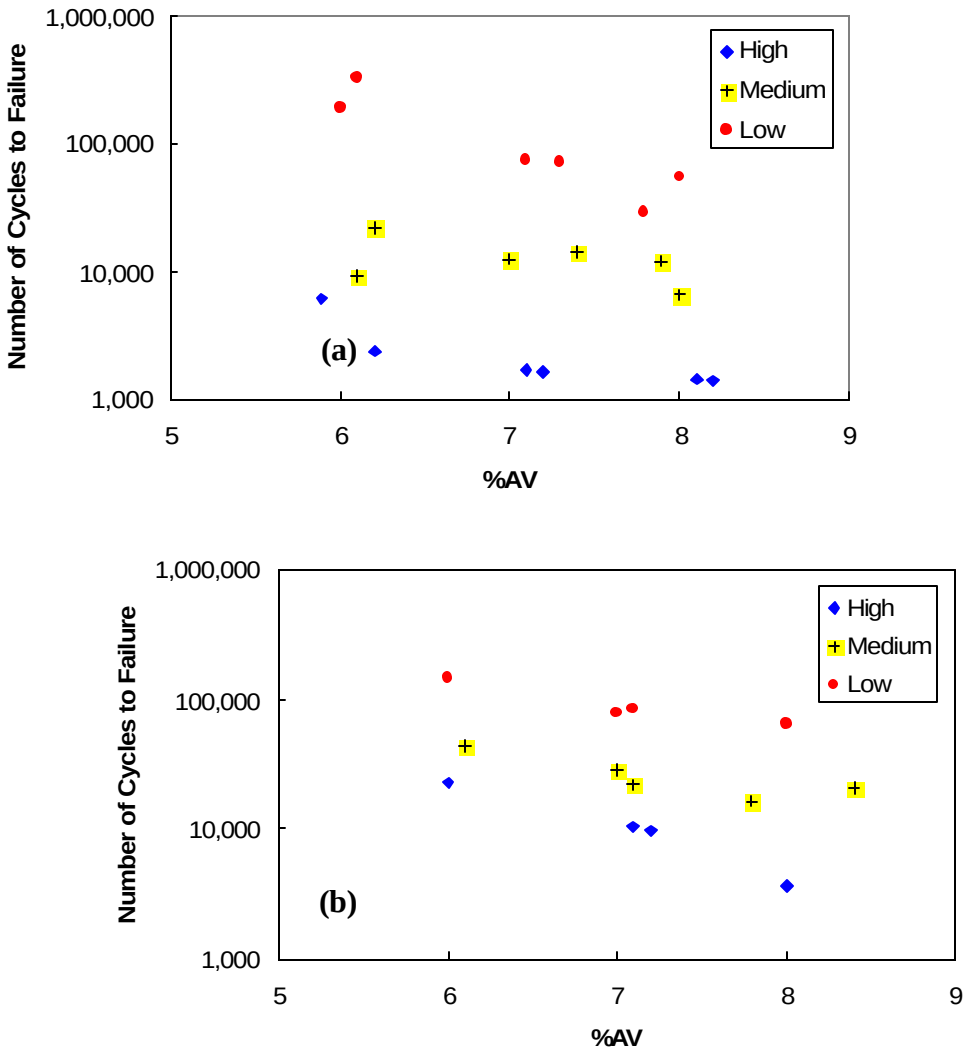

Figure 3-14. Reduction of fatigue life as a function of air void content for S9.5C mix: (a) 20°C; (b) 10°C

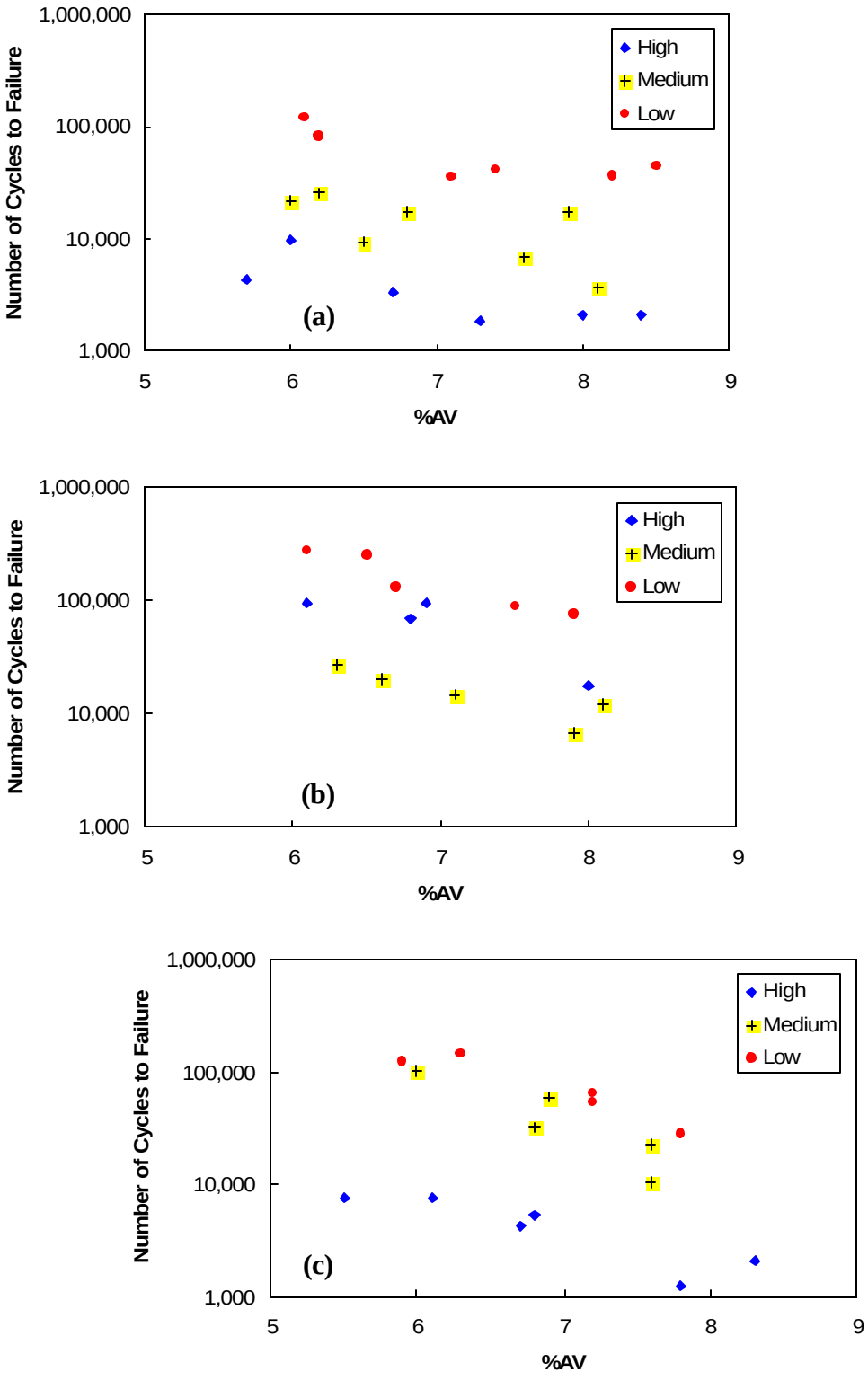

Figure 3-15. Reduction of fatigue life as a function of air void content for I19.0Cmix: (a) 20°C; (b) 10°C; (c) 1.5°C

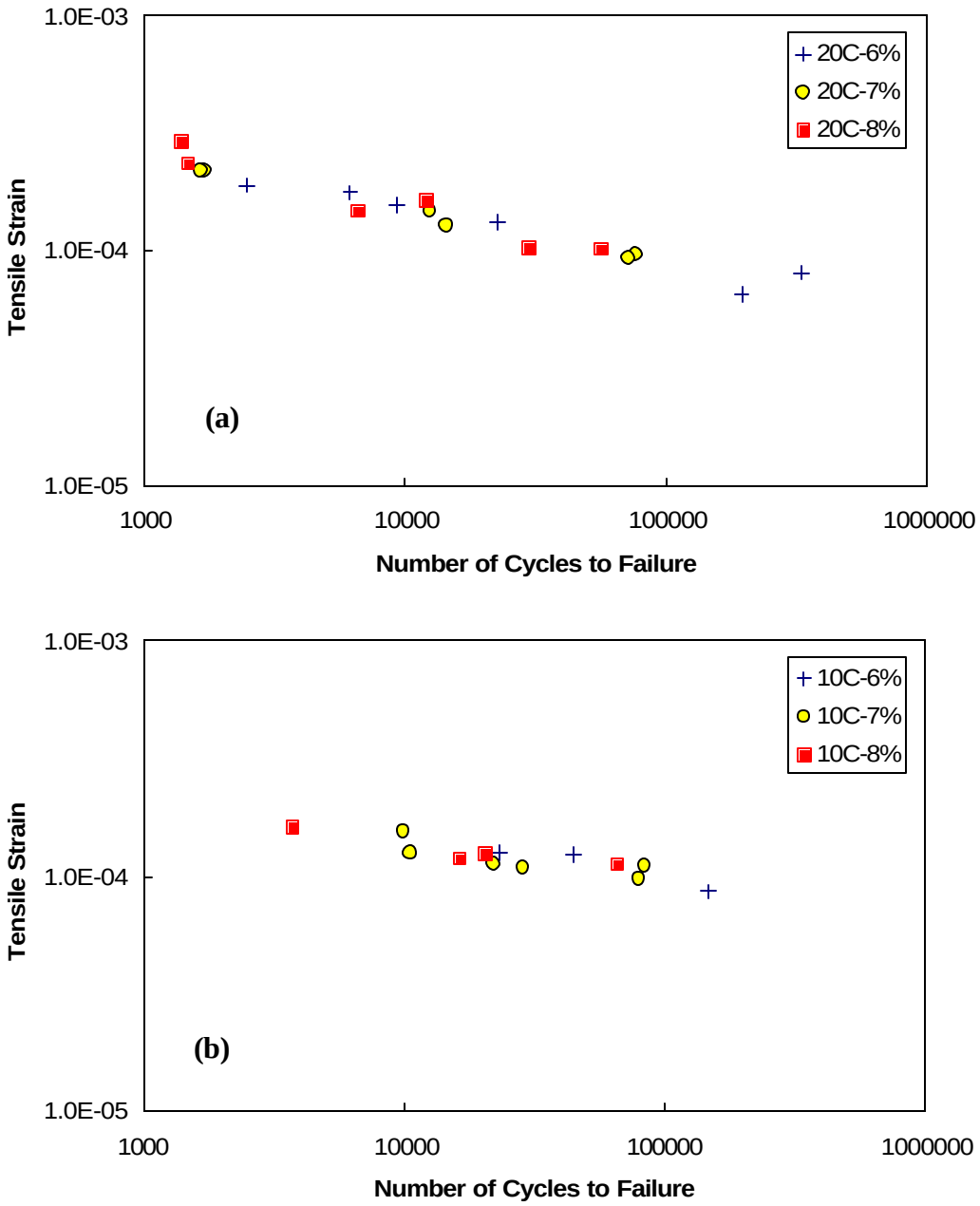

Figure 3-16. Comparison of fatigue cracking performance of S9.5C mix for different air void contents: (a) 20°C; (b) 10°C

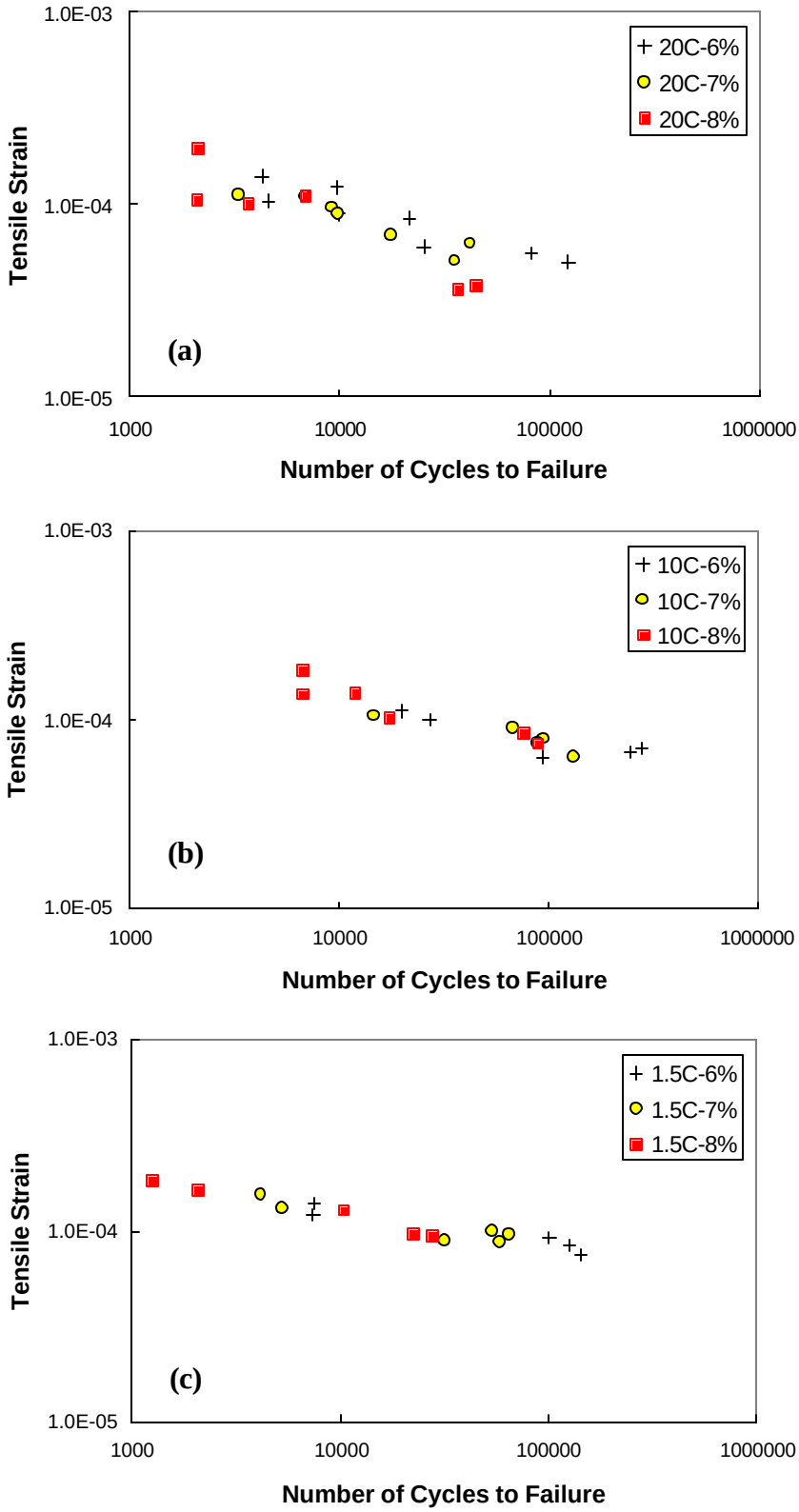

Figure 3-17. Comparison of fatigue cracking performance of I19.0C mix for different air void contents: (a) 20°C; (b) 10°C; (c) 1.5°C

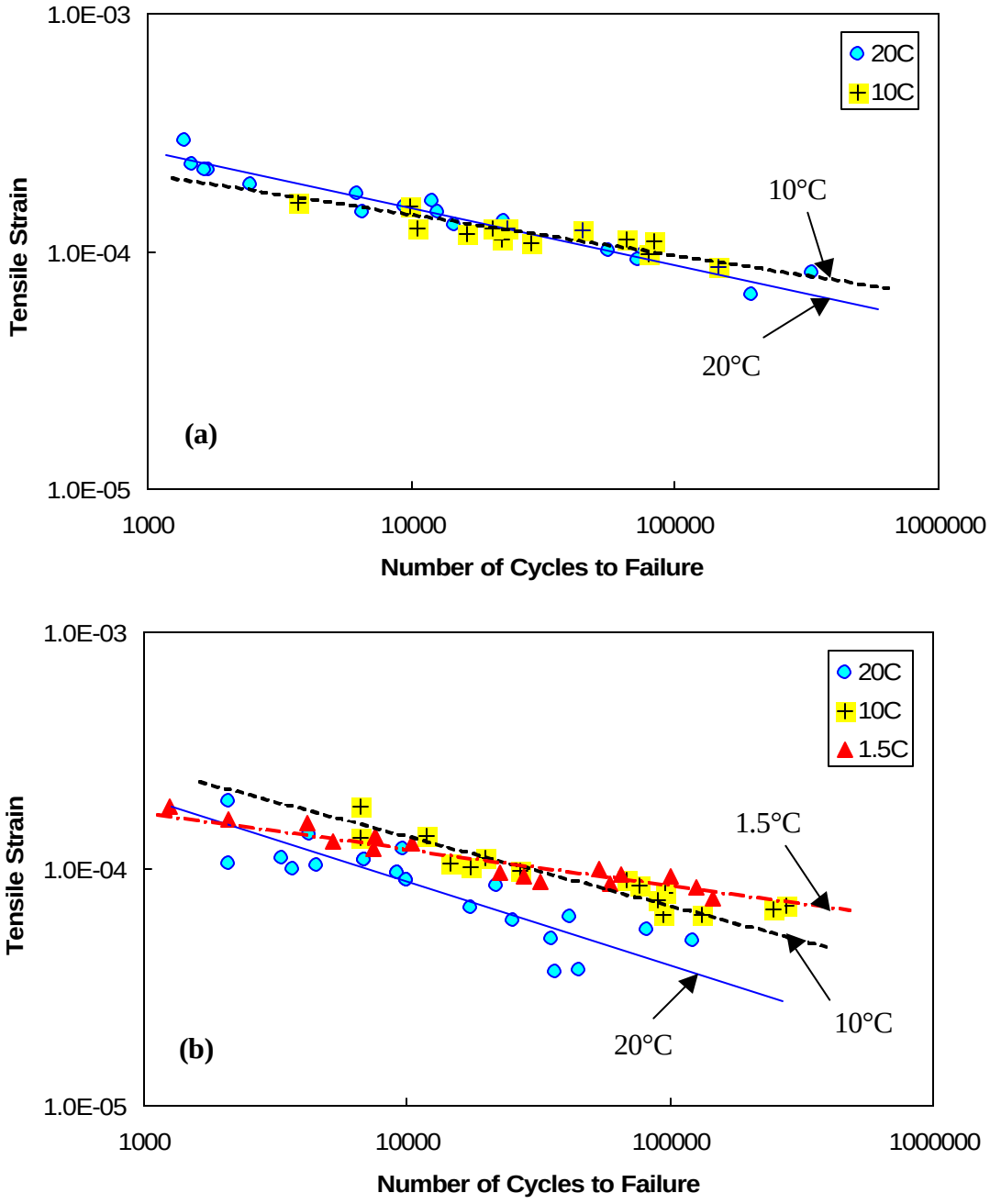

Figure 3-18. Effect of temperature on the fatigue performance: (a) S9.5C; (b) I19.0C

In this study, the phenomenological fatigue equation developed by the Asphalt Institute (1982) has been adopted to represent the fatigue behavior of asphalt concrete observed from the IDT fatigue testing. The AI fatigue equation is expressed as follows:

$$N_f = 14.72 \cdot C \cdot f_1 (e_t)^{-f_2} |E^*|^{-f_3} \quad (3\text{-}5)$$

where N_f = number of cycles to failure (i.e., fatigue service life);
14.72 = the laboratory-to-field shift factor for thin-layered pavement;
C = the correction factor based on mixture volumetrics;
e_t = tensile strain at the bottom of the asphalt layer;
$|E^*|$ = the dynamic modulus of the asphalt layer; and
f_1, f_2, f_3 = regression constants (2.9347E-4, 3.291, and 0.854, respectively).

The correction factor, C, shown below, is necessary to account for the difference in mixture properties between the mixture in question and the mixtures used in developing the AI equation:

$$C = 10^M \quad (3\text{-}6)$$

where

$$M = 4.84\left(\frac{V_b}{V_a + V_b} - 0.69\right) \quad (3\text{-}7)$$

and V_a and V_b represent the volume of the air void and asphalt binder, respectively.

It needs to be noted that the fatigue model in Eq. (3-5) has been developed based on a large database obtained from beam fatigue testing. Since the number of cycles to failure and tensile strain are measured from the IDT testing in this study, it is necessary to adjust Eq. (3-5) according to the following approach.

First, the mixture volumetrics for the IDT specimens and the fatigue data from the IDT testing were used to determine the coefficients for the following equation:

$$N_{f,IDT} = C' f_4 (e_{t,IDT})^{-f_5} |E^*|^{-f_6} \quad (3\text{-}8)$$

where $N_{f,IDT}$ = the number of cycles to failure measured from the IDT testing;
$e_{t,IDT}$ = tensile strain measured from the IDT testing;
$C' = 10^{m\left(\frac{V_b}{V_a + V_b} - n\right)}$; and
f_4, f_5, f_6 = regression constants.

Figure 3-17 shows the relationship between the number of cycles to failure and tensile strain found from the IDT testing for different temperatures and air void contents. The

nonlinear genetic algorithm program, Evolver 4.0, was used to determine the values of the regression constants in Eq. (3-8) using the data shown in Figure 3-17. It was found that f_4, f_5, and f_6 were relatively constant for different air void contents. The values of the regression constants are:

m = 3.3694, n = 0.9985, f_4 = 0.00432, f_5 = 3.291, f_6 = 0.854.

To convert the $N_{f,IDT}$ to N_f from the AI model in Eq. (3-5), the mixture volumetrics and IDT fatigue data were input to Eq. (3-5) without the laboratory-to-field shift factor. The modification factor, MF_{IDT}, was determined by calculating the ratio between the N_f from the AI model and N_f from Eq. (3-8).

It was found that the average value of MF_{IDT} under different conditions is 0.3383. The following equations can be used to describe the modeling approach:

$$\begin{aligned} N_f(field) &= 14.72 N_f(AI, Lab) \\ &= 14.72 MF_{IDT} N_f(IDT) \\ &= 14.72 MF_{IDT} C' f_4 (e_{tIDT})^{-k_5} |E^*|^{-k_6} \\ &= 14.72 MF_{IDT} 10^{m(\frac{V_a}{V_a+V_b}-n)} f_4 (e_{tIDT})^{-k_5} |E^*|^{-k_6} \end{aligned} \quad (3\text{-}9)$$

where MF_{IDT} = 0.3383, m =3.3694, n = 0.9985, f_4 = 0.00432, f_5 = 3.291, f_6 = 0.854.

The effect of air voids is reflected in Eq. (3-9) by three different parameters. First, $|E^*|$ in Eq. (3-9) was determined from Eq. (3-4) in which the air void content is one of the input parameters. The volume of air voids is used in Eq. (3-9) which, in turn, determines the *C'* value in Eq. (3-8). Finally, the tensile strain at the bottom of the asphalt layer (e_t) in Eq. (3-9) was determined from the layered elastic analysis using the dynamic modulus of the asphalt layer determined for the given air void content.

3.3 Permanent Deformation Model

In this study, the TRLPD test data were used to develop a relationship between permanent strain and testing and mixture variables. Figure 3-19 shows the typical relationship between the total cumulative plastic strain and the number of load cycles in normal and log-log scales. In Figure 3-19, three zones are defined along the cumulative permanent strain curve: primary, secondary, and tertiary. In the primary zone, permanent deformations accumulate rapidly. In the secondary zone, the incremental permanent deformations decrease, reaching a constant value. Finally, the incremental permanent deformations again increase, and permanent deformations accumulate rapidly in the tertiary zone. The cycle number at which tertiary flow starts is referred to as the *Flow Number*. It is important to note that well-performing mixes stay in the secondary zone and do not show any tertiary flow in normal loading conditions under standard axle loads (Kaloush and Witczak 2002).

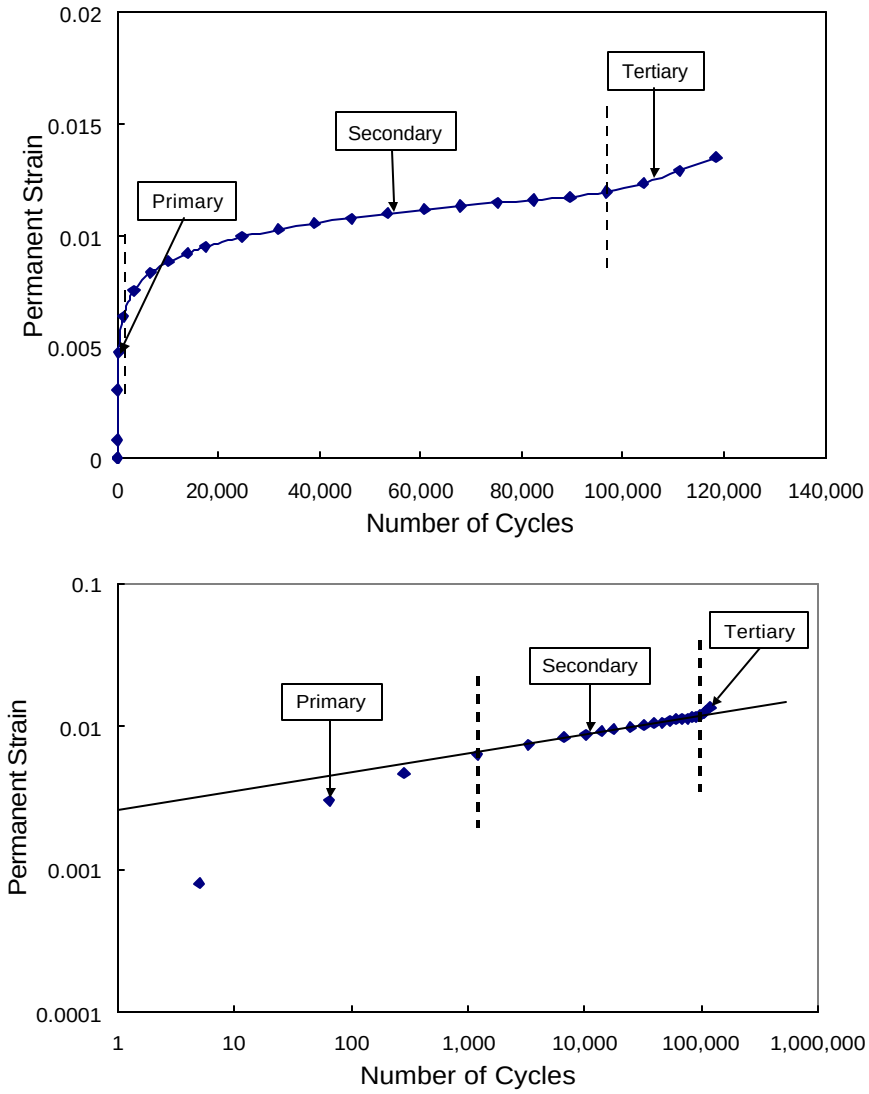

Figure 3-19. Typical relationship between permanent strain and number of load cycles: (a) normal scale; (b) log-log scale

In this research, only the secondary zone, in which the permanent strain versus the number of loading cycles relationship in a log-log scale shows a linear trend, was used to represent the permanent strain response of a mix. This portion can be expressed by the following classical power model:

$$e_p = aN^b \tag{3-10}$$

where "*a*" and "*b*" are regression constants. The intercept "*a*" represents the permanent strain at $N = 1$. The slope "*b*" represents the rate of change in log (e_p) as a function of the change in log (N). An alternative form of the mathematical model used to characterize the plastic strain per load repetition (e_{pn}) relationship can be expressed by:

$$\frac{\partial e_p}{\partial N} = e_{pn} = \frac{\partial (aN^b)}{\partial N} \tag{3-11}$$

or

$$e_{pn} = abN^{(b-1)} . \tag{3-12}$$

The resilient strain (e_r) is assumed to be independent of the load repetition value (N). As a result, the ratio of plastic to resilient strain components of the material can be defined by:

$$\frac{e_{pn}}{e_r} = (\frac{ab}{e_r})N^{b-1} . \tag{3-13}$$

Letting $m = \frac{ab}{e_r}$ and $a = 1-b$, one obtains:

$$\frac{e_{pn}}{e_r} = mN^{-a} \tag{3-14}$$

where e_{pn} is the permanent strain due to a single load application, i.e., at the N^{th} application. The coefficient, m, is the permanent deformation parameter representing the constant of proportionality between permanent strain and elastic strain. The exponent, a, is a permanent deformation parameter indicating the rate of decrease in incremental permanent deformation as the number of load applications increases.

Eq. (3-14) is further refined to the following permanent strain model in the NCHRP 1-37A MEPDG (AASHTO 2004):

$$\frac{e_p}{e_r} = a_1 T^{a_2} N^{a_3} \tag{3-15}$$

where e_p = accumulated plastic strain at N^{th} repetitions of load;
e_r = resilient strain of the asphalt material as a function of mix properties, temperature, and time rate of loading;
N = the number of load repetitions;
T = temperature; and
a_i = nonlinear regression coefficients.

Eq. (3-15) yields information regarding the relationships among the strain ratio, temperature, and number of loading cycles, but does not account for the effect of air void content. In this section, the TRLPD test data are analyzed to develop a similar relationship that includes the effect of air void content.

TRLPD test data are plotted in Figure 3-20 to Figure 3-25 for both S9.5C and I19.0C mixes at 30°, 40°, and 50°C. The strain values for each test were normalized by the dynamic modulus ratio between the reference and the fingerprint dynamic moduli values, as explained in Section 2.3.2. The dynamic modulus ratio was multiplied by the measured strain values to obtain the normalized strains. For example, if the test specimen is softer than the set of specimens used in the reference dynamic modulus testing, then the actual

dynamic modulus will be lower than the reference value, and the ratio will be less than one. Multiplying the measured strain by this ratio will reduce the strain values. Figure 3-20 to Figure 3-25 display these normalized TRLPD test data.

As expected, the strain increases as the temperature increases. Also, an examination of each graph reveals that the permanent strain increases with an increase in the air voids. In order to demonstrate the effects of temperature and air void content more clearly, the strains at 50,000 cycles are plotted in Figure 3-26 and Figure 3-27 as a function of air void content and temperature. It is clearly shown in this figure that the permanent strain increases as air voids and temperature increase.

The behavior of resilient strain throughout the TRLPD test is plotted in Figure 3-28 and Figure 3-29. The resilient strain remains relatively constant throughout the test, except during the early portion of the test. As expected, the resilient strain increases as the temperature increases. A representative resilient strain value was obtained for each TRLPD test by averaging the recoverable strains taken from different cycles throughout the test. The low resilient strain values that were observed at the beginning of the test were not included in this average. Then, these representative resilient strain values were used to determine the following relationships for the two mixes:

$$e_r = -0.00032974 + 0.0000002511 \times \%AV \times T + 0.0000130856 \times T + 0.0000001867 \times T^2$$
for the S9.5C mix; and
$$e_r = -0.00029209 + 0.0000008889 \times \%AV \times T + 0.0000108804 \times T + 0.0000001122 \times T^2$$
for the I19.0C mix (3-16)

where *%AV* is the air void content in percent, and *T* is the temperature in °C.

In order to find the proper form of the model for the permanent strain behavior seen in Figure 3-26 and Figure 3-27, the strain ratio of permanent strain to resilient strain was plotted against the number of loading cycles (*N*) for the I19.0C mixture. Figure 3-30 shows that the relationship between the strain ratio and *N* at different testing temperatures and air void contents is linear in a log-log scale. Also, it was found that the slope varies as a function of temperature, but is relatively constant among different air void contents for the same temperature. The intercept was found to be a function of both temperature and air void content. These observations suggest the following relationship for the strain ratio:

$$\frac{e_p}{e_r} = N^{f(T)} \cdot g(\%\mathrm{AV}, T) \quad (3\text{-}17)$$

It was found that this relationship also holds true for test data from the S9.5C mixture. The slopes of the linear relationships in Figure 3-30 are plotted against the temperature in Figure 3-31 to determine the form of function *f*. The following expression is used to fit the data in Figure 3-31:

$$f(T) = k_2 \ln(T) + k_3 \quad (3\text{-}18)$$

where ln is natural log and k_2 and k_3 are regression constants.

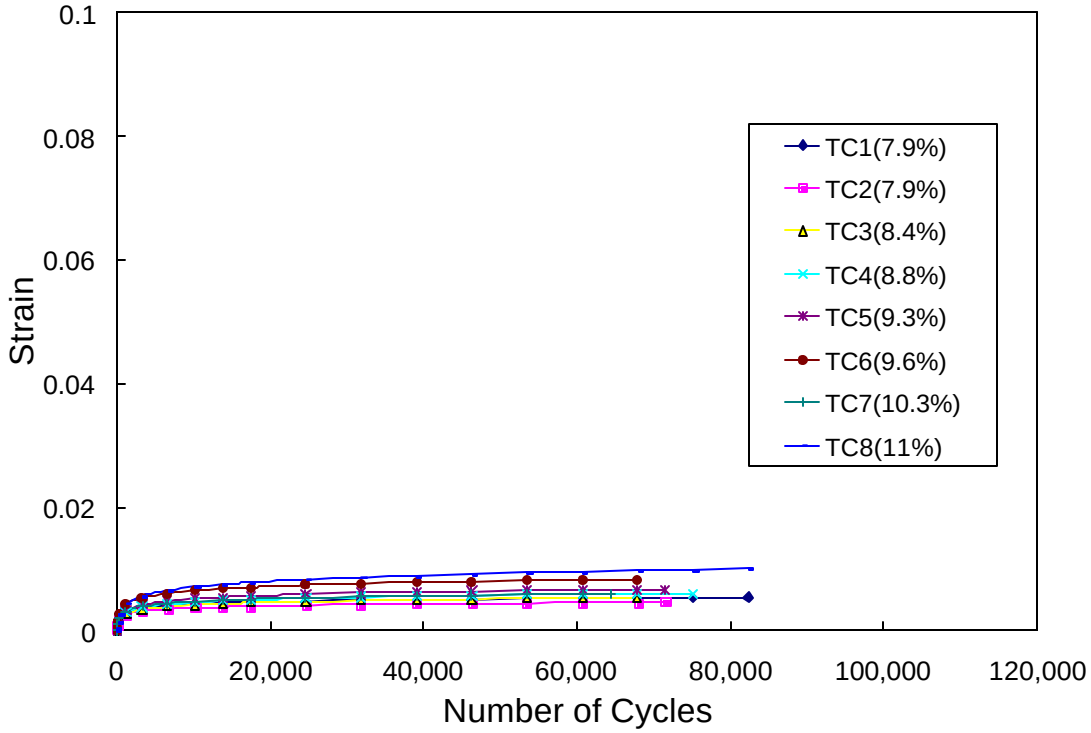

Figure 3-20. TRLPD data at 30°C (S9.5C)

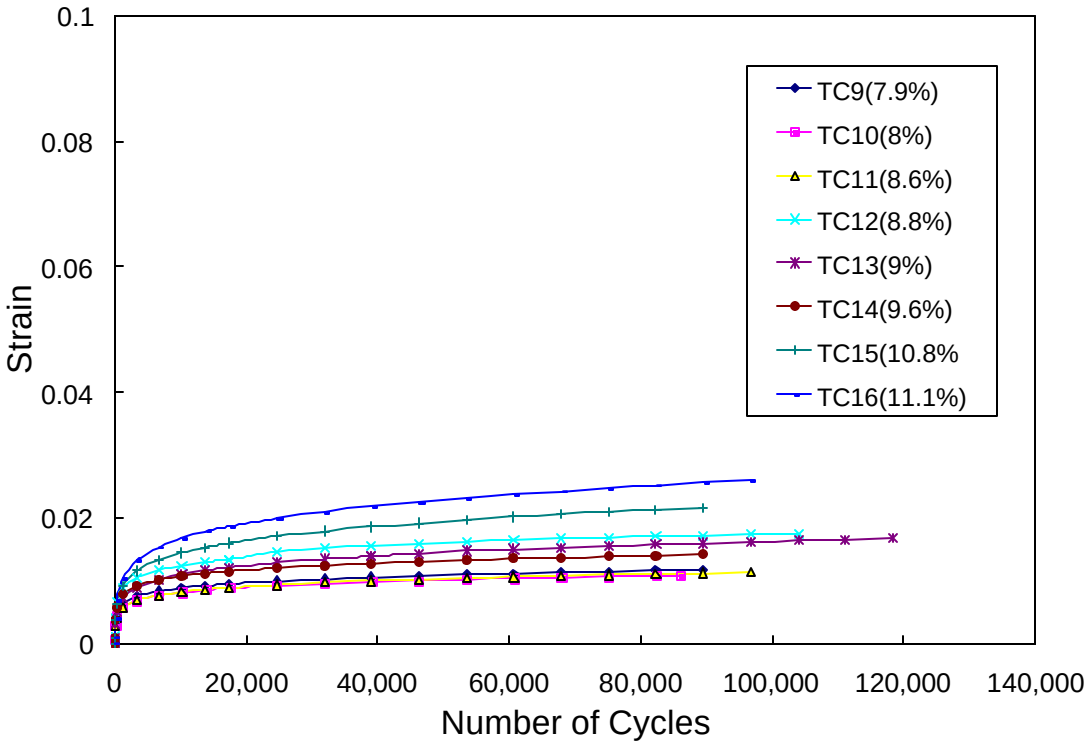

Figure 3-21. TRLPD data at 40°C (S9.5C)

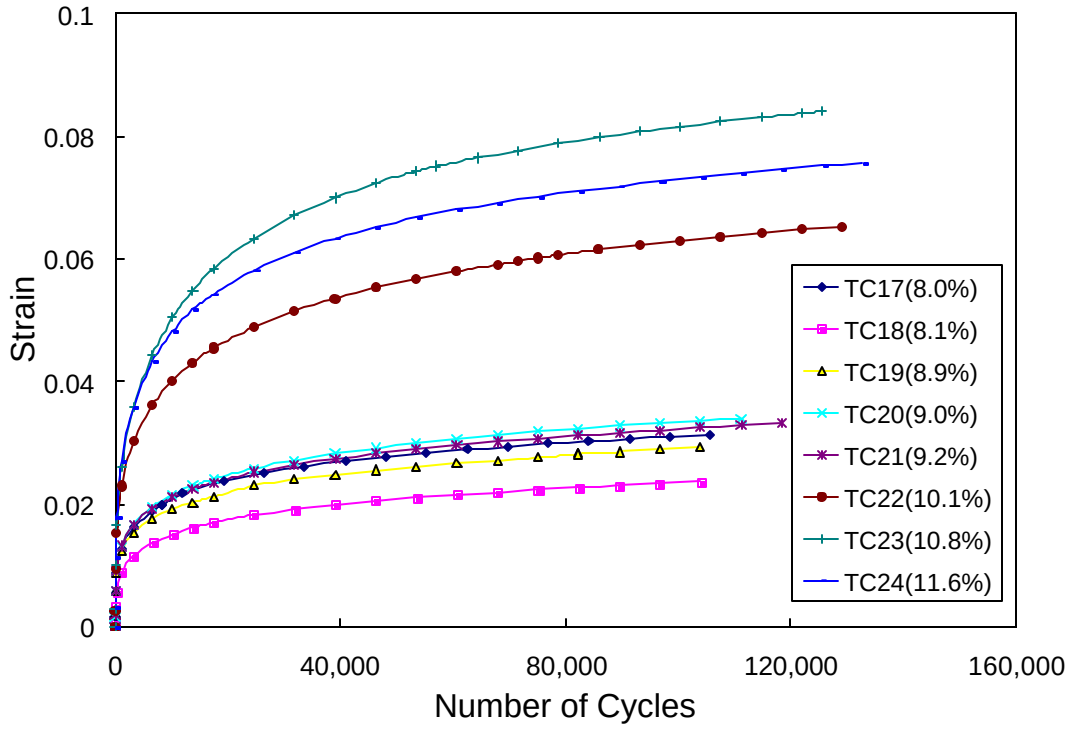

Figure 3-22. TRLPD data at 50°C (S9.5C)

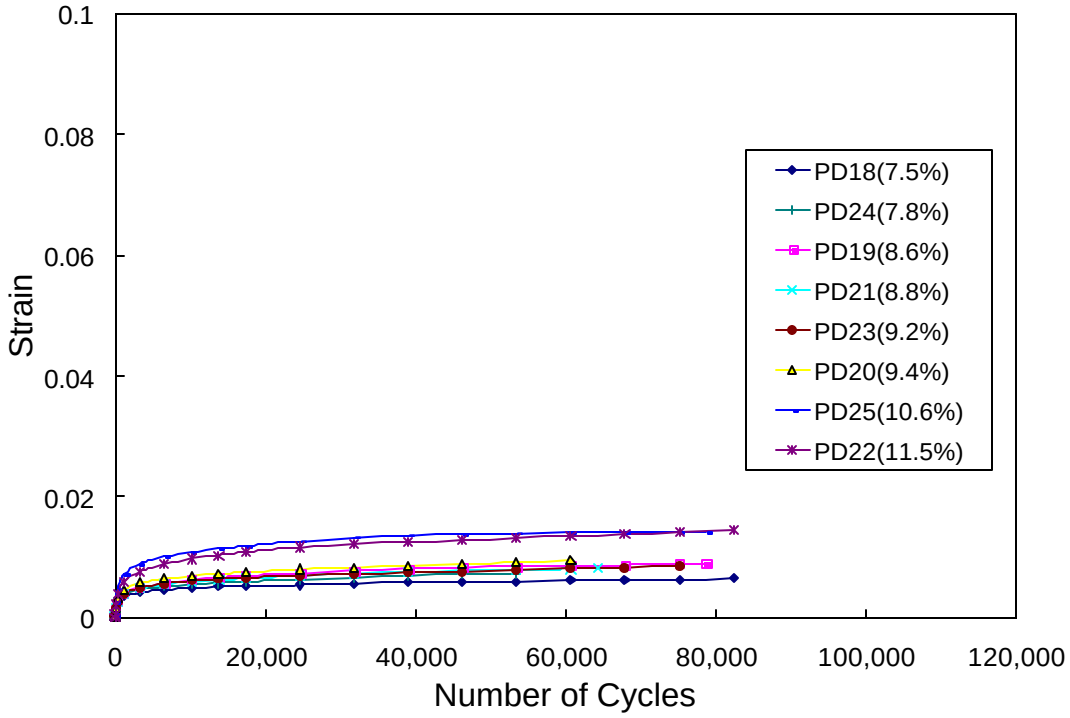

Figure 3-23. TRLPD data at 30°C (I19C)

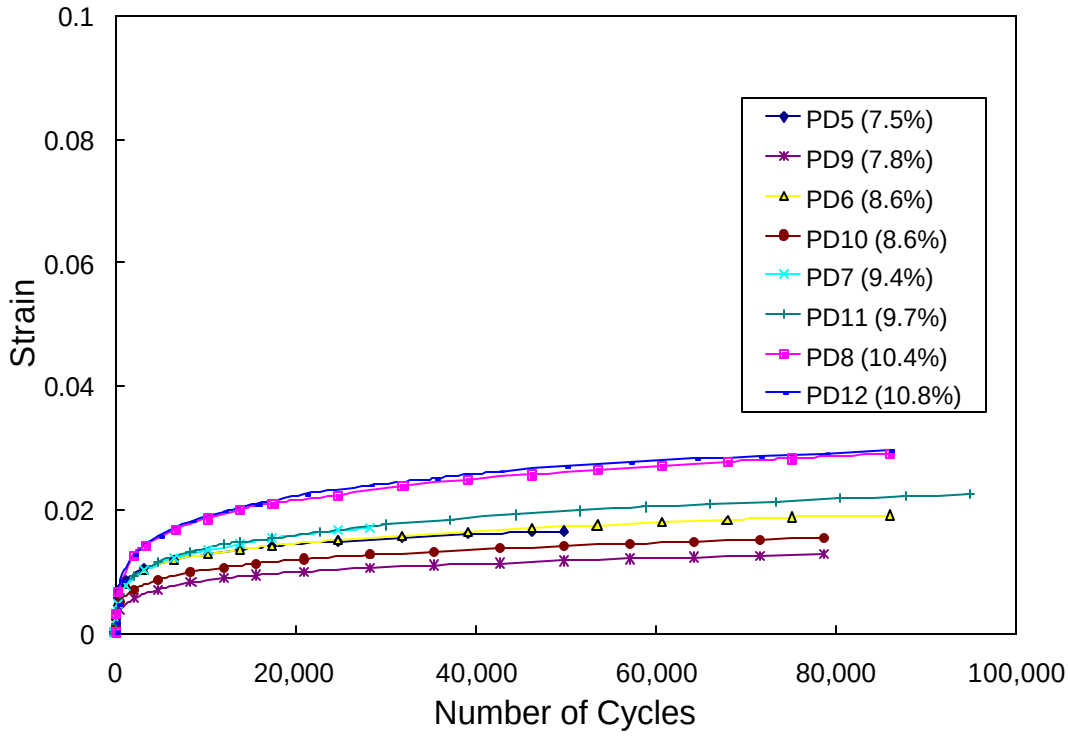

Figure 3-24. TRLPD data at 40°C (I19C)

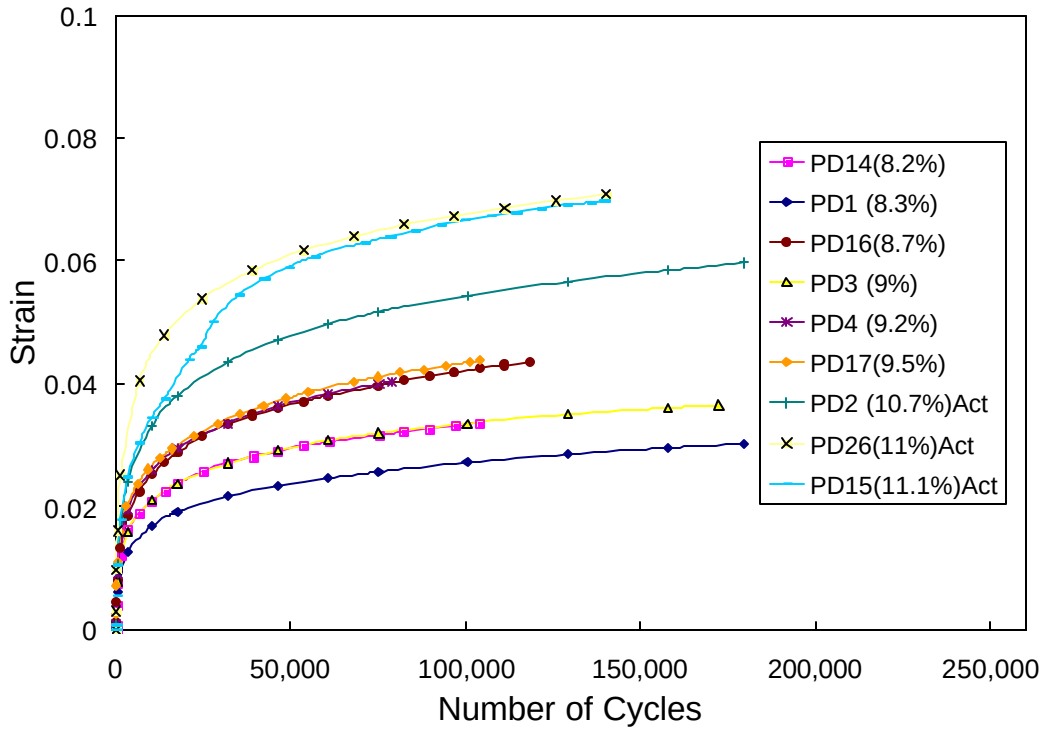

Figure 3-25. TRLPD data at 50°C (I19C)

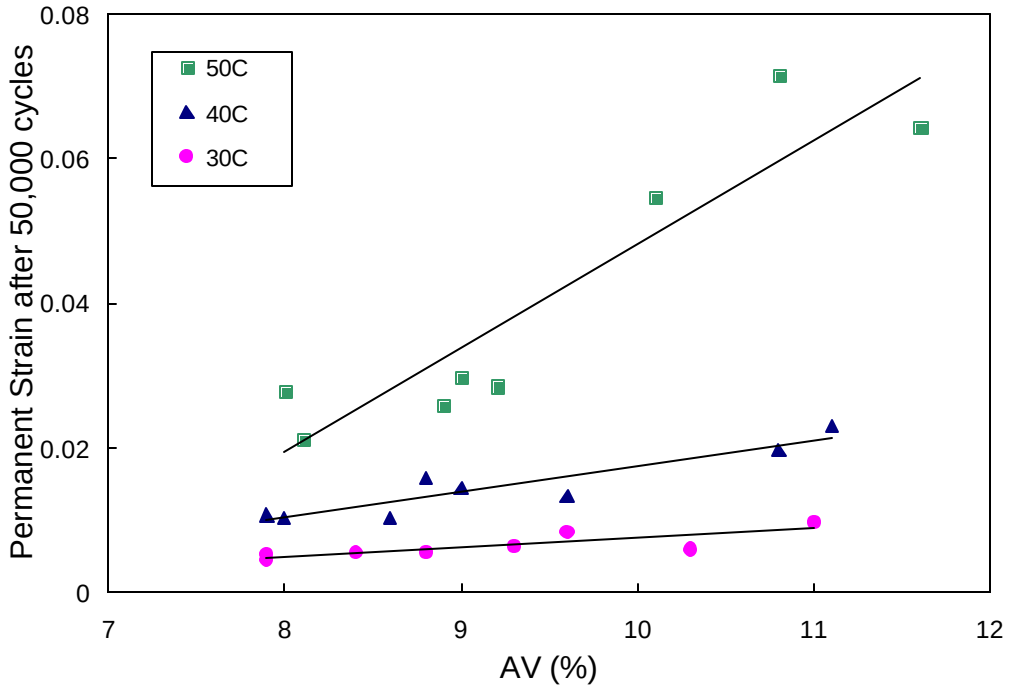

Figure 3-26. Effects of temperature and air void content on permanent strain (S9.5C)

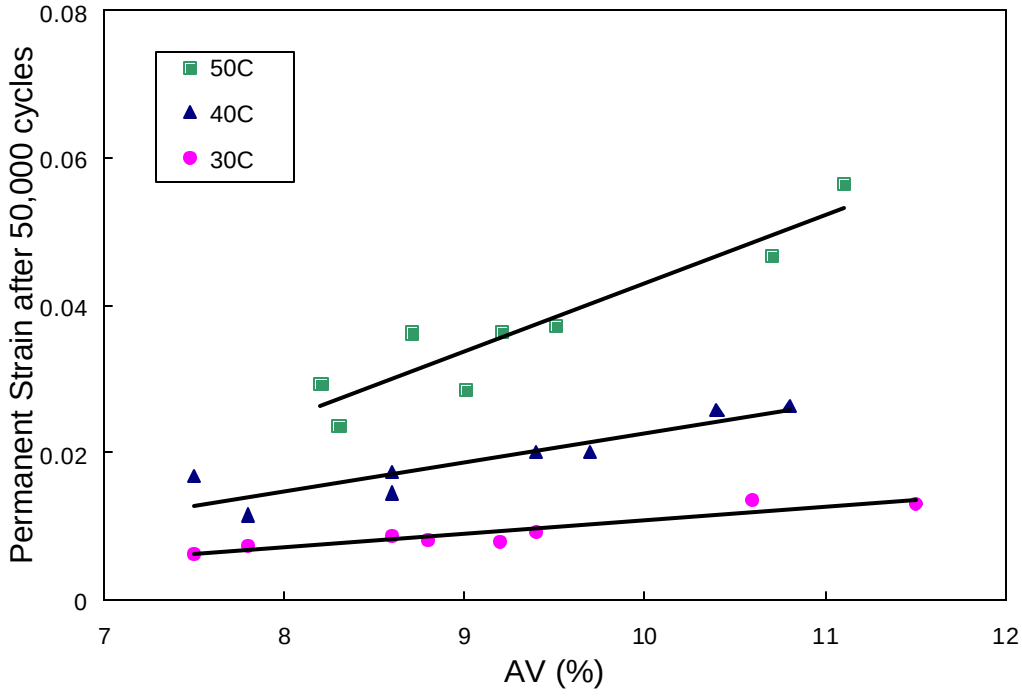

Figure 3-27. Effects of temperature and air void content on permanent strain (I19.0C)

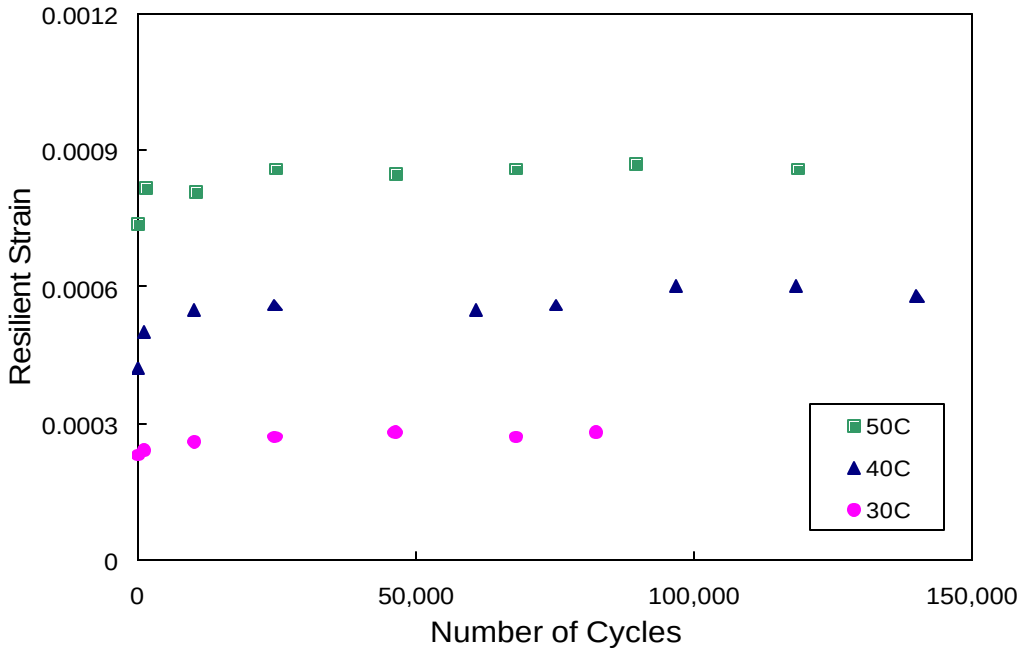

Figure 3-28. Resilient strain as a function of number of loading cycles (S9.5C)

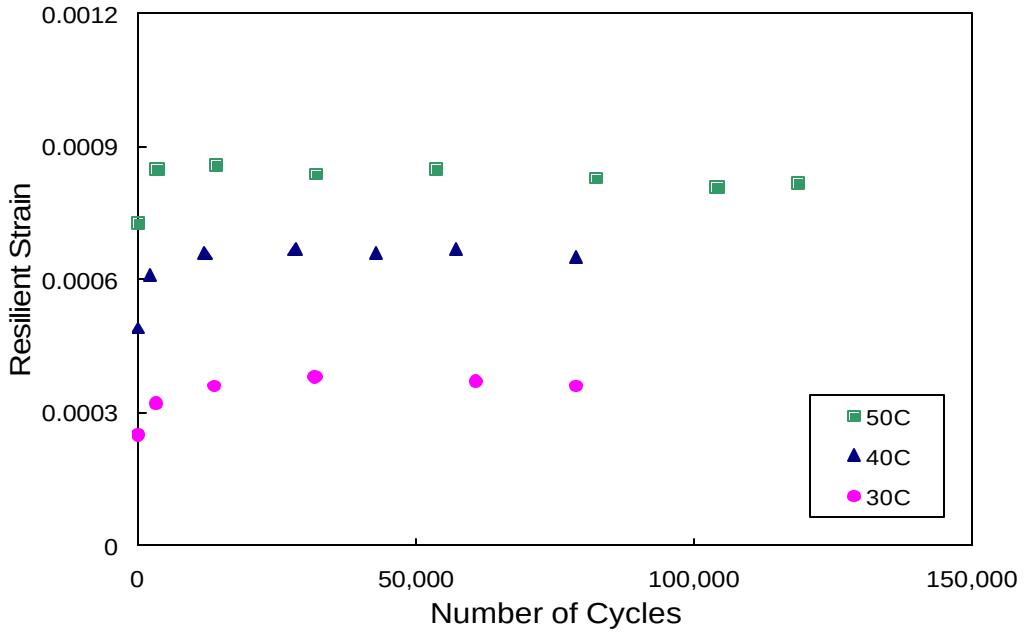

Figure 3-29. Resilient strain as a function of number of loading cycles (I19.0C)

To determine the form of function g, $\frac{e_p / e_r}{N^{f(T)}}$ was plotted against the temperature for different air void contents. As shown in Figure 3-32, it was found that the semi-log plot of the relationship may be represented by a power function. Therefore, the function, g, can be expressed as follows:

$$g = k_1 \times e^{k_4 T^{k_5 \times \%AV}} \tag{3-19}$$

where k_1, k_4, and k_5 are regression constants.

Combining Eqs. (3-17) - (3-19) yields:

$$e_p = e_r \times k_1 \times N^{[k_2 \cdot \ln(T) + k_3]} \times e^{k_4 \cdot T^{k_5} \times \%AV} \tag{3-20}$$

where e_r = resilient strain in microstrains;
T = temperature in degree Celsius; and
$\%AV$ = air void content in percentage.

The genetic algorithm was applied to the test data using the final form of the permanent deformation model in Eq. (3-20). The regression constants in this model are summarized in Table 3-5 for the two mixtures investigated in this study.

Table 3-5. Regression constants for permanent strain model in Eq. (3-20)

Variables	S9.5C	I19.0C
k_1	0.4000	1.7928
k_2	0.0205	0.0380
k_3	0.1042	0.0522
k_4	0.0241	0.0038
k_5	0.6429	0.8749

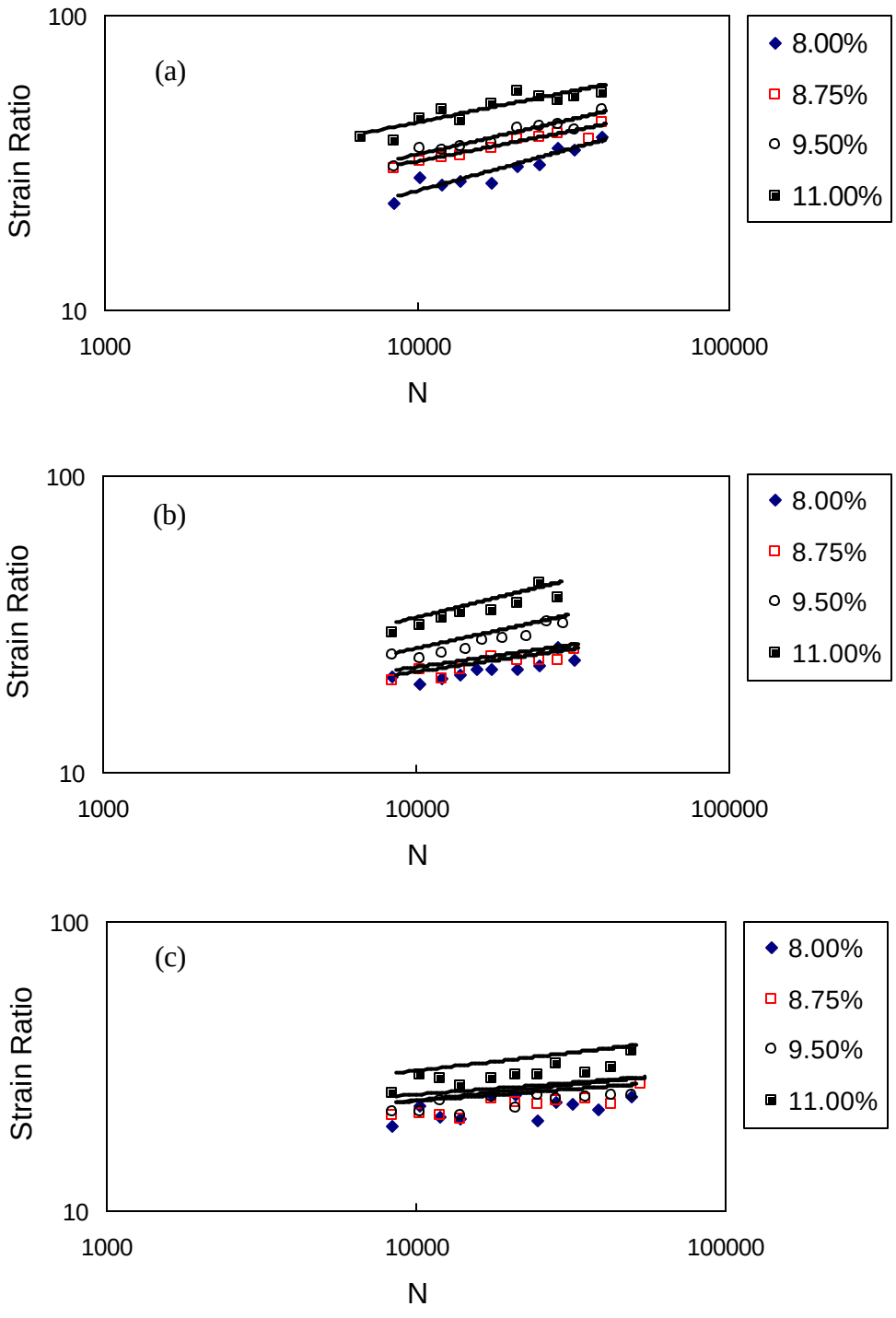

Figure 3-30. Air void effect on strain ratio versus number of loading cycles for I19.0C mix at: (a) 30°C; (b) 40°C; (c) 50°C

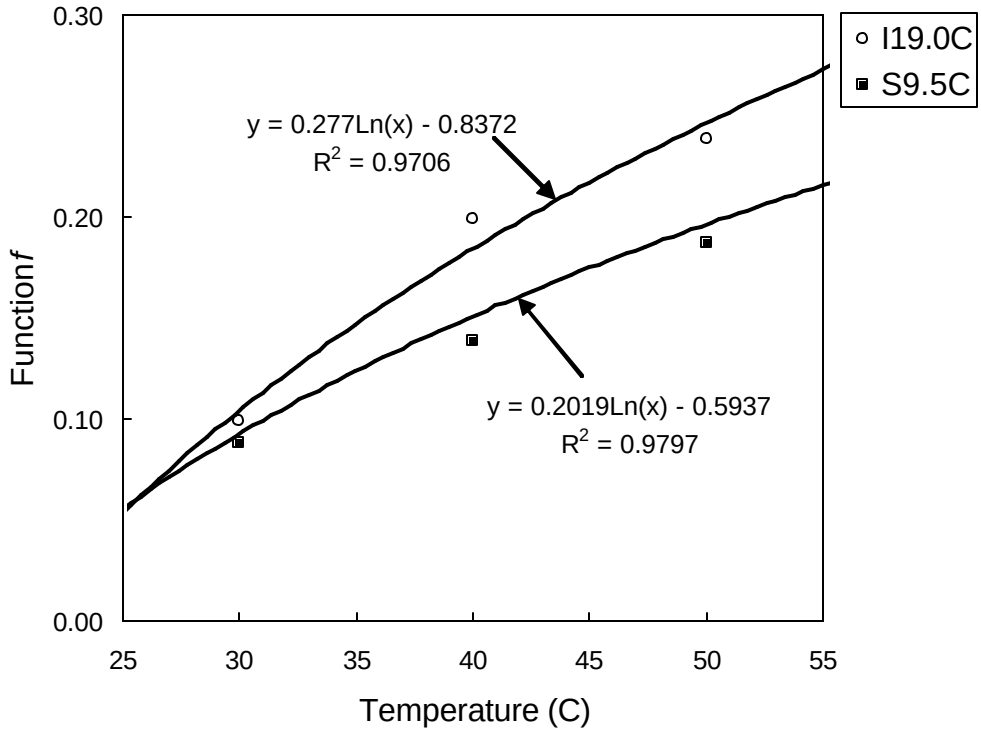

Figure 3-31. Function *f* versus temperature relationship

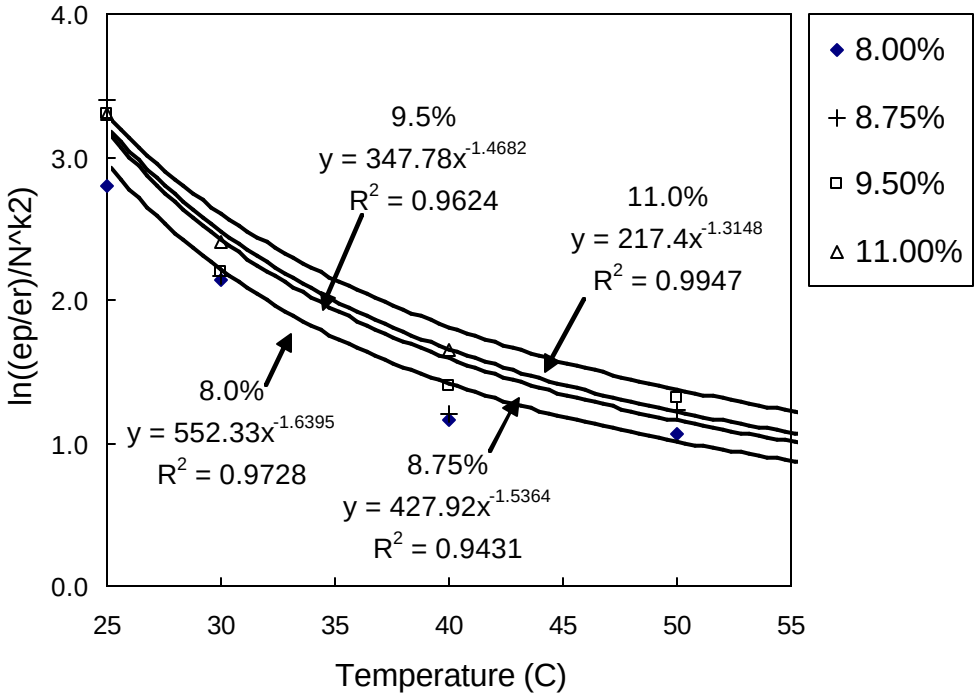

Figure 3-32. Function *g* as a function of temperature and air void content (I19.0C)

CHAPTER 4 ACCELERATED PAVEMENT TESTING USING MMLS3

A reliable performance prediction of asphalt pavements using laboratory models is a difficult task due to differences that exist between the field conditions and laboratory testing conditions. These conditions include, but are not limited to, stress state, loading history, material properties, temperature variations over time, and pavement depth, etc. A considerable amount of research has been conducted to correlate the field performance directly with the laboratory developed models. The major problem with this type of empirical approach is that when the prediction fails, it is difficult to identify the source(s) of the problem. Many times the laboratory constitutive and/or performance models are assigned the blame for this failure.

Accelerated pavement testing (APT) has been accepted as a means of bridging the gap between the laboratory and the field. The APT's abilities to control testing conditions (such as temperature, loading speed, etc.) minimize the differences between the laboratory material testing and the pavement testing and, therefore, allow researchers to evaluate the accuracy of the laboratory model more effectively.

In this research, a scaled-down APT device, the third-scale Model Mobile Loading Simulator (MMLS3) was used to evaluate the fatigue cracking and permanent deformation performance of asphalt pavements with varying air voids. The laboratory fatigue and rutting performance models developed in Chapter 2 were used in a mechanistic-empirical pavement design methodology, similar to the one adopted for the NCHRP 1-37A MEPDG (AASHTO 2004), to predict the fatigue cracking and permanent deformation performance of asphalt pavements loaded by the MMLS3. This prediction methodology includes the application of the time-temperature superposition principle with growing damage to account for the difference in loading frequency between the laboratory tests and the MMLS3. The measured and predicted performance measures were then compared to evaluate the reliability of the prediction methodology. The findings from the MMLS3 testing are reported in the following sections.

4.1 Laboratory Pavement Construction

The construction of the asphalt slabs was undertaken at the Constructed Facilities Laboratory (CFL) at North Carolina State University (NCSU). A steel wheel compaction roller with a vibrating force of 8.3 kN and a frequency of 50 Hz was used to compact the HMA mixture inside a steel mold.

The compaction was processed in three phases. In the first phase, the material was compacted by static rolling, without vibration, at the rate of about 1.1 km/hr up to 20 passes. The first pass began with the roller making slight contact with the material surface and, after each pass, the steel drum was manually placed about 1 mm lower in order to minimize the shear movement of the HMA during the next pass. This first phase usually took about 3 ~ 4 minutes. It was found that, during the first phase, slower speeds

produced denser compaction. In the second phase, vibration was applied to the mixture at around 100° to 110°C. The roller passed around 8 to 10 times at the rate of about 0.6 km/hr. Finally, the finish rolling was applied to provide a smooth surface at 85°~ 90°C. Since the mixture may have already cooled below the cessation temperature, this static rolling produced a mostly smooth surface. Figure 4-1 shows all the components involved in the slab construction and MMLS3 testing.

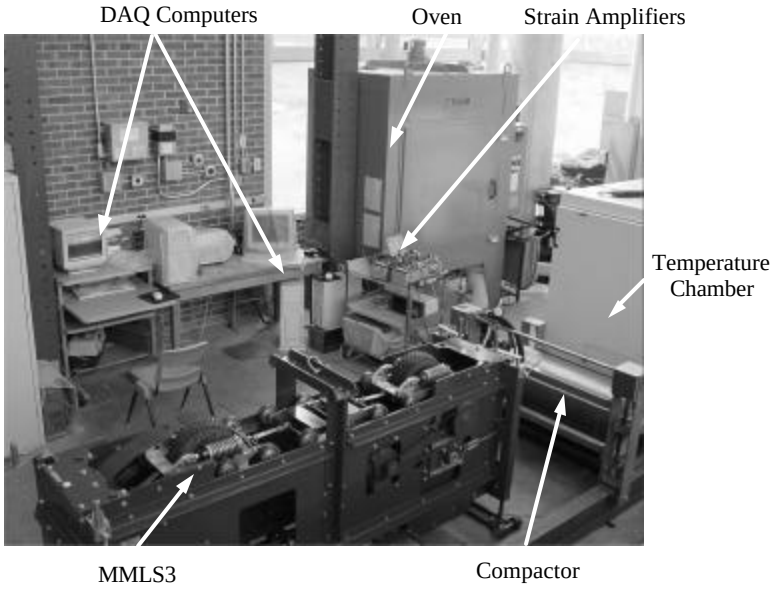

Figure 4-1. MMLS3 testing facility (Lee and Kim 2004)

For the fatigue testing, a 740 mm wide, 1,480 mm long, and 45 mm thick asphalt concrete (AC) layer was constructed on a 22.5 mm thick steel plate. After the compaction, the slab was cooled and taken out of the mold. Three 25 mm thick D60 neoprene sheets were placed on the steel plate as a base, and strain gauges and thermocouples were placed on the surface of the neoprene. A tack coat (MC-25) was applied between the neoprene base and the asphalt pavement to ensure good bonding between these layers. Then, the prepared asphalt slab was quickly cooled with dry ice in order to stiffen the slab to avoid possible damage during movement and placement of the asphalt slab on the neoprene base. Detailed steps involved in the development of the MMLS3 fatigue testing protocol are given in Lee and Kim (2004).

D60 neoprene was selected because its modulus is 360 MPa, which is similar to that of a typical aggregate base. The neoprene base was particularly helpful during the pavement construction because only the top sheet had to be replaced with a new sheet after each test. Although the neoprene base may not behave exactly the same way as aggregate base does under loading, the consistency and ease in construction that the neoprene base provided outweighed the negatives.

For permanent deformation testing, a 550 mm wide, 1,480 mm long, and 120 mm thick AC layer was constructed directly on the steel plate in the position where it was to be tested. The AC layer was constructed in two lifts with each lift thickness 60 mm, and a tack coat applied between the layers. The thickness of the AC layer was determined from the stress analysis using a multilayered elastic program such that the stress at the bottom of the AC layer was minimal. Because the permanent deformation tests were performed on thicker pavements there was no need for the neoprene layers, thus alleviating the need for them to be moved in and out of position, as in the fatigue testing.

One of the main objectives of this research is to determine the degree of change in performance as the HMA density becomes lower than the specified value. As discussed in Section 2.2, asphalt pavements with a density between 89% and 92% were considered for this research. Therefore, the target air void contents for MMLS3 testing were selected as 8, 9.5, and 11 %. Different air void contents were achieved by varying the total mass of HMA used in compaction.

After the slab was placed in the testing position, the MMLS3 was moved onto the slab. Then, the temperature chamber was placed on top of the MMLS3 to maintain the desired pavement temperature while the pavement was loaded by the MMLS3.

4.2 MMLS3 Test Protocol

The MMLS3 is a third-scale unidirectional vehicle-load simulator that uses a continuous loop for trafficking. It comprises four bogies with only one wheel per bogie. These wheels are pneumatic tires that are 300 mm in diameter, approximately one-third the diameter of standard truck tires. The wheels travel at the speed of about 5,500 wheel applications per hour, which corresponds to a dynamic loading of 3.3 Hz on the pavement surface. This loading consists of 0.3 sec haversine loading and a rest period of 0.3 sec. The dynamic load on the pavement surface by the MMLS3 in motion was measured by a Flexiforce® pressure sensor. The mean value of the maximum dynamic loads from the four wheels was approximately 3.57 kN. The contact area was measured to be approximately 34 cm^2 from the footprint of one MMLS3 wheel inflated to 700 kPa. Therefore, the surface contact stress was calculated to be approximately 1,049 kPa.

The fatigue tests were performed at 20°C with wheel wandering. The MMLS3 wheel-wandering mechanism provides lateral wheel movement perpendicular to the traffic direction to minimize permanent deformation. Wandering of the 80 mm wide wheel resulted in a wheel path of 180 mm in width. To achieve a normal lateral distribution of wheel loading, lateral displacement increments were programmed to occur at consistent time intervals. Permanent deformation tests were conducted at 40°C with channelized loading without wandering.

4.3 Measurements from the MMLS3 Testing

4.3.1 Fatigue Test

Strain

Strain gauges were installed to measure the tensile strain at the bottom of the AC layer. For strain measurements on nonhomogeneous material, it is preferable, in general, to select a gauge length that is several times larger than the nominal size of the aggregate. To satisfy this criterion, a strip-type strain gauge with a 50 mm gauge length was chosen and placed transverse to the traffic direction. Figure 4-2 shows the typical strain amplitude profile as wheel applications increase. The variation in the strain amplitude shown in Figure 4-2 is due to wheel wandering. When the wheel is located right above the strain gauge, the largest strain is recorded. As the wheel moves toward the edge of the wheel path, the strain becomes smaller. The fatigue life (N_f) of the asphalt pavement was determined using the measured tensile strain and the bisection method shown in Figure 4-3.

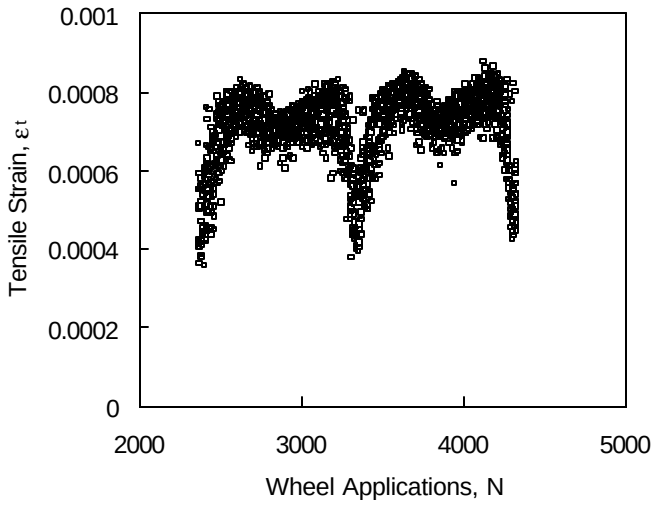

Figure 4-2. Typical tensile strain amplitude profile in the fatigue test

Temperature

The pavement surface and depth temperatures were measured using K-type thermocouples embedded in the pavements. As seen in Figure 4-4, the pavement temperature was kept fairly constant around the target temperature of 20°C throughout the thickness of the AC layer.

Fatigue Cracking

The length of fatigue cracks was determined using two different methods: manual crack mapping and analysis of digital images from the pavement surface. In the manual method, the cracks on the pavement surface were physically drawn on Plexiglas in different colors at various measurement periods. Also, the pavement surface images were taken using a digital camera. Using image analysis software, the cumulative crack length was determined.

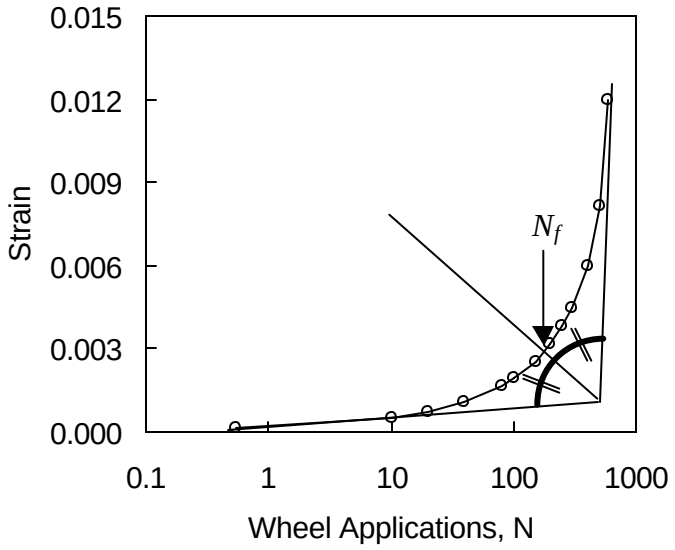

Figure 4-3. Determination of fatigue life using the bisection method

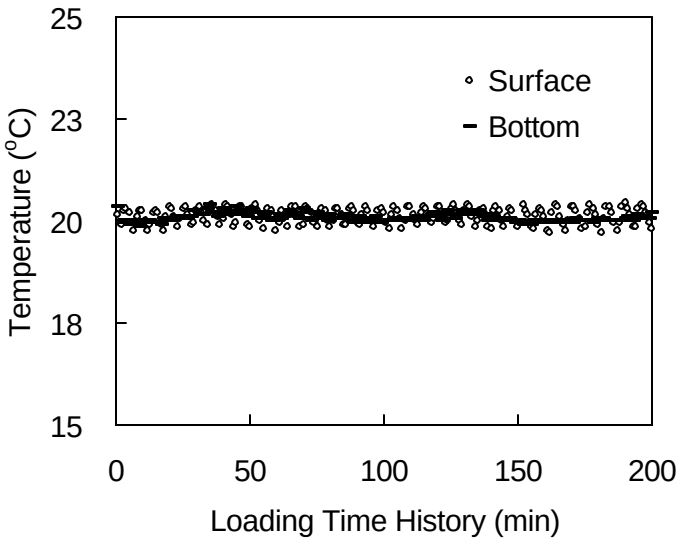

Figure 4-4. Temperature profile against loading time history for fatigue testing in the S9.5C pavement

4.3.2 Rutting Test

The following parameters were measured from the MMLS3 rutting tests.

Temperature

K-type thermocouples were used to monitor pavement temperatures at three different depths: surface, mid-depth, and bottom. The mid-depth temperature was used as a control. Figure 4-5 depicts a typical temperature history at three different depths. A temperature difference of about 10°C is observed between the top and bottom of the pavement. This temperature variation along the pavement depth should be taken into consideration for the rutting prediction. An increase in fluctuation of the temperature on the pavement surface is due to the heating system coming on and off to maintain the test temperature.

Rut Depth

Rut depths were measured using a Mitutoyo profilometer, which measures the transverse profile of the pavement surface at every 10 mm. The profilometer provides a comparison of the surface profiles measured during the intermittent periods of the MMLS3 testing with the initial profile. The change in these measurements throughout testing provides information related to the rutting evolution in the pavement. Figure 4-6 presents progressive surface deformation at different load applications for the I19.0C pavement.

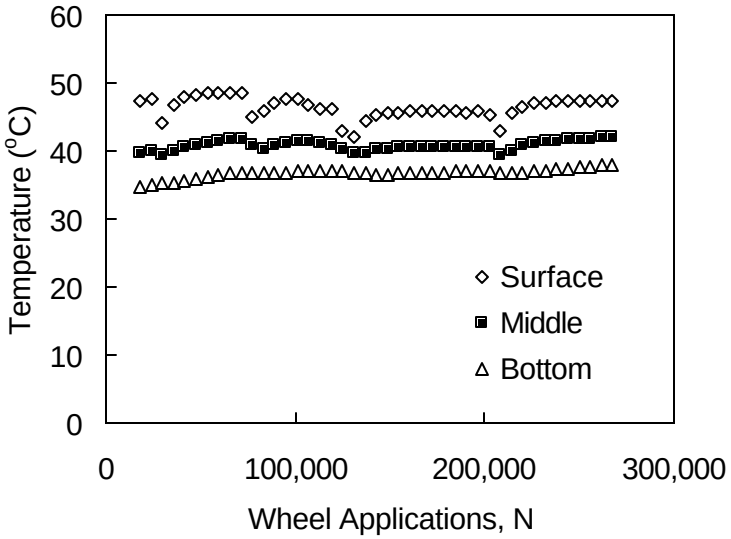

Figure 4-5. Typical temperature profiles in the MMLS3 rutting test

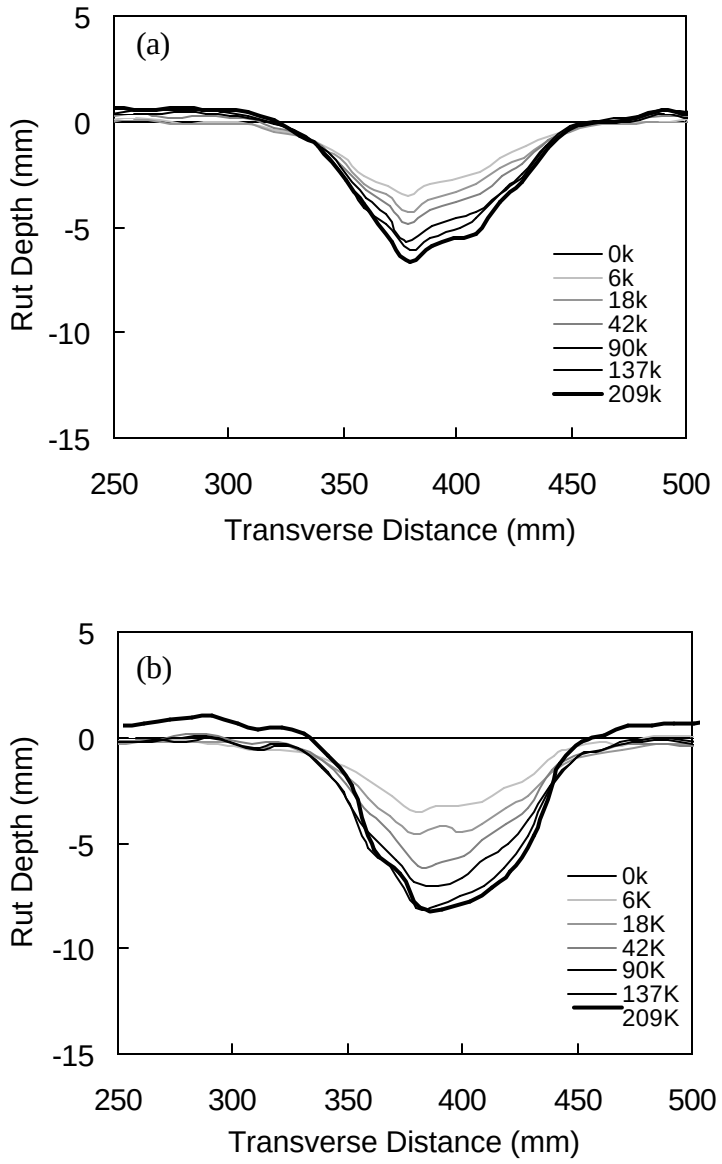

Figure 4-6. Rutting in the I19.0C pavement at air voids of: (a) 8.7%; (b) 10.2%

4.4 Performance Prediction Methodology

In this research, the fatigue cracking and rutting performance of asphalt slabs loaded by the MMLS3 were predicted using the laboratory performance models, the multilayered elastic program, and MMLS3 testing conditions. The predicted performance was compared with the measured performance to evaluate the performance prediction methodology developed in this research. In the following, the steps involved in the prediction process are described in detail.

4.4.1 Fatigue Life Prediction Method

Fatigue damage increases with applied loading cycles in a cumulative manner. Thus, a cumulative fatigue damage analysis, based on Miner's linear damage theory (1945), was adopted to assess the fatigue behavior of laboratory pavements loaded by the MMLS3. This damage model determines the incremental change in pavement wear caused by repetitions of dynamic load over time.

The phenomenological fatigue model in Eq. (3-5) was used in the fatigue life prediction with the inputs of the tensile strain at the bottom of the AC layer calculated from the multilayered elastic program and other mixture information specific to the pavement in question. It was deemed important to account for the following factors in the analysis:

- change in the loading frequency along the pavement depth;
- beneficial effects of rest periods that were introduced periodically to allow time to perform the crack survey and other nondestructive testing of the pavement; and
- wandering of the MMLS3.

The following describes how these factors are taken into account.

Change in Loading Frequency along Pavement Depth

The deformation behavior of asphalt concrete shows a *delayed response* from the time of applied loading due to the time-dependent behavior of viscoelastic materials. The loading time of 0.3 sec on the pavement surface and a tensile strain pulse time of 0.6 sec at the bottom (45 mm deep) of the AC layer were measured. According to Kim (1994), the longitudinal tensile strain pulse time and the depth beneath the pavement surface have a linear relationship. This relationship is used to describe the loading frequency under the MMLS3 loading, as shown in Figure 4-7 and expressed as follows:

$$Loading\ \ Frequency\ \ (Hz) = -0.037 \times depth + 3.33\ . \qquad (4\text{-}1)$$

Using Eq. (4-1), the loading frequency at mid-depth (22.5 mm) of the AC layer is determined to be 2.5 Hz. This frequency was used as the loading frequency in the fatigue analysis.

Although the loading frequency at the mid-depth of the AC layer caused by the MMLS3 is different from that used in the IDT testing, correction was not considered necessary because this difference is already included in the laboratory-to-field conversion factor (14.72) inherent in the AI fatigue model in Eq. (3-5). As will be shown later, the performance prediction analysis for permanent deformation is different in that respect because no correction factor is included in the permanent deformation model.

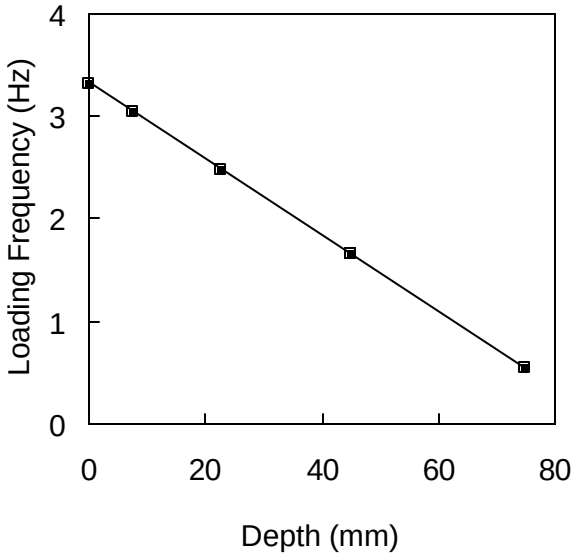

Figure 4-7. Loading frequency variation along depth

Rest Periods

During the MMLS3 testing, the test was halted periodically in order to perform a crack survey and other nondestructive testing. It is well known that rest periods have a beneficial effect on the fatigue life of asphalt pavement. Since this beneficial effect was not taken into account in the cumulative damage analysis, the fatigue life determined from the strain time history measured from the strain gauge under the AC layer should be corrected to eliminate the rest period effect. Since the degree of the beneficial effects of rest periods is not fully known, a simple procedure of shifting the strain time history along the time (or number of loading cycles) axis was applied to the test results. This procedure is shown graphically in Figure 4-8, and the adjusted fatigue life is summarized in Table 4-1.

MMLS3 Wandering

The MMLS3 fatigue test protocol incorporates a wandering mechanism to minimize the rutting and to cause alligator cracking. Therefore, the wandering had to be taken into account in the cumulative damage analysis. The wandering mechanism was programmed so that the wheel path comprised 21 stations. Figure 4-9 presents the ratio of the number of loading cycles on the i^{th} station to the number of cycles in one wandering period. These ratios were applied to the total number of loading cycles to determine the number of loading cycles at different stations. Then, the multilayered elastic analysis was conducted to determine the tensile strain (e_t) at the bottom of the asphalt layer in the center of the wheel path caused by the wheel load at each wandering station.

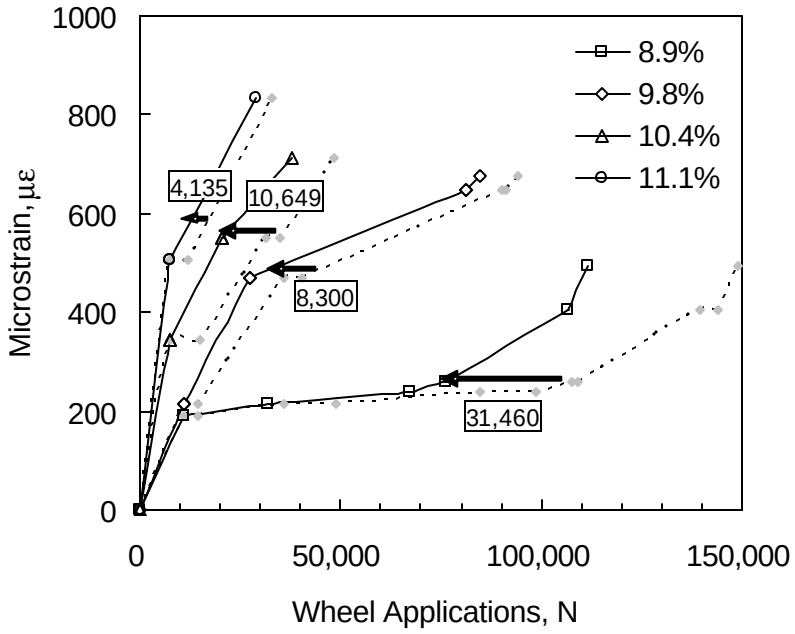

Figure 4-8. Fatigue life determination by eliminating rest period effect in the I19.0C pavement (arrow length corresponds to the corrected number of wheel applications)

Table 4-1. Determination of fatigue life without rest periods

Mix	Air Voids (%)	Rest Period	No. of Cycles at the Rest	N_f before Adjustment	N_f after Adjustment
S9.5C	8.0	1	7,575	148,823	98,134
		2	5,001		
		3	9,511		
		4	28,602		
	11.4	1	3,694	65,000	40,143
		2	18,031		
		3	3,132		
	12.2	1	3,771	36,355	26,679
		2	5,905		
I19.0C	8.9	1	3,800	102,875	71,415
		2	13,280		
		3	14,380		
	9.8	1	3,827	49,868	41,568
		2	4,473		
	10.4	1	7,163	37,880	27,231
		2	3,486		
	11.1	1	4,135	28,000	23,865

Assuming linear energy accumulation, the measure of damage (D) is defined as the sum of all the individual damage ratios (D_i). The damage ratio at the i^{th} loading station is defined as the ratio between the actual and allowable number of load repetitions of a load at the i^{th} wandering location. This concept is expressed mathematically as follows:

$$D = \sum_{i=1}^{n} D_i \tag{4-2}$$

where

$$D_i = \frac{N_i}{N_{f,i}}. \tag{4-3}$$

N_i = the actual number of load repetitions at the ith station; and
$N_{f,i}$= the allowable number of load repetitions at the ith station.

Using this cumulative damage analysis, the pavement fatigue life can be determined when the damage ratio is equal to one. The application of Eq. (3-5) to Eqs. (4-2) and (4-3) results in the following equation for the determination of the fatigue life of asphalt pavement loaded by the MMLS3 with wandering:

$$N_f = \frac{1}{\sum_{i=1}^{21} \frac{r_i}{4.9798 \times C \times f_1 \times e_{ti}^{-f_2} \times |E^*|^{-f_3}}} \tag{4-4}$$

where r_i is the fraction of wheel loads at the i^{th} loading station during one wandering period.

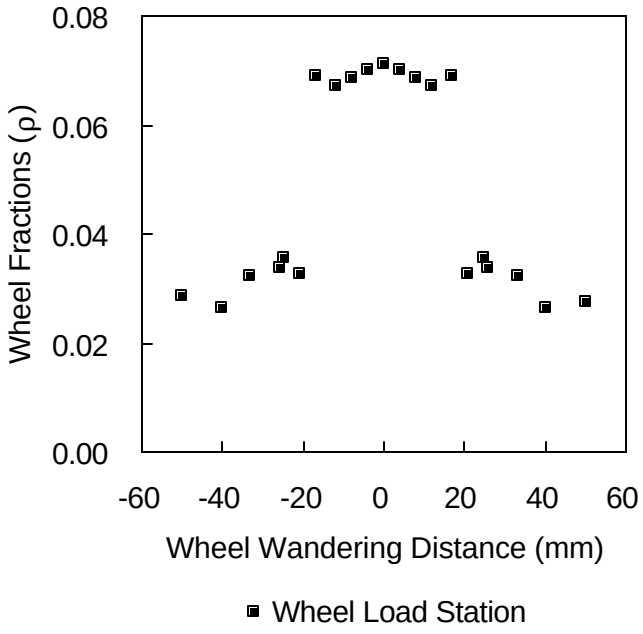

Figure 4-9. Wheel fractions at different stations in one wandering period

Figure 4-10 shows the growth of tensile strain measured from the bottom of the pavement as a function of the number of wheel applications. The strain increases rapidly at the initial stage, and then the rate of increase of strain becomes relatively constant until it is accelerated to final failure. The bisection method described earlier was used to determine the fatigue life of each pavement.

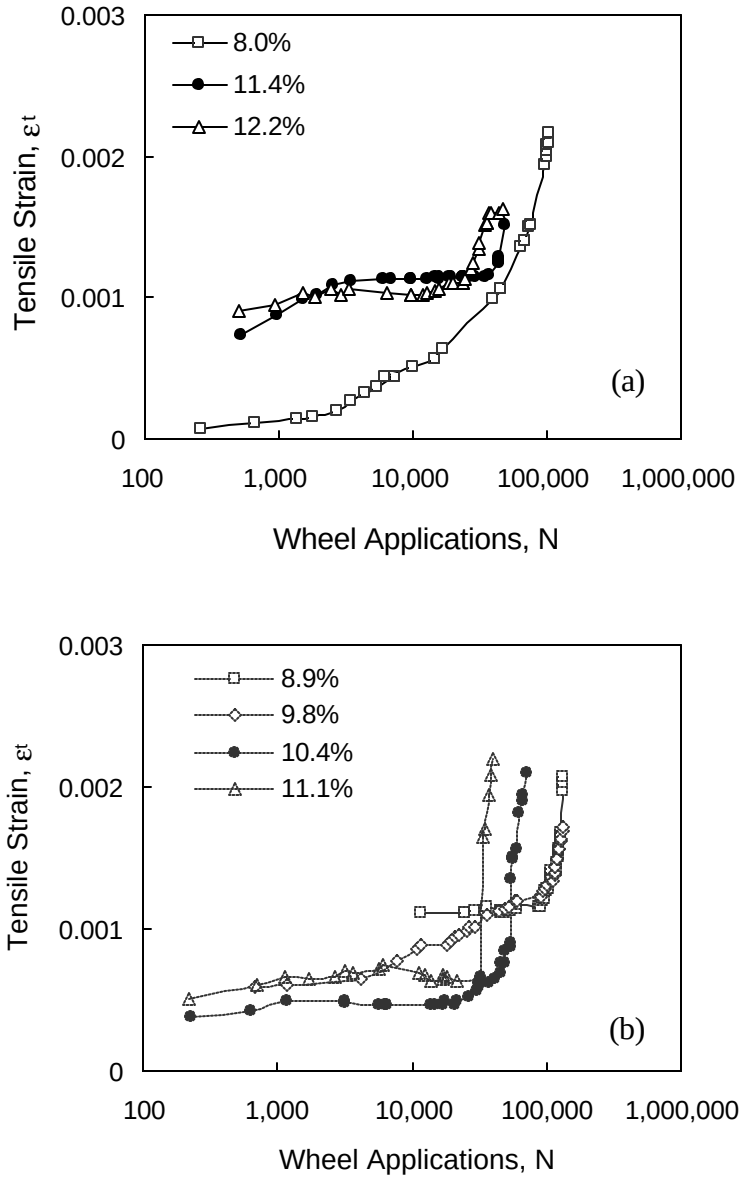

Figure 4-10. Tensile strain growth: (a) S9.5C; (b) I19.0C

Table 4-2 summarizes the measured and predicted fatigue lives and the estimated damage ratio at the end of the measured fatigue life. In general, the prediction is reasonable, except for the 8% S9.5C pavement. As can be seen in Figure 4-10(a), this pavement shows a different pattern of tensile strain growth compared to the other pavements, which

probably caused the error in the measured fatigue life. The proposed fatigue cracking prediction methodology results in the damage ratios at the end of the measured fatigue life, ranging between 0.8 and 1.2, excluding the 8% S9.5C pavement. It is noted that the increase of air voids from 8% to 11% causes the reduction of fatigue life by a factor of two to three.

Table 4-2. Summary of MMLS3 fatigue performance prediction

Mix	% AV	Measured N_f	Predicted N_f	Damage Ratio (D) at Measured N_f
S9.5C	8.0	98,134	133,324	0.74
	11.4	40,143	38,623	1.04
	12.2	26,679	32,468	0.82
I19.0C	8.9	71,415	65,688	1.09
	9.8	41,568	35,510	1.17
	10.4	27,231	28,636	0.95
	11.1	23,865	22,579	1.06

4.4.2 Permanent Deformation Prediction Method

The permanent deformation of the laboratory pavement under MMLS3 loading was predicted using the permanent strain prediction model in Eq. (3-20) and strain values computed from the multilayered elastic analysis. A sublayering method was adopted in which the permanent deformation in each sublayer was predicted and then summed to determine the permanent deformation in the entire AC layer. The 120 mm thick pavement was divided into four sublayers. Since more permanent deformation occurs in the upper portion of the AC layer, the thickness of the sublayer in the upper portion of the layer is smaller than that in the lower portion of the layer. The sublayer thicknesses were 15, 15, 30, and 60 mm for the four sublayers from top to bottom, respectively. The sublayering and temperature measuring points are depicted in Figure 4-11.

As with the fatigue analysis, some factors in the MMLS3 testing are important to consider in the permanent deformation prediction. These factors include:

- change in the temperature along the pavement depth;
- change in the loading frequency along the pavement depth; and
- frequency difference between the MMLS3 loading and the loading used in the TRLPD test.

Temperature and Frequency Changes along the Pavement Depth

As is shown in Figure 4-12, there was about a 10°C change in the temperature from the top to the bottom of the pavement. Since the permanent deformation of the HMA is a strong function of the temperature, this temperature change must be taken into account in the analysis.

The temperature of each sublayer was determined from the mid-depth of the sublayer. Since the thermocouples were not embedded exactly in those mid-depth locations, the mid-depth temperatures were interpolated from the measured depth temperatures using the following equation:

$$DepthTemp.\ (°C) = 0.0819 \times Depth\ (mm) + 45.665. \quad (4\text{-}5)$$

The mid-depth temperatures of the four sublayers were determined to be 45.0°, 43.8°, 42.0°, and 38.3°C, from the top to the bottom.

As was discussed in the fatigue analysis, the loading frequency changes as the pavement depth changes. The loading frequencies in the sublayers were determined using Eq. (4-1) and tabulated in Table 4-3.

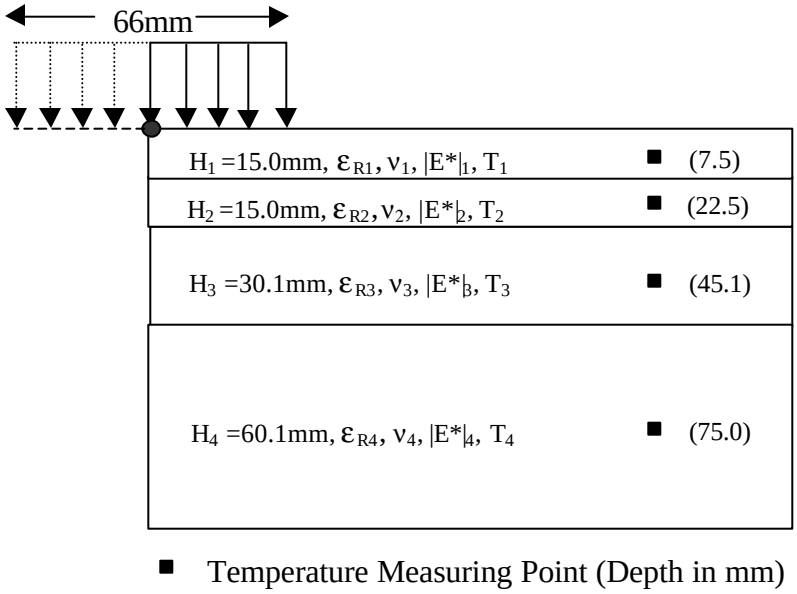

Figure 4-11. Layer characteristics of the MMLS3 pavement for permanent deformation prediction

(H_i = thickness; e_{Ri} = resilient strain; n_i = Poisson's ratio; $|E^*|_i$ = dynamic modulus; T_i = temperature in °C; and subscript i = the sublayer number)

Table 4-3. Loading frequencies at different depths

Depth (mm)	7.5	22.5	45.1	75.0
Loading Frequency (Hz)	3.06	2.50	1.66	0.56

Loading Frequency Difference between MMLS3 and TRLPD Tests

One of the major differences between the MMLS3 test and the TRLPD test is the loading frequency (to be more exact, the loading history). The TRLPD test employs a 0.1 sec loading and a 0.9 sec rest period, whereas the loading history of the MMLS3 test results in about a 3 Hz loading on the pavement surface and 0.56 Hz loading in the lowest sublayer. In order to account for this difference in the rutting performance prediction, the time-temperature superposition principle with growing damage (Chehab et al. 2003) was adopted.

The time-temperature superposition principle with growing damage states that the stress-strain behavior of HMA at two different temperatures can be the same if the loading histories in reduced time are the same. The reduced time at a reference temperature is defined as the value of the physical time at the temperature in question divided by the time-temperature shift factor determined from the dynamic modulus testing. Although the loading histories used in the MMLS3 testing and the TRLPD testing do not have the same reduced time loading histories, the application of this principle reduces the errors due to the difference in loading histories.

The most convenient way to apply the time-temperature superposition principle is to adjust the temperature of the permanent deformation analysis from the TRLPD test. For example, suppose that the i^{th} sublayer has a loading frequency of 2 Hz and a temperature of 43°C. To calculate the permanent strain in this sublayer using the TRLPD test results based on 10 Hz loading, the temperature in the analysis is adjusted so that the dynamic modulus of the HMA at the adjusted temperature at 10 Hz is the same as that at the sublayer temperature of 43°C and 2 Hz loading frequency. In this example, the adjusted temperature would be higher than 43°C because the loading frequency at the adjusted temperature is higher than that at the sublayer temperature. The amount of adjustment is based on the time-temperature shift factor determined from the dynamic modulus testing.

The approach described above was applied to the sublayers of all the pavements tested in this research. These adjusted temperatures are summarized in Table 4-4. They are used in the permanent deformation prediction model in Eq. (3-20) to predict the permanent strains in the sublayers.

The moduli of the sublayers were determined from the dynamic modulus model in Eq. (3-4) using the loading frequencies shown in Table 4-3 and the adjusted temperatures shown in Table 4-4. The multilayered elastic analysis was performed using the calculated moduli of the sublayers in order to determine the compressive strain in each sublayer.

The compressive strain, adjusted temperature, and percent air voids were input to Eq. (3-20) to determine the permanent strain in each sublayer. In order to correct for the difference in contact pressure between the MMLS3 test (1,047 kPa) and the TRLPD test (827 kPa), the permanent strain under the MMLS3 was obtained by multiplying the obtained permanent strain by a factor of 1.268 (i.e., 1,047/827). The permanent deformation for the sublayer can be computed by multiplying the i^{th} permanent strain by

the i^{th} sublayer thickness (h_i),. Finally, the total permanent deformation is obtained by adding the displacement contributions from each of the sublayers, as follows:

$$Rut\ \ Depth = \sum_{i=1}^{N} [e_p(i) \times h_i] \tag{4-6}$$

where i is the number of sublayers, N is the total number of sublayers, and $e_p(i)$ is the permanent strain in the i^{th} layer.

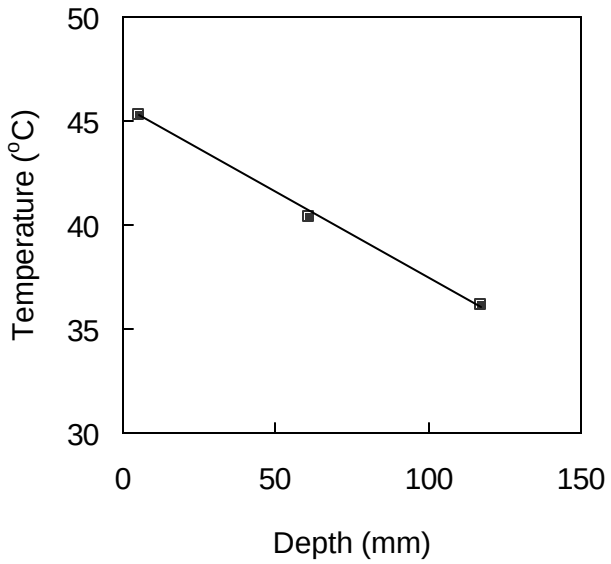

Figure 4-12. Temperature variation along pavement depth

Table 4-4. Measured and adjusted temperatures

Mix	Sublayer	Measured Temperature, °C (Loading Frequency, Hz)	Adjusted Temperature, °C, at 10 Hz
S9.5C	1	45.3 (3.06)	50.1
	2	44.1 (2.50)	49.7
	3	42.4 (1.66)	49.5
	4	40.1 (0.56)	51.5
I19.0C	1	45.0 (3.06)	50.9
	2	43.8 (2.50)	50.7
	3	42.0 (1.66)	50.8
	4	38.3 (0.56)	52.2

Figure 4-13 and Figure 4-14 present the development of measured and predicted permanent deformation as wheel loads are applied. In these figures, the prediction data with and without the adjusted temperatures are presented to demonstrate the importance of using the time-temperature superposition principle to match the loading frequency and temperature between the MMLS3 test and the TRLPD test. The prediction improves significantly by using the adjusted temperatures.

Table 4-5 summarizes the accuracy of the rutting prediction methodology using permanent deformation at 170,000 wheel applications. A comparison between the measured and predicted permanent deformation reveals that the proposed prediction methodology is reasonable in predicting the permanent deformation of asphalt pavement loaded by the MMLS3. The prediction errors are greater in the S9.5C pavement than in the I19C pavement. The exact cause of this difference is not known.

Several possible reasons may explain the prediction errors shown in this comparison, including, but not limited to, errors involved in estimating the sublayer loading frequency and temperature, errors involved in accounting for different contact pressures using linear extrapolation, and errors that originated from the fact that the reduced time loading histories in the MMLS3 and TRLPD tests are not the same. A mechanistic material model is necessary to address these issues in a more fundamental and accurate way.

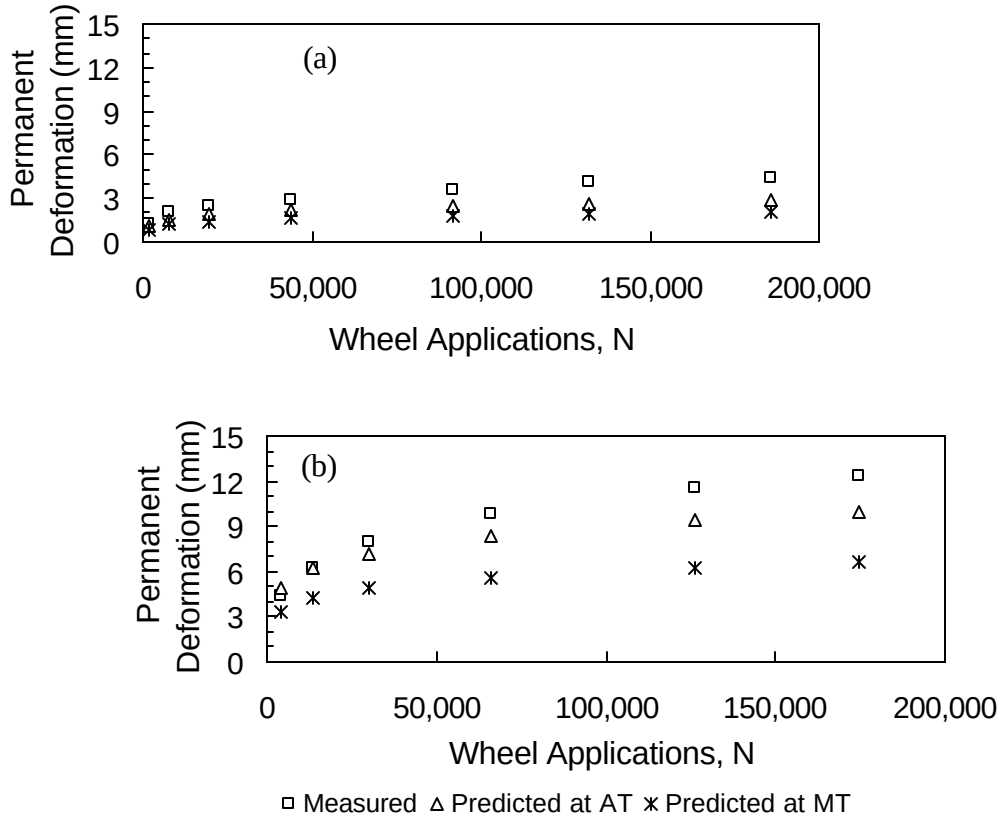

Figure 4-13. Measured and predicted permanent deformation of S9.5C pavements with air voids of: (a) 8.3%; (b) 11.7% (AT: Adjusted Temperature, MT: Measured Temperature)

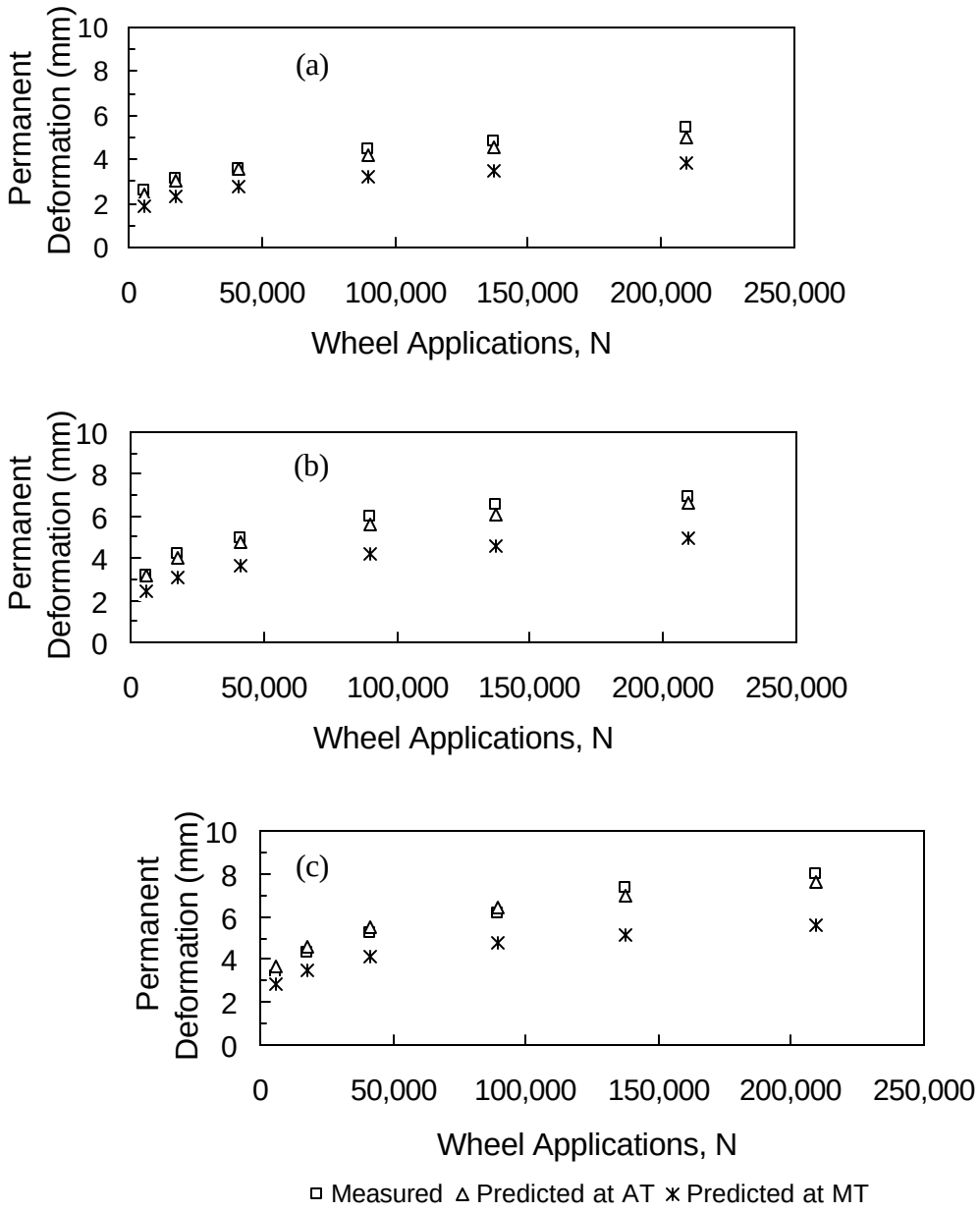

Figure 4-14. Measured and predicted permanent deformation of I19.0C pavements with air voids of: (a) 8.7%; (b) 9.7%; (c) 10.2% (AT: Adjusted Temperature, MT: Measured Temperature)

Table 4-5. MMLS3 permanent deformation (PD) prediction at 170,000 wheel applications

Mix	% AV	Measured PD (mm)	Predicted PD (mm) at Reduced Temperature	Predicted PD (mm) at Measured Temperature
S9.5C	8.3	4.33	2.78	2.06
	11.7	12.27	9.89	6.64
I19.0C	8.7	5.08	4.77	3.65
	9.7	6.73	6.31	4.72
	10.2	7.60	7.25	5.38

Note: Values between measurement intervals were determined by the linear interpolation method.

CHAPTER 5 ASPHALT PAVEMENT PERFORMANCE PREDICTION PROGRAM (AP^4)

The pavement performance prediction methodology described in CHAPTER 4 is a complex procedure that involves processing multiple inputs in various steps. In order to execute this methodology for a specific problem in a routine manner, it was deemed necessary to develop a computer program with graphic user interface (GUI). The following sections describe the framework, input parameters, and various modules incorporated into this program.

5.1 Damage Calculation

The Asphalt Pavement Performance Prediction Program (AP^4) is a stand-alone executable computer program written in LabView 6.0. The purpose of this program is to predict the service life of asphalt pavement based on fatigue cracking and rutting performance. The algorithm adopted in the AP^4 for the damage calculation is very similar to that used in the NCHRP 1-37A MEPDG (AASHTO 2004). This program is applicable to aggregate base pavement and full-depth pavement.

The AP^4 is based on the incremental damage concept in which the total damage during the analysis period is calculated by summing up the incremental damage computed for each analysis time period. Since the traffic and temperature change throughout a day, it is desirable to compute the damage on an hourly basis. However, preliminary assessment revealed that the computing time for this approach is too long for it to be adopted as a routine operation at the NCDOT. Considering the changes in temperature and traffic throughout a day, one day was divided into five time groups in which the temperature and traffic changes are not significant. These time groups are suggested by the NCHRP 1-37A MEPDG and summarized in Table 5-1.

Table 5-1. Five time groups used in the AP^4

Group Number	Time
1	midnight – 6 am
2	6 – 10 am
3	10 am – 4 pm
4	4 – 8 pm
5	8 pm - midnight

The two primary models in the AP^4 are the pavement response model and the performance prediction model. The pavement response model calculates the stresses and strains in the pavement system based on given loading conditions, pavement layer thicknesses and types, and layer material properties. A general purpose finite element code, FEP++, is used in the AP^4 as the pavement response model. Linear elastic, two-

dimensional analysis is performed in the AP[4] to calculate the stresses and strains in the pavement.

In the pavement response calculation, each asphalt layer is divided into sublayers to account for the temperature and loading frequency variations along the pavement depth and to provide a more accurate representation of the strain variation along the depth. The required material properties in the FEP++ include the dynamic moduli of asphalt sublayers, the elastic moduli of the aggregate base and subgrade, and Poisson's ratio of each layer. The dynamic moduli of asphalt sublayers are determined from Eq. (3-4) using the loading frequency and temperature for each sublayer. The loading frequencies at different sublayers are calculated from Eq. (4-1), and the temperatures in the middle of the sublayers are computed from the temperature prediction program.

The pavement responses used in the fatigue cracking and rutting performance predictions are the tensile strain at the bottom of the lowest asphalt layer and the compressive strain at the mid-depth of each asphalt sublayer, respectively. A preliminary analysis was performed on a typical asphalt pavement structure using the approaches presented in CHAPTER 4. It was found that the rutting analysis resulted in reasonable values within the analysis period of 20 years, whereas the fatigue analysis yielded a very short fatigue life. In order to correct the fatigue analysis, the MEPDG reports (which became available toward the end of this project) were studied. It was found that in the MEPDG fatigue analysis the AI fatigue model was modified by additional factors. The fatigue analysis used in the MEPDG is presented below and implemented into the final version of the AP[4] program.

The fatigue performance prediction model in the MEPDG is:

$$N_f = 0.00432 \times k_1^{'} \times C \left(\frac{1}{e_t} \right)^{3.9492} \left(\frac{1}{|E^*|} \right)^{1.281} \tag{5-1}$$

where

$$k_1^{'} = \frac{1}{0.000398 + \frac{0.003602}{1 + e^{(11.02 - 3.49 \times h_{ac})}}}; \tag{5-2}$$

$$C = 10^M \text{; and} \tag{5-3}$$

$$M = 4.84 \left(\frac{V_b}{V_a + V_b} - 0.69 \right). \tag{5-4}$$

The dynamic modulus of the HMA layer in Eq. (5-1) is determined by using Eq. (3-4) with the loading frequency and temperature at the mid-depth of the entire HMA layer.

Once N_f is determined, the damage (D) is calculated from:

$$D = \sum_{i=1}^{T} \frac{n_i}{N_{f,i}} \quad . \tag{5-5}$$

Once D is determined, the fatigue cracking is calculated from the fatigue damage using the following relationship:

$$FC_{bottom} = \left(\frac{6000}{1 + e^{(C_1 \times C_1' + C_2 \times C_2' \times \log 10(D \times 100))}} \right) \times \frac{1}{60} \tag{5-6}$$

where FC_{bottom} = bottom-up fatigue cracking, percent lane area;
D = bottom-up fatigue damage;
C_1 = 1.0;
C_1' = -2 × C_2';
C_2 = 1.0; and
C_2' = -2.40874-39.748 × $(1+h_{ac})^{-2.856}$.

According to the coefficients in Eq. (5-6), the cumulative damage ratio of one represents the 50% fatigue cracking in the lane area.

In the AP[4], the damage is calculated for one hour in each time group using the average temperature and average traffic for each time group, and then is multiplied by the number of hours in each time group. The average pavement temperature is determined from hourly pavement temperatures in a time group that are computed using the pavement temperature prediction program, developed in Fortran from the previous NCDOT project 23241-95-1 *Statewide Calibration of Asphalt Temperature Study from 1992 and 1993*.

The damage ratios for the five time groups are summed up to determine the damage ratio in one day. This process for the determination of a daily damage ratio is repeated for each day during the analysis period with changing ESALs and temperatures. A cumulative damage ratio is then calculated by adding the daily damage ratios. When the cumulative damage ratio becomes one, the pavement is considered to be failed in fatigue cracking, and the time that has elapsed from the initial trafficking to that point is the fatigue life of the pavement in question.

For rut depth prediction, the sublayering technique (Eq. (4-6)) and the permanent strain model in Eq. (3-20) are used. The basic analysis time unit is each time group, as was the case in the fatigue cracking analysis. The mid-depth temperature and air void content of each sublayer, ESALs, and compressive strain in the mid-depth of the sublayer are used in Eq. (3-20) to calculate the permanent strain. It needs to be noted that one cannot plug in these values to Eq. (3-20) to determine the permanent strain in a specific time group. The algorithm must account for where the time group in question is located on the permanent strain growth curve. To make this point more clear, Figure 5-1 shows permanent strain growth curves at five different temperatures. In this figure, $N(i)$, $T(i)$, and $e_p(i)$ represent the ESALs, temperature, and permanent strain of the i^{th} time group. The permanent strain in each time group is determined by accounting for the loadings in

the previous time groups. Each permanent strain is multiplied by the thickness of the sublayer to determine the permanent deformation in the sublayer.

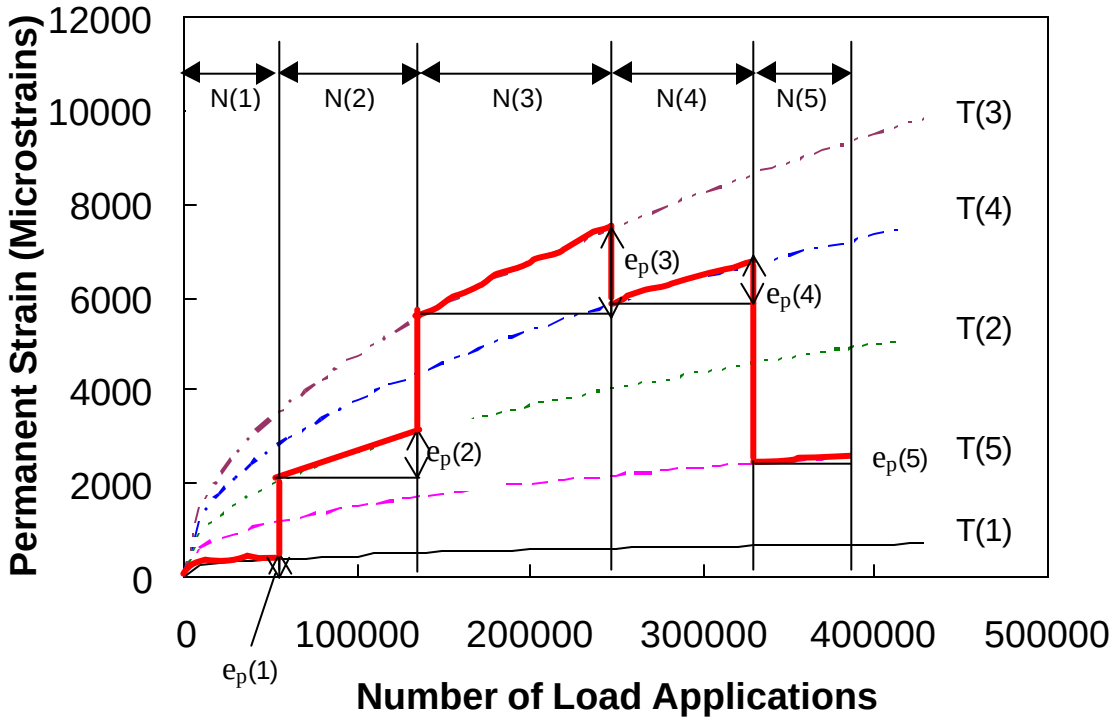

Figure 5-1. Schematic of the permanent strain calculation method

5.2 Input Parameters

The following parameters are necessary to run the AP[4]:

1. Location of the project. Locations are categorized into six counties where complete temperature data are available: Durham, Wake, New Hanover, Wilkes, Polk, and Pitt Counties.
2. Date (month/day). This month/day does not indicate the construction completion date, but the first date when the pavement in question is open to traffic.
3. Design period, in years.
4. Total design ESALs and traffic growth rate.
5. Tire load and contact pressure.
6. Traffic speed (10/35/55 mph).
7. Critical rut depth.
8. Material information.
    A. HMA type (S9.5C or I19.0C)
    B. Air void contents of asphalt layers
    C. Moduli and Poisson's ratios of aggregate base and subgrade

5.3 Pavement Response Model

The finite element code written in C++, FEP++, is used in the AP[4] as the pavement response model. A pre- and post-processor (3P) code for layered elastic modeling of asphalt concrete with FEP++ was developed and implemented in the AP[4]. The 3P is an executable code written in Visual Basic 6.0 and compiled on the Windows XP platform.

The 3P creates the finite element mesh based on the user's inputs of the layer thicknesses and types. The asphalt layers are divided into sublayers: 1 in. thick for the first 4 sublayers from the pavement surface and 2 in. thick for the rest of the asphalt layers. If the thickness of the lowest sublayer is less than the specified thickness, that layer was combined with the sublayer above. The schematic of a finite element model for a pavement structure is shown in Figure 5-2.

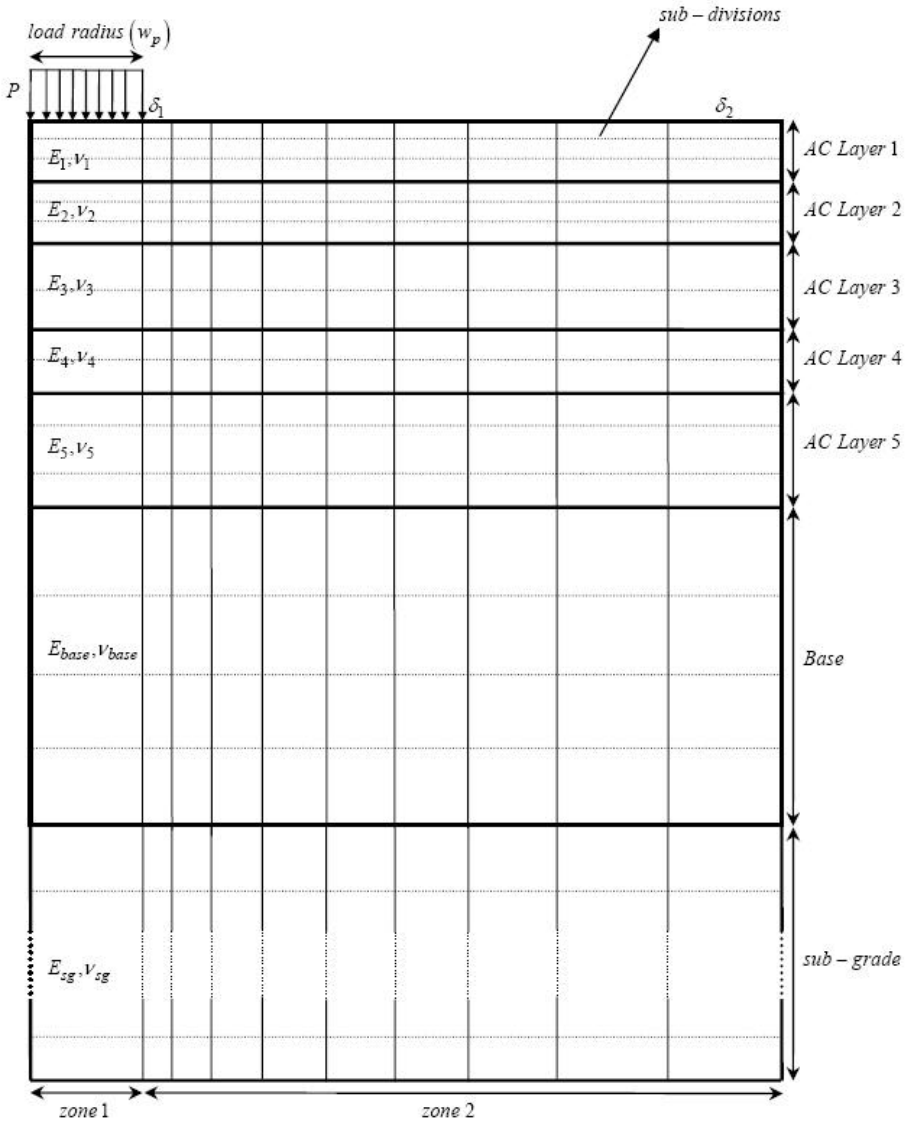

Figure 5-2. Schematic of a pavement structure

The pavement responses calculated from the FEP++ are the tensile strain at the bottom of the lowest asphalt layer and the compressive strain at the mid-depth of each asphalt sublayer, respectively. These responses are used in the performance prediction models to calculate the extent of fatigue cracking damage and rut depth.

The FEP++ model is verified against the EverStress 5.0, multilayered elastic pavement analysis program, developed by the Washington State DOT, using a typical pavement example. Table 5-2 shows the comparison of the vertical displacements calculated from the EverStress and the FEP++. The results are essentially identical.

Table 5-2. Comparison of vertical displacements calculated from EverStress and the FEP++

	Displacement (inch)	
Depth (inch)	EverStress	FEP++
0.0	2.642	2.641
0.5	2.557	2.557
1.0	2.456	2.457
1.5	2.354	2.355
3.0	2.070	2.071

5.4 Material Properties

Since the laboratory testing described in CHAPTER 2 was performed on the S9.5C and I19.0C mixtures, the coefficients for the dynamic modulus air void model are available only for the two mixtures described in Section 2.1. Therefore, the asphalt mixture selection in the AP^4 is available only for these two mixtures. When the pavement in analysis is a full-depth asphalt pavement with an asphalt concrete base, it is recommended to use the I19.0C mixture instead of the base mixture. Since the primary purpose of using the AP^4 is to determine the service life difference between density-deficient and in-specification pavements, the effect of this type of approximation is expected to be minimal.

For asphalt concrete, the dynamic modulus is determined for each asphalt sublayer as a function of loading frequency and temperature in the mid-depth of the sublayer and the air void content of the sublayer using Eq. (3-4). The following relationship is used to determine the loading frequency as a function of pavement depth:

$$f_i = a_1 \times d_i + a_2 \tag{5-7}$$

where f_i = loading frequency at the i^{th} sublayer (Hz);
d_i = depth of the i^{th} sublayer (in.); and
a_1, a_2 = regression constants depending on traffic speed (Table 5-3).

Table 5-3. Values of a_1 and a_2 for different traffic speeds

Traffic Speed	a_1	a_2
10 mph	-1.147	14.49
35 mph	-4.611	44.44
55 mph	-4.44	52.63

Poisson's ratio of the asphalt layer is calculated using the following equation:

$$n_{ac} = 0.15 + \frac{0.35}{e^{(-0.04 \times {}^{\circ}F + 3.18)} + 1} \quad . \tag{5-8}$$

The aggregate base and subgrade are assumed to be linearly elastic, and appropriate values of Young's moduli and Poisson's ratios for these layers are input by the user. Typical modulus and Poisson's ratio values for these unbound materials are given in Table 5-4.

Table 5-4. Typical modulus and Poisson's ratio values for unbound materials

Layer Type	Modulus (psi)	Poisson's Ratio
Aggregate Base	30,000 – 80,000	0.3 – 0.4
Subgrade - Sandy	7,000 – 25,000	0.35
Subgrade - Clayey	5,000 – 25,000	0.4

5.5 Traffic Module

The algorithm used in the traffic module begins with the current NCDOT procedure for calculating the 18 kip (80 kN) equivalent single-axle loads (ESALs) for pavement design. The following traffic inputs are required in the NCDOT procedure: initial year ADT, projected year ADT, percent duals, percent TTST, and directional distribution percentages. The term, *TTST*, represents various combinations of multiple unit and multiple axle trucks.

The NCDOT procedure is based on the following traffic growth law:

$$Total\ ESALs = \sum_{i=0}^{DL} IESAL \times (1 + \frac{GR}{100})^{i} \tag{5-9}$$

where DL = design period in years;
$IESAL$ = first year ESALs; and
GR = growth rate in percent.

Eq. (5-9) can be further refined using various traffic factors, as shown below:

$$Total\ ESALs = AE + IADT \times \left\{ \left(1 + \frac{GR}{100*365.25} \right)^{365.25 \times DL} - 1 \right\} \times \left(1 + \frac{GR}{365.25 \times 100} \right)^{(CY - IY) \times 365.25}$$

$$\times \left(\frac{PTT}{100} \times FTT + \frac{PD}{100} \times FD \right) \times \frac{DDP}{100} \times \frac{LD}{\ln\left(1 + \frac{GR}{100 \times 365.25} \right)} \qquad (5\text{-}10)$$

where

AE = additional ESALs, such as military loadings;
GR = growth rate, percent;
DL = design life, year (flexible pavement = 20 and rigid pavement = 30);
IADT = initial year ADT;
CY = construction year;
IY = initial year;
PTT = TTST, percent;
FTT = truck factor for TTST (Table 5-6);
PD = DUALS, percent;
FD = truck factor for DUALS (Table 5-6);
DDP = directional distribution percentages, percent;
LD = lane distribution factor determined from Table 5-5; and
LN = natural logarithm.

The projected year ADT is normally for a 20-year period. Loadings from automobiles are considered to be negligible. The lane distribution factors and the truck factors are tabulated in Table 5-5 and Table 5-6, respectively. A lane distribution factor of 0.5 will be used for the design of inside (median) lane widening of existing facilities with 2 or more lanes per direction.

Table 5-5. Lane distribution factor

Lane Distribution Factor	No. of Lanes in One Direction
1.0	1
0.9	2
0.8	3 or more

Table 5-6. Truck loading factors

	Truck Loading Factors	
Road Type	Duals (*FD*)	TTST (*FTT*)
Rural Freeway	0.30	1.15
Rural Other	0.30	0.95
Urban Freeway	0.30	0.85
Urban Other	0.25	0.80

Since the incremental damage analysis is performed in the AP^4 on a time group basis, the annual ESALs calculated from Eq. (5-10) need to be distributed to individual time groups. This distribution is accomplished first by dividing the annual ESALs by 365.25 days to obtain the daily ESALs and then distributing the daily ESALs into the ESALs in the 5 time groups using the percent truck values shown in Table 5-7. The ESALs for each time group are equally divided into the hours in the time group to determine the hourly ESALs. Table 5-7 shows the hourly ESALs, assuming that the daily ESALs are 1000.

Table 5-7. Traffic distribution in five time groups (AASHTO)

Time	% Truck	ESALs in Each Time Group Based on 1000 Daily ESALs	Hourly ESALs Based on 1000 Daily ESALs
Midnight-6 am	*14.0*	*141.12*	*23.5*
6 – 10 am	*19.8*	*199.58*	*49.9*
10 am - 4 pm	*35.1*	*353.80*	*58.9*
4 – 8 pm	*18.5*	*186.48*	*46.6*
8 pm - midnight	*12.6*	*127.00*	*31.8*

5.6 Temperature Model

For the estimation of the hourly pavement temperature, the Fortran program developed from the previous NCDOT project, *Statewide Calibration of Asphalt Temperature Study from 1992 and 1993,* was utilized. This program is based on fundamental principles of heat transfer and predicts the pavement depth temperature from the pavement surface temperature history, which is determined using the *yesterday* maximum air temperature and cloud conditions, and the minimum air temperature of the *today* morning. This information was obtained from the National Climatic Data Center for five climatic divisions in North Carolina. The temperature database for these five divisions accompanies the AP^4 program to provide the hourly pavement temperatures at different depths for the determination of the dynamic modulus of the asphalt sublayer and the calculation of fatigue cracking and rutting damage. The hourly pavement depth temperature is used to determine the average pavement depth temperature for each time group. This step is automatically included in the main program after selecting a county. A detailed procedure for the construction of the temperature database can be found in Kim et al. (1996).

CHAPTER 6 DETERMINATION OF PRICE REDUCTION FACTORS

In this project, the price reduction factor (PRF) is defined as follows:

$$PRF = \frac{\Gamma_{Deficient}}{\Gamma_{In-Specification}} \tag{6-1}$$

where $\Gamma_{Deficient}$ and $\Gamma_{In\text{-}Specification}$ represent service lives for density deficient and in-specification pavements, respectively. If the life-cycle costs or amount of distress at the end of the project period are used in the PRF calculation, the definition in (6-1) needs to be inverted. Once the PRF value is determined, the following equation can be used to calculate the price reduction:

$$\Delta P = (1 - PRF) \times CP \tag{6-2}$$

where ΔP = price reduction in dollars; and
CP = contract price in dollars.

The most ideal way of defining the PRF is to use the life-cycle costs. However, the use of the life-cycle costs requires the accurate and realistic prediction of pavement performance. As will be discussed later, the lack of calibration of the AP[4] with actual field performance makes the life-cycle cost analysis unreliable. Therefore, the PRF is calculated in this study using the life or the amount of distress at the end of the project period.

In this chapter, the following three approaches are described as a means of determining the PRF for density deficient HMAs:

1. material level laboratory performance tests (i.e., the IDT fatigue test for fatigue cracking and the TRLPD test for rutting);
2. MMLS3 fatigue and rutting tests; and
3. case studies of actual density deficient pavements using the AP[4]

In order to understand the strengths and weaknesses of these different approaches, one must first understand the various factors that affect the performance of deficient pavements. These factors include, but are not limited to, the following:

1. boundary condition (i.e., presence of sublayers and pavement thickness);
2. pavement layer type and condition;
3. temperature and loading frequency variations along the pavement depth;
4. location (i.e., depth) and thickness of deficient HMA;
5. traffic speed; and
6. environmental conditions of the project location.

Table 6-1 tabulates the ability of each analysis method to account for these factors. Undoubtedly, the AP^4 analysis provides the most accurate and rational information regarding the performance of density deficient pavements. However, this approach requires the NCDOT to perform the AP^4 analysis in each case and does not provide a simple set of factors or equations for price reduction. In the following sections, findings from each of these methods are reported and their strengths and weaknesses are discussed.

Table 6-1. Factors addressed in different analysis methods

	Material Level Performance Test	MMLS3 Test	AP^4 Analysis on Pavement Structure
Presence of Sublayers	N/A[a]	?[b]	?
Pavement Thickness	N/A	Fixed	?
Pavement Layer Type and Stiffness	N/A	Fixed	?
Temperature-Depth Variation	N/A	Fixed	?
Loading Frequency-Depth Variation	N/A	?	?
Location and Thickness of Deficient HMA	N/A	Entire AC Layer	?
Traffic Speed	N/A	Fixed	?
Project Location	N/A	Fixed	?

Note: [a]Not Addressed; [b]Addressed properly

6.1 Material Level Laboratory Performance Tests

In this section, the results from the IDT fatigue test and the TRLPD test are analyzed further to determine the PRFs. For the fatigue cracking, the data shown in Figure 3-14 and Figure 3-15 are fitted to determine the relationship between N_f and the air void content. It is noted that the air void contents shown in these figures are those of the IDT specimens. The corresponding *initial* air void contents of the HMA pavements are summarized in Table 2-3. The regression equations between N_f and the IDT air void content obtained from Figure 3-14 and Figure 3-15 and the relationship between the IDT and *initial* air void contents in Table 2-3 are used to determine the PRFs at different air void contents.

The results are plotted in Figure 6-1 for both mixtures. Due to the variability in the fatigue data, no significant trend in the PRF vs. air void content relationship was found as a function of mixture type, temperature, and the load level. The regression of the data in Figure 6-1 results in the following equation:

$$PRF = 5.0237 \times e^{-0.2007 \times \%AV} \quad \text{for the IDT fatigue test} \qquad (6\text{-}3)$$

where %AV is the air void content in percentage.

The rutting analysis was performed using Eqs. (3-16) and (3-20). To determine the number of cycles to failure due to rutting, a failure criterion was needed. The failure criterion of a 0.5 in. rut depth was employed with the assumption that the rutting occurs within the top 4 in. of the asphalt layer. These conditions resulted in the critical permanent strain of 0.125. This value was input to Eq. (3-20) to solve for the number of cycles to failure due to rutting. These values were then used to determine the PRFs for different air void contents. The results are plotted in Figure 6-2. The regression analysis of the data in Figure 6-2 yields:

$$PRF = 10{,}954 \times e^{-1.1633 \times \%AV} \quad \text{for the TRLPD rutting test.} \tag{6-4}$$

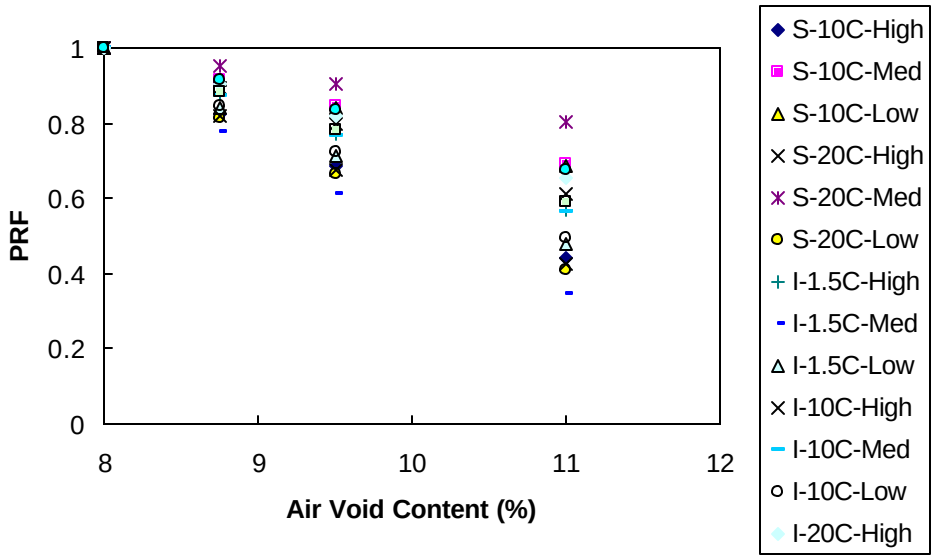

Figure 6-1. PRFs determined from the IDT fatigue tests (S: S9.5C, I: I19.0C)

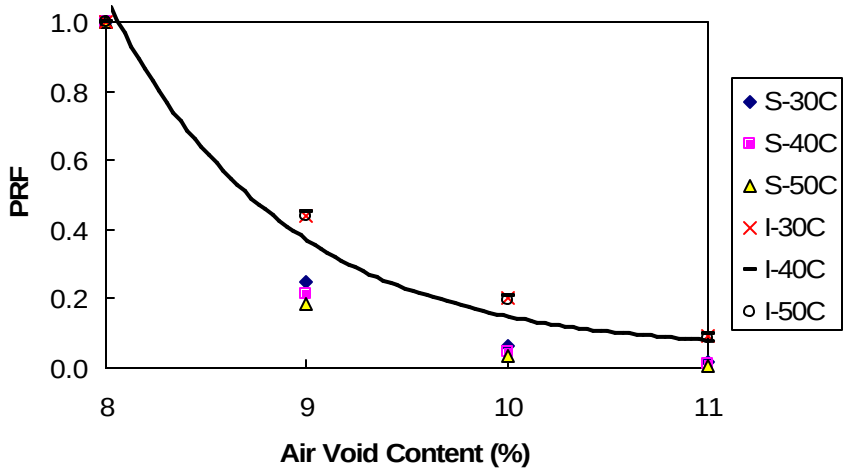

Figure 6-2. PRFs determined from the TRLPD rutting tests (S: S9.5C, I: I19.0C)

6.2 MMLS3 Tests

The MMLS3 test results for fatigue cracking and rutting are further analyzed in this section to determine the PRF. For the fatigue cracking analysis, the number of cycles to failure for different air void contents are summarized in Table 4-2 and plotted in Figure 6-3. For the rutting analysis, a failure criterion is necessary to determine the number of cycles to failure from Figure 4-13 and Figure 4-14. The NCDOT uses a 0.5 in. rut depth as the failure criterion. Since the MMLS3 is a third-scale machine, the rut depth of 0.5 in. in an actual pavement is equal to 0.17 in. Power form equations were obtained between the rut depth and the number of loading cycles from the data in Figure 4-13 and Figure 4-14 and solved for the number of cycles to failure at the rut depth of 0.17 in. The results are shown in Figure 6-4.

The results shown in Figure 6-3 and Figure 6-4 are used to determine the PRFs based on the number of cycles to failure, which are plotted against the air void contents in Figure 6-5. The regression analysis of the data in this figure results in the following equation:

$$PRF = -0.215 \times (\%AV) + 2.72 \quad \text{for fatigue cracking;} \tag{6-5}$$

$$PRF = 2446.8 \times e^{-0.9753 \times \%AV} \quad \text{for rutting.} \tag{6-6}$$

Eqs. (6-3) to (6-6) are used to calculate the PRF values at different air void contents. These values are tabulated in Table 6-2.

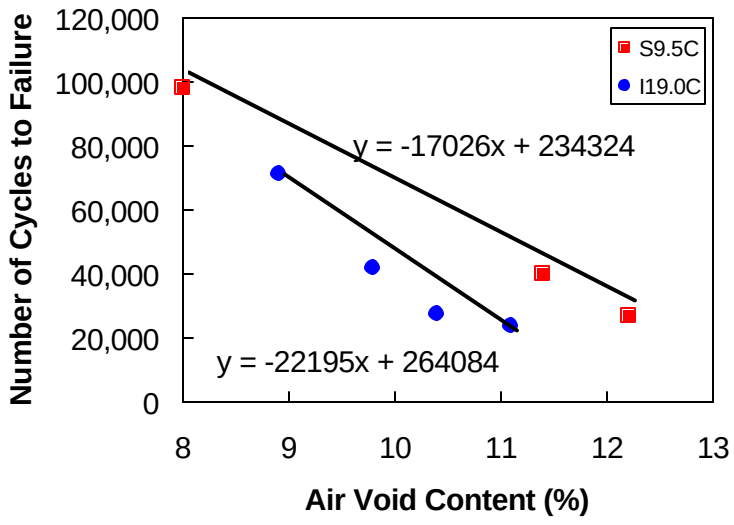

Figure 6-3. Service life measured by the MMLS3 as a function of air void content based on the fatigue cracking analysis

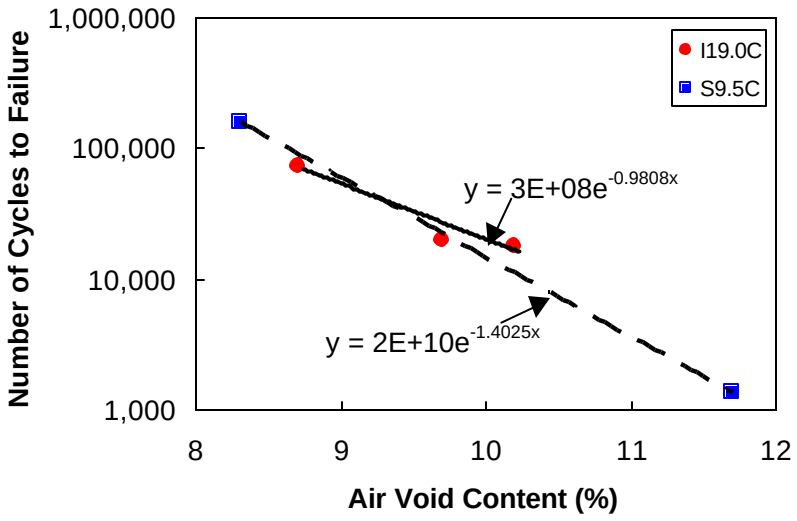

Figure 6-4. Service life measured by the MMLS3 as a function of air void content based on the rutting analysis

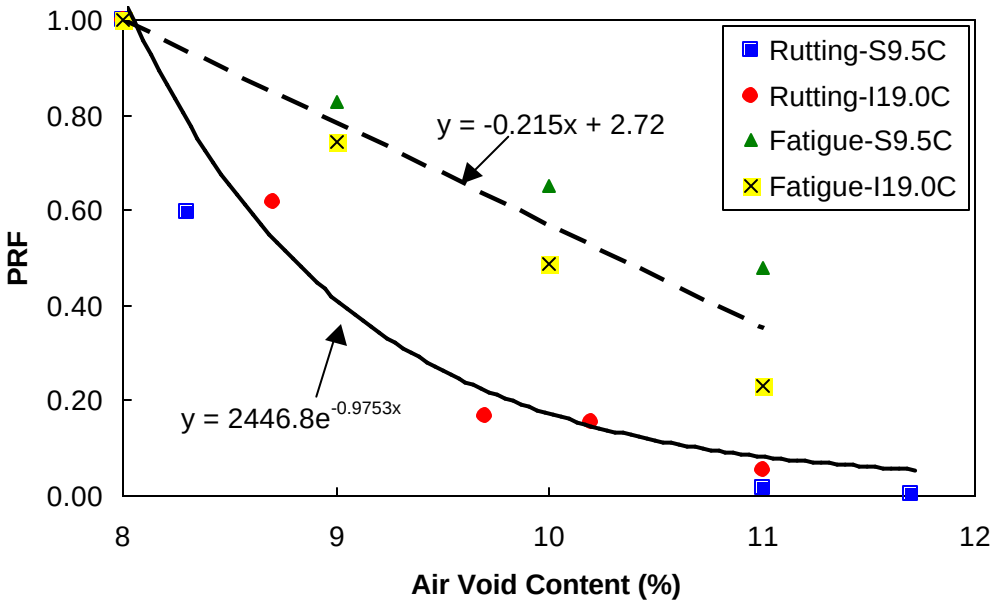

Figure 6-5. PRFs determined for different air void contents using the MMLS3 data

Table 6-2. PRF values for different air void contents

	PRF			
	IDT	TRLPD	MMLS3	
%AV	Fatigue Cracking	Rutting	Fatigue Cracking	Rutting
8	1.00	1.00	1.00	1.00
9	0.83	0.31	0.79	0.38
10	0.68	0.10	0.57	0.14
11	0.55	0.03	0.36	0.05

It can be seen from Table 6-2 that the PRF values for a specific performance characteristic (i.e., fatigue cracking or rutting) are not significantly affected by the means of determining those values (i.e., IDT or TRLPD testing vs. the MMLS3 testing). A much greater difference is observed between the values for fatigue cracking and the values for rutting. The PRFs obtained from the fatigue analysis are closer to the current NCDOT policy of a 50% price reduction for a 3% air void deficiency, and the PRFs calculated from the rutting analysis are much lower than those determined from the fatigue analysis.

It is noted here that the PRFs determined from the material level performance tests and MMLS3 tests assume that the deficient HMA is present through the entire thickness of the HMA layer. In reality, the deficient HMA is present in only a portion of the entire thickness of the HMA layer and, therefore, the PRFs shown in Table 6-2 need to be considered as the lower bound.

In the next section, case studies are presented with the purpose of demonstrating the methodology in which the effect of deficient HMAs in a pavement structure is assessed.

6.3 Case Studies Using the AP^4

In this section, five price reduction cases from Carteret County are studied using the AP^4. These cases are actual cases obtained from the NCDOT Construction Unit. Around 30 cases all together were obtained from the Construction Unit; these five cases were selected for the analysis because they represent the widest range of conditions. Information on the input parameters used in the case studies is as follows:

- Design life = 20 years
- Initial year ADT = 60,800
- Traffic growth rate (%) = 5.21
- Starting date = May 1st
- % Duals = 6
- % TTST = 18
- Modulus and Poisson's ratio of aggregate base = 60 ksi and 0.35
- Modulus and Poisson's ratio of subgrade = 15 ksi and 0.45
- Failure criterion for fatigue cracking: cumulative damage ratio of one
- Failure criterion for rutting: rut depth of 0.25 in.

The pavement structure and the air void contents of the asphalt layers in each pavement are summarized in Table 6-3. Cases 1, 2, and 3 are aggregate base pavements, and Cases 4 and 5 are full-depth pavements. The total asphalt layer thickness ranges from 2 in. (Case 1) to 13 in. (Case 5). In Cases 2 the density was deficient in the intermediate course, whereas the surface course was the problem for Cases 1, 3, 4, and 5. The extreme case of an 11.1% air void content is reported in Case 2.

The AP^4 was run for these five and their corresponding in-specification cases for the analysis period of 20 years. The in-specification cases assume that all the conditions are the same as the corresponding deficient cases, except that the air void contents of all the asphalt layers are 8%. The results from this analysis are summarized in Table 6-4.

Even though the equations in the MEPDG were used in the fatigue analysis, the service lives from the fatigue analysis are unreasonably short. This error is probably due to the differences between the MEPDG and AP^4, including, but not limited to, the effects of seasonal variation on the aggregate base and subgrade moduli. The lab-to-field correction factor in Eq. (5-1) was developed by comparing the fatigue life predicted from the MEPDG with the actual fatigue life observed from the field. Therefore, unless exactly the same algorithms are used in the fatigue life prediction, the correction factor is expected to be invalid.

However, it is believed that the primary objective of this research can be accomplished using the AP^4 because the PRF is the ratio of the life of the deficient pavement and that of the in-specification pavement. Since the correction factor in the fatigue performance equation (Eq. (5-1)) is multiplied to the rest of the equation, this correction factor is cancelled when the ratio of two fatigue lives is calculated.

The following observations can be made from Table 6-4 for each case.

Case 1: Since the pavement in Case 1 has only two in. of HMA, the calculated horizontal strain at the bottom of the asphalt layer was in compression. The compressive strain makes the use of the fatigue performance prediction model invalid. Therefore, rutting becomes the critical distress for the PRF determination in this case.

Case 2: The PRFs from the fatigue and rutting analyses are similar. The density deficiency of 3.1% in the intermediate layer resulted in about 54% in price reduction.

Cases 3 and 4: In these cases, the deficiency lies in the surface layer. Since these pavements are relatively thick, the rutting performance is the critical parameter for the PRF determination. Although the density deficiencies are 1.6% and 1.2% for Cases 3 and 4, respectively, the price reduction is about 40% because the deficient layer is the surface layer and the rutting occurs at the top few inches of the pavement.

Case 5: The rutting performance is the critical parameter for the PRF determination. About 13% of the price reduction resulted from a 1.1% deficiency in the surface layer. The comparison of the fatigue life between Cases 4 and 5 demonstrates the importance of

HMA layer thickness in extending the fatigue life of asphalt pavements. The increase in the total HMA layer thickness from 9.5 in. in Case 4 to 13.5 in. in Case 5 (about 50% increase) causes the fatigue life to increase almost 9 times.

Table 6-3. Pavement structures and air void contents for the five cases

Case No.	Materials	Thickness (inch)	Air voids (%)
1	S9.5C	2.0	8.9
	I19.0C	N/A	N/A
	Aggregate Base	8.0	N/A
2	S9.5C	2.5	8.0
	I19.0C	2.5	11.1
	Aggregate Base	8.0	N/A
3	S9.5C	2.75	9.6
	I19.0C	4.3	8.0
	Aggregate Base	6.0	N/A
4	S9.5C	3.0	9.2
	I19.0C	6.5	8.0
	Aggregate Base	N/A	N/A
5	S9.5C	2.5	9.1
	I19.0C	11	8.0
	Aggregate Base	N/A	N/A

Note: Shaded areas represent the layers with a deficient density.

Table 6-4. AP^4 analysis results and the calculated PRF values

Case No.	Distress Type	Service Life (Years)		PRF	% Air Deficiency and Location
		In-Spec.	Deficient		
1	Fatigue Cracking	-	-	-	1.9% - S[a]
	Rutting	4.94	4.47	0.90	
2	Fatigue Cracking	0.13	0.07	0.53	3.1% - I
	Rutting	7.95	3.62	0.46	
3	Fatigue Cracking	0.56	0.46	0.82	1.6% - S
	Rutting	13.07	7.44	0.57	
4	Fatigue Cracking	0.92	0.78	0.84	1.2% - S
	Rutting	9.57	6.14	0.64	
5	Fatigue Cracking	7.06	6.48	0.92	1.1% - S
	Rutting	17.13	14.90	0.87	

Note: Shaded areas represent the controlling distress type.
[a]S and I stand for the surface and intermediate courses, respectively.

CHAPTER 7 CONCLUSIONS AND RECOMMENDATIONS

7.1 Conclusions

This report presents an experimental study on the development of air void models for the dynamic modulus and performance prediction of HMAs. Two typical HMAs used in North Carolina, S9.5C and I19.0C, were tested. The material level test methods employed in this study include:

- Axial compression dynamic modulus test with and without confining pressure
- Indirect tensile (IDT) fatigue test
- Triaxial repeated load permanent deformation test

The findings from these tests are as follows:

Dynamic Modulus

- The dynamic modulus decreases as air void content increases, regardless of the temperature and loading frequency, whereas the time-temperature shift factor is not affected by the air void content.
- The effect of the confining pressure on the dynamic modulus is minimal at low temperatures and high frequencies, whereas at high temperatures and low frequencies this effect becomes significant. This observation can be explained by the fact that, as temperature increases and the loading frequency becomes slower, the asphalt binder becomes softer, and the effect of confinement on the aggregate structure becomes more significant.
- The effect of the confining pressure is more significant in the I19.0C mixture with larger aggregate than in the S9.5C mixture. In the I19.0C mixture, the effect of air voids on the dynamic modulus becomes slightly greater as the confining pressure is added.
- The sigmoidal function used in the MEPDG for representing the dynamic modulus master curve can be successfully modified to incorporate the effect of the air void content.

Fatigue Cracking

- In general, larger variations in the fatigue behavior were observed from the IDT fatigue test than from the other tests. However, it is clear that the fatigue life decreases as the air void content increases, regardless of the mixture type and load level used in the fatigue test.
- The effect of the air void content on the tensile strain versus the number of cycles to failure relationship is not significant, whereas the effect of temperature on the relationship is evident.
- A correction factor can be used to correlate the AI fatigue model that is based on beam fatigue testing with the results from the IDT fatigue testing.

Permanent Deformation

- The effect of the air void content on the permanent strain is very significant. The permanent strain increases as the air void content increases.
- The resilient strain remains fairly constant throughout the TRLPD testing. The resilient strain increases with the increase of both temperature and air void content.
- The permanent strain model in the MEPDG is not adequate to incorporate the effects of the air void content. A new model correlates the ratio of the permanent strain and the resilient strain with the number of loading cycles, temperature, and the air void content.

The effect of the air void content on the fatigue and rutting performance of asphalt slabs was investigated using the third-scale accelerated pavement testing machine, MMLS3. Expected results were obtained; that is, the service life based on the fatigue and rutting failure decreases as the air void content increases.

Performance prediction methodologies were developed that predict the fatigue life and permanent deformation growth of the asphalt pavement under the MMLS3 loading using the material level performance models and multilayered elastic analysis. In the prediction process, the differences between the MMLS3 test and the laboratory tests were identified, and attempts were made to correct for those variations. Some attempts were empirical because of the lack of knowledge and research in those areas. It was found that the prediction methodologies that incorporate these corrections yield reasonable predictions of fatigue life and permanent deformation growth under the MMLS3 loading. A more mechanistic model that can account for these different testing conditions between the MMLS3 and the laboratory tests could help reduce the prediction errors.

Among many other factors, the difference in the loading histories between the MMLS3 test and the laboratory tests appears to be an important factor in the accuracy of the prediction. The time-temperature superposition principle with growing damage was successfully used to account for this difference.

The results from the material level performance tests and the MMLS3 tests allowed the calculation of the PRF values. It was found that the PRF values are not sensitive to the testing methodology used (i.e., the MMLS3 vs. IDT or TRLPD tests); rather they are significantly different depending upon which performance characteristic is used (i.e., fatigue cracking vs. rutting).

Since the effect of density deficient HMAs on the pavement performance is dependent on many factors related to the pavement structure (e.g., location of the deficient mix, layer thickness, etc.), a more realistic means of determining the price reduction than the material level performance tests or MMLS3 test is to use the combination of pavement response model and performance prediction model. In this research, the AP^4 is developed as a stand-alone executable computer program written in LabView 6.0 with graphic user interface. The purpose of this program is to predict the service life of asphalt pavement

based on fatigue cracking and rutting performance. The algorithm adopted in the AP^4 for the damage calculation is very similar to that used in the NCHRP 1-37A MEPDG (AASHTO 2004).

Case studies of five pavements with varying thicknesses and layer types were analyzed using the AP^4 program. These cases were obtained from the Construction Unit at the NCDOT. A comparison of the predicted performances from in-specification and deficient pavements resulted in reasonable PRFs. Although the service life calculated from the AP^4 may not be accurate due to the lack of field calibration, the mechanistic approach implemented in the program provides a more rational and dependable foundation for the calculation of the price reduction.

7.2 Recommendations

The following recommendations are offered for future research:

1. The seasonal variations of the moduli of unbound materials should be incorporated in the damage calculation.
2. The lab-to-field transfer functions should be developed by comparing the performance predicted from the AP^4 with the field performance.
3. Once the performance prediction algorithm is calibrated with the field performance, the life-cycle cost analysis should be implemented for the PRF determination.
4. The HMA rutting performance model in the MEPDG does not have the air void content as an input variable, thus prohibiting the use of the MEPDG for the calculation of the price reduction due to deficient densities. A methodology to change the model form or model coefficients should be developed to take advantage of the most powerful current pavement analysis program that has been already calibrated.

REFERENCES

AASHTO (2004). "Design of New and Rehabilitated Pavement Structures," NCHRP Project 1-37A, American Association of State Highway and Transportation Officials.

Anderson, D.A., D.R. Luhr, and C.E. Antle (1990). "Framework for Development of Performance-Related Specifications for Hot-Mix Asphaltic Concrete," NCHRP Report 332.

Asphalt Institute (1982). "Research and Development of the Asphalt Institute's Thickness Design Manual (MS-1), Ninth Edition," Research Report No. 82-2 (RR-82-2).

Barksdale, R.D., J. Alba, N.P. Khosla, Y.R. Kim, P.C. Lambe, and M.S. Rahman (1997). Laboratory Determination of Resilient Modulus for Flexible Pavement Design, Final Report, National Cooperative Highway Research Program 1-28 Project.

Buttlar, W.G. and R. Roque (1994). "Development and evaluation of the strategic highway research program measurement and analysis system for indirect tensile testing at low temperature," Transportation Research Record.

Buttlar, W.G. and M. Harrell (1998). "Development of End-Result and Performance-Related Specifications for Asphalt Pavement Construction in Illinois," Crossroads 2000, Iowa State University and Iowa Department of Transportation, Ames, Iowa.

Chehab, G.R., Y.R. Kim, R.A. Schapery, M.W. Witczak, and R. Bonquist (2003). "Characterization of Asphalt Concrete in Uniaxial Tension Using a Viscoelastoplastic Continuum Damage Model," Asphalt Paving Technology: Association of Asphalt Paving Technologists-Proceedings of the Technical Sessions, Vol. 72, pp. 315-355.

Daniel, J.S., G.R. Chehab, and Y.R. Kim (2004). "Issues Affecting Measurement of the Complex Modulus of Asphalt Concrete," ASCE Journal of Materials in Civil Engineering, Volume 16, Number 5, pp. 469-476.

Fernando, E.G., D.A. Anderson, D.R. Luhr, C.E. Antle, and Z. Siddiqui (1987). "A Conceptual Framework for Development of Performance-Based Specifications," Journal of Association of Asphalt Paving Technologists, Vol. 56, Reno, Nevada.

Hafez, I.F. (1997). "Development of a Simplified Asphalt Mix Stability Procedure for Use in Superpave Volumetric Mix Design," Ph.D. dissertation, University of Maryland, College Park, Md.

Hanson, D.I., Mallick, R.B., and Brown, E.R. (1994), "Five-Year Evaluation of HMA Properties at the AAMAS Test Projects," Transportation Research Record, 1454, pp. 134-143.

Hondros, G. (1959) Evaluation of Poisson's Ratio and the Modulus of Materials of a Low Tensile Resistance by the Brazilian (Indirect Tensile) Test with Particular Reference to Concrete. Austr. J. Appl. Sci., Vol. 10, No. 3, pp. 243-268.

Hughes, C.S. (1984). "Performance Related Specifications for Bituminous Concrete," FHWA-VA-85-11 Final Rpt.

Kaloush, K.E. (2001). "Simple Performance Test for Permanent Deformation of Asphalt Mixtures," Ph.D. dissertation, Arizona State University, Tempe, Arizona.

Kaloush, K. E. and M. W. Witczak (2002). Tertiary Flow Characteristics of Asphalt Mixtures. Journal of the Association of Asphalt Paving Technologists.

Kim, N. (1994). "Development of Performance Prediction Models for Asphalt Concrete Layers," Ph.D. dissertation, North Carolina State University, Raleigh, NC.

Kim, Y.R., S. Park, and L. Shao (1996). "Statewide Calibration of Asphalt Temperature Study from 1992 and 1993," Final report submitted to North Carolina Department of Transportation.

Kim, Y.R. and H. Wen (2002). "Fracture Energy from Indirect Tension Testing," Journal of Association of Asphalt Paving Technologists, Vol. 71, pp. 779-793.

Lee, S.J. and Kim, Y.R. (2004). "Fatigue Investigation of Laboratory Asphalt Pavement Using the Third Scale Model Mobile Loading Simulator," Proceedings of the 5th International RILEM Conference on Cracking in Pavements, Limoges, France.

Miner, M.A. (1945). "Cumulative Damage in Fatigue," Transaction of the ASME, Vol. 67, pp. A159-A164.

NCHRP 1-28 (1997). "Laboratory Determination of Resilient Modulus for Flexible Pavement Design: Final Report," National Cooperative Highway Research Program.

NCHRP 1-37A Draft Test Method DM-1 (2002[a]). "Standard Test Method for Dynamic Modulus of Asphalt Concrete Mixtures."

NCHRP 1-37A Draft Test Method W2 (2002[b]). "Simple Performance Test for Permanent Deformation Based upon Repeated Load Test of Asphalt Concrete Mixtures."

National Center for Asphalt Technology (2002). Verification of the Gyrations in the Ndesign Table for North Carolina #1: I-85, NCHRP 9-9 (1).

Roque, R. and W.G. Buttlar, The Development of a Measurement and Analysis System to Accurately Determine Asphalt Concrete Properties Using the Indirect Tensile Mode, Proceedings, The Association of Asphalt Paving Technologist, pp. 304-333, 1992.

Seo, Y., El-Haggan, O., Lee, S.J., and Kim, Y.R., "Development of Air Void Models for Dynamic Modulus and Performance of Asphalt Concrete," Paper submitted to the ASCE Journal of Materials in Civil Engineering, 2004.

Shook, J.F., M.A. Diaz, M. Stroup-Gardiner, and S.B. Seeds (1993). "Performance-Related Specifications for Asphalt Concrete," FHWA-RD-91-070, NCP 3E8b1032.

Weed, R.M. (1999). "Practical Framework For Performance-Related Specifications," Transportation Research Record, Vol. 1654.

Witczak, W.M., Kaloush, K., Pellinen T., El-Basyouny M., and Quintus H.V. (2000), "Simple Performance Test for Superpave Mix Design," NCHRP Report 465, National Research Council, Transportation Research Board, Washington, D.C.

Yoder, E.J. and M.W. Witczak (1975). Principles of Pavement Design, 2nd Edition.